STRUCTURE AND CATALYTIC PROPERTIES OF MODEL MULTINUCLEAR TRANSITION METAL COMPLEXES ENCAPSULATED IN POROUS INORGANIC SOLIDS

A THESIS SUBMITTED TO THE

UNIVERSITY OF PUNE

FOR THE DEGREE OF

DOCTOR OF PHILOSOPHY

IN

CHEMISTRY

BY

CHAVAN SUHAS ARUNKUMAR

CATALYSIS DIVISION

NATIONAL CHEMICAL LABORATORY

PUNE 411 008, INDIA

FEBRUARY 2002

CERTIFICATE

It is certified that the work incorporated in the thesis "**Structure and Catalytic Properties of Model Multinuclear Transition Metal Complexes Encapsulated in Porous Inorganic Solids,"** submitted by Mr. Chavan Suhas Arunkumar, for the degree of **Doctor of Philosophy in Chemistry**, was carried out by the candidate under my supervision, in the Catalysis Division, National Chemical Laboratory, Pune, India. Materials obtained from other sources have been duly acknowledged in the thesis.

Dr. D. Srinivas

Research Guide

CANDIDATE'S STATEMENT

I hereby declare that the work incorporated in the present thesis "**Structure and Catalytic Properties of Model Multinuclear Transition Metal Complexes Encapsulated in Porous Inorganic Solids,"** is original and has not been submitted to any University / Institution for the award of a Diploma or Degree. I further declare that the results presented in the thesis and considerations made therein contribute in general to the advancement of knowledge in **Chemistry** and particularly to the field of **Spectroscopy and Catalysis**.

Chavan Suhas Arunkumar

ACKNOWLEDGEMENT

This has indeed been a philosophical endeavor. During the time that has elapsed, I had the privilege to share an association with many well-wishers who have, each in their own ways, influenced my individuality and understanding of a professional attitude to Life and Chemistry in particular. I wish to acknowledge them because had not been for them, this work may not have been completed.

I wish to express my sincere gratitude to Dr. Paul Ratnasamy, Director, National Chemical Laboratory, Pune, for giving me this unique opportunity to work at the National Chemical Laboratory and for actively supporting my research and encouraging me throughout the course of this educational quest.

I am indebted to my Research Guide Dr. D. Srinivas for his invaluable guidance, care and encouragement, which has helped me to realize my goal.

I sincerely thank Dr. A. V. Ramaswamy, Head, Catalysis Division, for permitting me to use the laboratory facilities to carry out my research work at the National Chemical Laboratory.

I especially thank Dr. S. Sivasanker, Dr. C. Gopinathan, Dr. (Mrs.) Sarada Gopinathan and Dr. S. B. Halligudi for the encouragement during the course of my work. I place on record my thanks to Dr. Tamhankar (for help in AAS-analyses), Mrs. N. Jacob (for help in TG-DTG analyses), Mr. Suresh Waghmode (for help in molecular modeling) and Mr. Sonawane, C-MET, Pune (for help in ICP-AES analysis). I thank Dr. Robert Raja, Dr. C. V. Rode and Dr. R. V. Chaudhari for their interest in my work.

I wish to express my sincere gratitude to the scientists of the Catalysis Division for their valuable suggestions. My thanks are due to all my friends and colleagues at

the Catalysis Division, and to Avinash, Shrikant, Nandkumar, Shyam, Lawrence, Ramani, Ebenezer and Satya for making my stay at NCL memorable.

Finally, I thank my wife Geeta and aunt, Mrs. Suhasini M. Pawar, for being with me at each step of this remarkable journey.

"You cannot acquire experience by making experiments. You cannot create experience. You must undergo it."

--Albert Camus (1913 - 1960)

TABLE OF CONTENTS

CHAPTER-1 GENERAL INTRODUCTION

CHAPTER-2 **EXPERIMENTAL METHODOLOGY**

Chapter-1

General Introduction

1.1 Introduction

The high efficiency and fine-controlled catalytic activity exhibited by metalloenzymes and proteins in biochemical transformations are attributed to the facile redox behavior of the active site and the conformational flexibility of the protein moiety (1, 2). Enzymes are polyfunctional catalysts containing several groups, some of which bind and orient substrates while others participate in consecutive chemical reactions. In the presence of enzyme catalysts, energy and entropy barriers are lowered substantially, and the reaction proceeds along the most favorable reaction path. The sufficient rigidity, compact structure and optimal molecular dynamic mobility are the causes for the dynamic adjustment of the active site, resulting in high specificity of the metalloenzymes. However, the tedious extraction procedures and the requirements of highly defined, controlled, conditions e.g., pH, temperature etc., limit their use in large industrial applications. An alternative approach, while maintaining the high activity and selectivity in chemical transformations, is to encapsulate active metallic centers or their complexes inside porous inorganic solids like zeolites (3, 4). The active site of the enzyme mimics a microscopic reaction vessel in which the substrate is confined and the chemical transformation of the bound substrate takes place (5). The substrate is adsorbed on the external surface of the protein tertiary structure of the enzyme, followed by that the substrate molecules are sieved, such that, only those molecules capable of diffusing through the protein mantle can access the internally located active site. It is, here the selectivity of the substrate transformations is achieved, since the active site has size and shape characteristics. In analogous zeolite-encapsulated complexes the protein mantle

is replaced by the zeolite framework, and the active site by the metal complex. The porous inorganic mantle provides the required steriochemistry to the metal complex. It also imposes certain restrictions to the access of the active site, by the substrate molecules, resulting in size and shape selectivity (6). The novel, encapsulated complexes combine the engineering advantages of heterogeneous catalysts like ruggedness, easy catalyst separation etc., with those advantageous features of homogeneous catalysts like a well-defined unique structure that can be elucidated and correlated with catalytic activity (3 – 5). Hence, the solid, encapsulated metal complex catalysts have attracted the attention of catalyst researchers in recent times. A variety of metal complexes containing Schiff base, diimine, phthalocyanine and porphyrin ligands have been encapsulated in zeolite molecular sieves (7 – 10). However, a majority of the studies are confined to mononuclear metal complexes.

Multinuclearity is a common phenomenon in metalloenzymes. The multinuclear active sites are responsible for multi-electron redox transformations and energy generating reactions in biological pathways, such as, nitrogen fixation, oxidative phosphorylation, reduction of nitrates and sulphites, oxidation of ascorbic acid, binding and activation of dioxygen, hydroxylation of saturated hydrocarbons and metabolism of molecular hydrogen (11, 12). Hence, studies on multinuclear metal complexes and their encapsulation in porous inorganic solids are important. The present work deals with this subject.

1.2 Multinuclear Metal Clusters in Enzymes and Proteins

Representative examples of metalloenzymes containing multinuclear metal active sites are as follows. The nitrogenases derived from *C. pasteurinum*

have 2Mo and 24Fe metal centers (13), while xanthine oxidase (14) and sulphite dehydrogenase (15) have 2Mo, 8Fe and 2FAD centers and 1Mo and 20Fe centres, respectively. The Fe-containing proteins (16) have 3.45 to 4.05Fe centers while the Ni-containing dehydrogenases obtained from *D. salexigens* (17) have 1Ni, 1Fe and 1Se centers. The multinuclear Cu-containing metalloenzymes and proteins are not only efficient carriers and activators of dioxygen but are also capable of mediating many oxidations selectively. In cytochrome c oxidase are present 2Cu centers and 2 heme groups (18), while in the blue Cu proteins and enzymes such as cerrulloplasmin (19), ascorbate oxidase (19) and laccase (20), which catalyze the reduction of oxygen to water, are present 4 to 8Cu centers. Monooxygenases like dopamine oxidase (16) and tyrosinase (21) contain 2Cu centers and catalyze efficiently the hydroxylation of aromatic substrates. The Cu-containing oxidases with 1 to 3 Cu centers catalyze the oxidation of amines and galactose and the reduction of oxygen to H_2O_2 (19). The electron carrier proteins usually have 1 to 2 copper centers (22, 23). The thyllakoid membrane of the Photosystem-II of plant chloroplasts contains a Mn-complex of nearly 4Mn centers per one reaction center comprising four hundred chlorophyll molecules, pheophytin and a primary acceptor P 680^+ (24 – 26). The composition and integrity of the metal cluster active site is highly important, for example, removal of any one of the Mn centers results in the malfunctioning of Photosystem-II.

1.3 Porous Inorganic Solids - Zeolites

Porous inorganic solids are defined as ordered crystalline structures enclosing within themselves a measurable void in the form of pores, channels and cages. The wide spectrum of porous inorganic solids includes a variety of

oxides, aluminosilicates (zeolites), high silica (silicalites), aluminophosphates and layered materials like clays and pillared clays (27 – 31). Variation in pore shape (elliptical, circular etc.), dimensionality of the pore system (1-, 2- and 3-dimensional), presence and absence of cages, the strength, location and distribution of the acid sites, hydrophilic or hydrophobic surface properties, the void volume (nearly 50%) and the framework composition are distinctly observed in these porous solids and define their specific application in chemical industry. Porous solids have extensive commercial applications as adsorbents, catalysts and catalyst supports due to their high surface area.

Table 1.1 Pore Size and Structure of Some Porous Inorganic Solids

Class of materials	Examples	Pore structure	Pore size (nm)
Aluminosilicates (Zeolites)	Faujasites (X, Y-type, Beta, ZSM-5)	Small, medium and large pores	0.3 – 0.7
Silica molecular sieves (Silicalites)	Metallosilicates (Ti, V, Sn, Cr-silicates)	Medium and large pores	0.5 – 0.8
Phosphate-based molecular sieves	$AlPO_4$'s and SAPO's	Medium and large pores	0.5 – 1.0
Clays, Pillared clays	Smectite, K-10 intercalated with metal oxides, PILC's	Large pore (2-dimensional)	> 1.0
Mesoporous materials	Silica, silicaalumina MCM-41 and MCM-48	Large pore (1-dimensional)	> 2.0

The porous, inorganic solids are essentially characterized by the pore size and by uniformity in pore structure. It is on this fundamental principle, the shape selective catalysis can be brought about using these porous inorganic solids as catalysts or catalyst supports (32 – 34). According to IUPAC

definition, the porous materials are divided, based on their pore dimensions, into microporous (< 20 Å), mesoporous (20 – 500 Å) and macroporous (> 500 Å) materials. (35). The pore size and structure of selected classes of porous inorganic materials are given in Table 1.1 (36 – 39).

Zeolites are natural or synthetic, crystalline aluminosilicates with a 3-dimensional microporous framework made up of corner sharing of SiO_4 and AlO_4 tetrahedra. Isomorphous substitution of Si^{4+} by Al^{3+} in the silicate lattice creates an excess negative charge compensated by exchangeable cations. A general formula of aluminosilicates can be written as

$$M_{x/n}^{n+}[(AlO_2^-)_x(SiO_2)_y].zH_2O$$

where n is the valence of the charge compensating cation M; x assumes values between 0 and 0.5. According to the Loewenstein rule (40), the ratio x/y is smaller than or equal to unity. The individual silicon and aluminium tetrahedra are always close to regular, but the shared oxygen linkage can accommodate T-O-T angles from 130-180º. The tetrahedra can be combined to form a variety of framework structures. Zeolites with different framework topology have pores varying in size, shape and dimensionality. The aperture of the pores range from 4 to 8 Å, depending on the number of tetrahedra constituting these rings. The main properties of zeolites from the catalytic point of view are their ability for molecular sieving, cationic exchange, high surface area, variable acidity and chemical and thermal stability. Traditional aluminosilicate zeolites are widely used as heterogeneous catalysts in petroleum and petrochemical industries as well as in environmental pollution control (41).

Zeolite-Y belongs to the Faujasite (FAU) family and exhibits 3-dimensional pore structure, with pores perpendicular to each other and is made

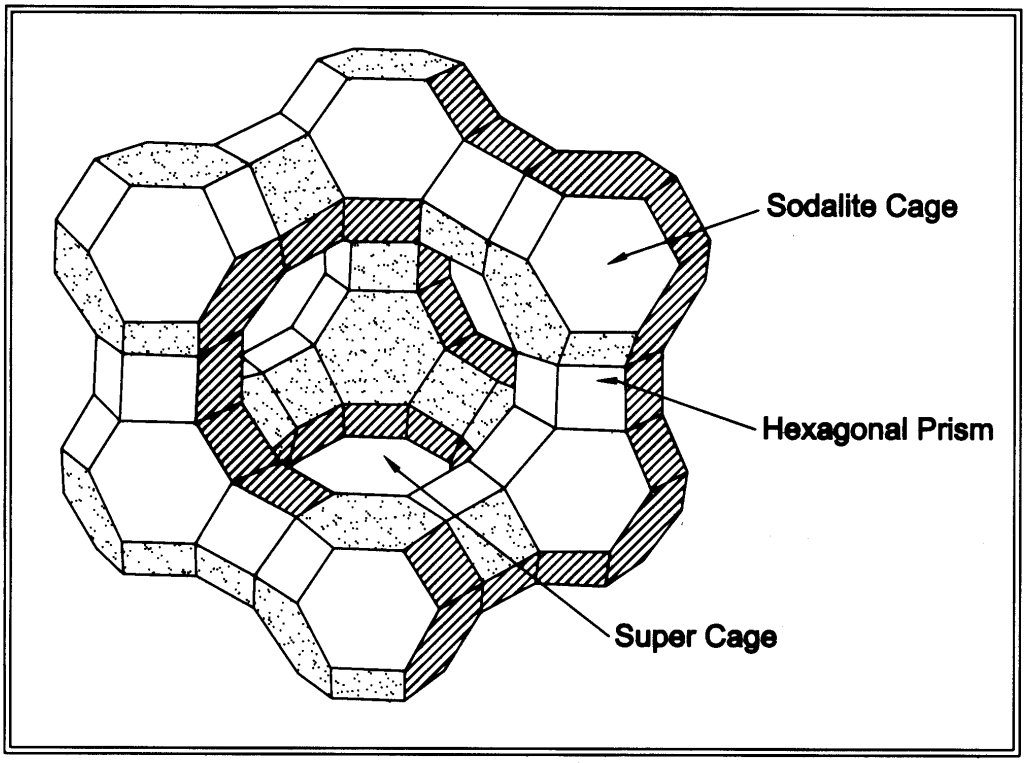

Fig. 1.1 Structure of zeolite-Y

up of 4, 6, and 6-6 secondary building units (42 - 44). The diameter of the aperture of zeolite-Y is about 7.4 Å, since a 12-member oxygen ring defines it. It leads into a larger cavity or supercage, possessing a diameter of ~12 Å. Zeolite-Y is widely used as a cracking catalyst. It is used in acidic form to increase the yield of gasoline and diesel fuel from crude oil feedstock by cracking heavy paraffins into gasoline grade napthas, in petroleum refinery catalytic cracking units. It is also used in the hydrocracking units as a Pt/Pd support to increase aromatic content of reformulated refinery products. The microporosity of zeolite-Y also provides means for physically trapping of guest molecules as opposed to external surface attachment (45, 46). The structure of zeolite-Y is illustrated in Fig. 1.1.

1.4 Zeolite Encapsulated Metal Complexes - Zeozymes

A majority of large-scale industrial chemical processes employ heterogeneous catalysts because of their ease of separation from products, use in fixed bed and continuous flow through operations, eco-friendly nature, thermal stability and amenability to regeneration and reusability (47 – 50). However, homogeneous catalysts offer advantages like greater selectivity and controllability because of the presence of only one type of active site. Heterogenization of homogeneous catalysts ensures the cross-fertilization of most of the advantages of both the systems (51). If the commonly encountered problem of metal leaching is avoided, the hybrid-catalysts provide unique opportunity in synthetic chemistry and chemical processing. Immobilization of metal complexes can be achieved either by encapsulating the complex in the pores of zeolite or by anchoring or tethering to the inert support (52 – 57, Fig. 1.2). The grafting and tethering refer to covalent attachment of the metal complex, either directly (grafting) or through a spacer ligand (tethering). However, encapsulation (ship-in-a-bottle) is a convenient and ideal approach of heterogenization because the complex, once formed inside the pore of zeolite, is too large to diffuse out. As these composite materials mimic biological enzymes, they are also called zeozymes (*acronym* for zeolite mimics of enzymes). On confinement in zeolite matrix, the metal complex loses some of its degrees of freedom, adopts unusual geometries and stabilizes by coordination to zeolite-surface functional groups. Thus, in a general sense, they mimic the facile nature of natural systems in constrained environments while simultaneously exhibiting high redox activity (58 – 62).

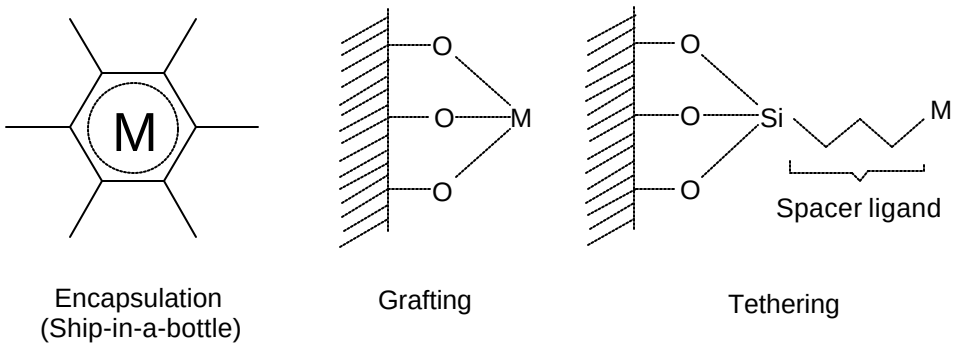

Fig. 1.2 Immobilization of metal complexes (M).

1.4.1 Methods of Encapsulating Metal Complexes

Metal complexes are encapsulated in zeolites and other molecular sieves by the following three methods viz., (i) flexible ligand method, (ii) template synthesis or *in situ* synthesis method and (iii) zeolite synthesis method (63 – 67).

1.4.1.1 Flexible Ligand Synthesis Method

In the flexible ligand synthesis method, the ligands are diffused through the zeolite pores and a metal complex is obtained by their complexation with metal ions that have been already exchanged in the zeolite. The metal complexes, possessing dimensions larger than the diameter of the pore opening, once formed within the zeolite cannot exit unless they undergo decomposition or there is a collapse of the zeolite structure. In this approach, the ligands should have a reasonably low melting point or sublimation point and should be sufficiently small enough to enter through the pores. Once the zeolite void volume is filled homogeneously with the ligand molecules, complexation can be initiated thermally. Once formed, the complexes are sterically hindered in the constrained environments of the zeolite supercages. A wide variety of Schiff base (68 – 70), bipyridine (71, 72), terpyridine and

trimethyltriazacyclononane (73) complexes have been encapsulated in Faujasite supercages using this method.

1.4.1.2 Template Synthesis Method

Ligands with molecular dimensions exceeding 7 Å cannot diffuse into the pores of zeolites. In such cases the template synthesis method is used wherein the ligand itself is constructed inside the zeolite matrix. The mechanism of complexation involves condensation of ligand precursors around the metal ion acting as a template (74). The complex formed cannot exit through the narrow pore of the zeolite. A typical template synthesis method, in the preparation of encapsulated metal phthalocyanine complexes, involves the reaction of a metal ion exchanged zeolite with dicyanobenzene at 423 – 573 K and reduced pressures. Some workers also call this process "*in situ* synthesis" method.

Carbonyl clusters are encapsulated in zeolites by this method. The metal exchanged zeolite is interacted with CO/H_2 or CO/H_2O to form the encapsulated metal carbonyl clusters through reductive carbonylation of intrazeolitic metal ions in the presence of H_2 or H_2O.

1.4.1.3 Zeolite Synthesis Method

The zeolite synthesis method involves building of a zeolite mantle around the metal complex, similar to "building the bottle around the ship" (75 – 81). This method is advantageous as it can be employed to encapsulate well defined, stable complexes. Besides, this method does away with the problems of contamination by the free ligand and uncomplexed or partially complexed metal ions. The only disadvantage is that the metal complex dimensions may be more than that of the zeolitic voids. The stable complex is mixed with silica,

alumina, NaOH and water and heated to ~373 K. The silicate and aluminate species present in the gel are allowed to react with the metal complex in such a manner, that a portion of the complex is incorporated within the zeolite crystal structure. However, if this same methodology was to be adopted for metal complex encapsulation in aluminophosphates by addition of the metal complex to a similar aluminophosphate gel or if the metal complex was added to an aluminate solution, then one observes virtually no encapsulation. Metal complexes are encapsulated in ZSM-5 and mordenite using this method. The metal complex usually plays the role of the template, directing the synthesis. Problems like the aggregation of metal complexes can be overcome by carefully designing the zeolite synthesis procedure. However, the stability of the complex at all stages of the synthesis is necessary. Another frequently observed problem is that in the case of zeolites requiring supplementary template molecules, it is during the process of removal of this template by calcination that the encapsulated complex could also be damaged.

1.4.2 A Brief Review of Zeolite -Encapsulated Metal Complexes and their Catalysis

1.4.2.1 Zeolite-Encapsulated Mononuclear Complexes

Synthetic Faujasite type zeolites (X and Y) have been used extensively for metal complex encapsulation primarily due to the large size of the supercage. A variety of mononuclear complexes have been encapsulated as models for cytochrome P 450. Several researchers (53, 82 – 90) have reviewed the methods of encapsulation, characterization and catalysis. Workers at Du Pont were among the early pioneers to exploit the chemistry of natural enzymes (91, 92). In an attempt to prepare analogs of hemoglobin and myoglobin, which

reversibly bind molecular oxygen, Co(Salen) complexes were encapsulated in zeolite-Y (67). The encapsulated complexes formed more stable dioxygen adducts than the complexes in homogeneous solutions. In a similar attempt to prepare analogs of cytochrome P-450, iron phthalocyanine complexes were encapsulated in zeolite-Y, which exhibited remarkable substrate- and regio-selectivities in the oxidation of unactivated alkanes (64). Interestingly, encapsulation suppressed dimerization that usually occurs in homogenous solutions leading to formation of inactive oxo- and peroxo-bridged metal complexes(64).

Encapsulation of large complexes within the micropores of zeolites has been pioneered by the studies of Jacobs and co-workers (93). They reported a composite catalyst system, that achieved realistic mimicry of cytochrome P-450 by incorporating Fe-phthalocyanine complex in the crystals of zeolite-Y, which are in turn embedded in a polydimethylsiloxane membrane (93). This system oxidized cyclohexane, at room temperature, at rates comparable to those of the enzymes.

Phthalocyanine complexes of Fe and Cu encapsulated in zeolites exhibited high activity and selectivity for direct conversion of methane to methanol with O_2/*tert*-butyl hydroperoxide oxidants. Raja and Ratnasamy (65, 94) have reported the oxyhalogenation of organic substrates using zeolites X, Y and L encapsulated substituted phthalocyanine complexes of Cu, Fe and Co, in liquid phase, at low temperatures, using O_2 as the oxidizing agent and HCl and alkali chloride/bromides as sources of halogens. The encapsulated phthalocyanines catalyzed the aerial oxidation of cyclohexane at ambient temperatures.

Extensive studies have been reported on the selective oxidation of organic compounds using singlet oxygen sources (H_2O_2, *tert*-butyl hydroperoxide and PhIO). Jacobs et al (84) have encapsulated Mn complexes of 2,2-bipyridine, 1,10-phenanthroline, triazacyclononane in Faujasite, HMS and MCM-41, as models for the methane monooxygenases. In solutions, the catalytic activity of Mn(II)-bipyridine is limited by its catalase activity (tendency to decompose H_2O_2 catalytically). When *cis*-$[Mn(bpy)_2]^{2+}$ complexes were encapsulated within the micropores of zeolites X and Y, however, they acted as effective alkane epoxidation catalysts without complications of competing processes such as self-oxidation or catalase activity. Mn porphyrin complexes embedded in polydimethylsiloxane (PDMS) exhibited high activity in selective oxidation of cyclic alcohols to ketones in the presence of *tert*-butyl hydroperoxide oxidant (95).

Jacob et al (96) reported the oxidation of *para*-xylene to *para*-toluic acid using encapsulated substituted Salen complexes. Encapsulated Co(Salophen) complexes were efficient O_2 activators in the Pd catalyzed aerobic oxidation of 1,3-cyclohexadiene to 1,4 diacetoxy-2-cyclohexene (97). Diegruber et al (98) reported the selective oxidation of propene to formaldehyde and acetone with dioxygen using $Co(dmg)_2$-X and Co(py)-X catalysts. Copper amino acid complexes encapsulated in zeolite-Y catalyzed the oxidation of cyclohexane, benzyl alcohol, 1-pentanol and cyclohexene with *tert*-butyl hydroperoxide as oxidant (99, 100). Oxidation of benzene to phenol using molecular oxygen as oxidant was also reported with those complexes.

Recently, zeolite-encapsulated metal complexes are being used in enantioselective oxidations (101). Ogunwumi and Bein (102) and Sabater et al

(103) have extended the use of encapsulation to prepare heterogeneous catalysts for enantioselective epoxidation. The catalysts are based on Jacobson homogeneous oxidation catalyst. Epoxidation of prochiral alkenes were studied using NaOCl as oxidant. Ogunwumi and Bein (102) have reported high *ee* in the epoxidation of *cis*-β-methylstyrene. Piaggio et al (104) have found that the Mn(III) chiral Salen complex immobilized in Al-MCM-41 is an effective epoxidation catalyst for *cis*-stilbene.

Fe-phthalocyanine encapsulated in zeolite-Y was used in the hydrogenation of butadiene and toluene (105, 106) and Pd(Salen) complexes were used for the hydrogenation of cyclohexene and 1-hexene. (69). Ernst et al (107) reported, for the first time, the enantioselective hydrogenation of olefinic double bonds over zeolite (FAU and EMT) encapsulated chiral Pd-Salen complexes.

1.4.2.2 Metal Cluster Complexes

The reports on encapsulated metal cluster complexes are mostly related to metal carbonyls. Knoezinger et al (108) reported characterization of Pd carbonyl clusters encapsulated in zeolite-Y. Ichikawa et al (109) reported the encapsulation and catalytic activity of hexanuclear bimetallic carbonyl clusters of Rh-Ir and Rh-Fe in zeolite-Y. The encapsulated cluster systems were strongly structure-sensitive and efficiently catalyzed C_2H_6 hydrogenolysis to yield C2 - C4 olefins. Schulz-Ekloff et al (110) reported studies on anionic high nuclearity Pt carbonyl complexes encapsulated in Li^+, Na^+, K^+ and Cs^+ exchanged zeolite-X. Though the electronic transitions of the encapsulated clusters remained unaffected, the vibrational frequencies of the CO ligands changed appreciably due to the interaction of the linear CO ligands with the O

atoms of the zeolite lattice. $Pt_{15}(CO)_{30}$ clusters encapsulated in mesopores like FSM-16 exhibited high activity in the water-gas shift reaction than those encapsulated in zeolite-Y(111).

Raja and Ratnasamy (112) reported, for the first time, that dimeric copper acetate encapsulated in molecular sieves Y, MCM-22 and VPI-5 mimics the enzymatic activity of tyrosinase. The encapsulated catalysts exhibited efficient activity in the oxidation of various phenols to *ortho*-dihydroxy and *ortho*-quinone compounds; L-tyrosine was oxidized to L-DOPA. Later, Easwaramoorthy et al (113) reported encapsulation of copper acetate in cubic mesoporous materials. Heteropolyacid $H_3PW_{12}O_{40}$ that was encapsulated in the supercage of Faujasite, exhibited increased activity and modified selectivity in isomerization and disproportionation of *m*-xylene(114).

The encapsulated complexes exhibited enhanced activity and in some cases modified selectivity. Deshpande et al (115) and Seelan et al (116) used UV-visible and EPR spectroscopic studies to explore the causes for the enhanced activities of Salen and phthalocyanine complexes of Cu after they are encapsulated in zeolite-Y. The studies revealed a low-symmetry geometric distortion of the metal complexes after encapsulation in zeolite-Y that resulted in an admixed electronic ground state and subsequent enhanced activity of the metal complexes.

1.5 Activation of Dioxygen

Selective oxidation of organics is an important reaction in bulk and fine chemical manufacturing (117). Selective oxidations can be achieved by harnessing dioxygen and incorporating it into the substrates to yield oxygenated products. Though thermodynamically dioxygen can react with

organic compounds, kinetically it is inert. Dioxygen is a paramagnetic molecule in a triplet ($^3\Sigma_g^-$) ground state with two unpaired electrons in degenerate antibonding orbitals. Its reactivity must follow rules governing the conservation of spin in a reaction. Therefore, dioxygen must either react with another radical or form products with a triplet ground state. Such processes are rare and thus lead to the kinetic inertness of oxygen. Dioxygen can overcome this kinetic barrier of its unpaired electrons and triplet ground state by excitation to its first excited state ($^1\Delta_g$), in which all electrons are paired. This species (singlet oxygen) is generally too reactive and short-lived. However, dioxygen complexation to a transition metal can also result in activation and create stable complexes that can be utilized in further reactions in a controlled manner.

1.5.1 Activation of Dioxygen by Enzyme Tyrosinase

In nature, the binding and activation of dioxygen is performed by a specific group of metalloenzymes called "oxygenases" and "oxidases". The oxygeneses are further categorized into monooxygenases and dioxygenases. Dioxygenases catalyze regio- and stereo-selective oxidations incorporating both the oxygen atoms of the dioxygen molecule into the substrate, while the monooxygenases responsible for the catalytic epoxidation of unsaturated C-C bonds and hydroxylation of the aromatic ring or C-H bond in saturated hydrocarbons, incorporate one oxygen atom into the substrate. The other oxygen atom is converted into water.

An important Cu-containing monooxygenase is tyrosinase. The enzyme tyrosinase oxidizes tyrosine to melanin in mammals and causes the browning reaction in many fruits and vegetables. Due to its ability to reversibly bind

dioxygen, tyrosinase mediates the oxidation of L-tyrosine to L-DOPA and exhibits simultaneous monophenolase and diphenolase activities in the *ortho*-hydroxylation of monophenols to *ortho*-quinones (Fig. 1.3) (118).

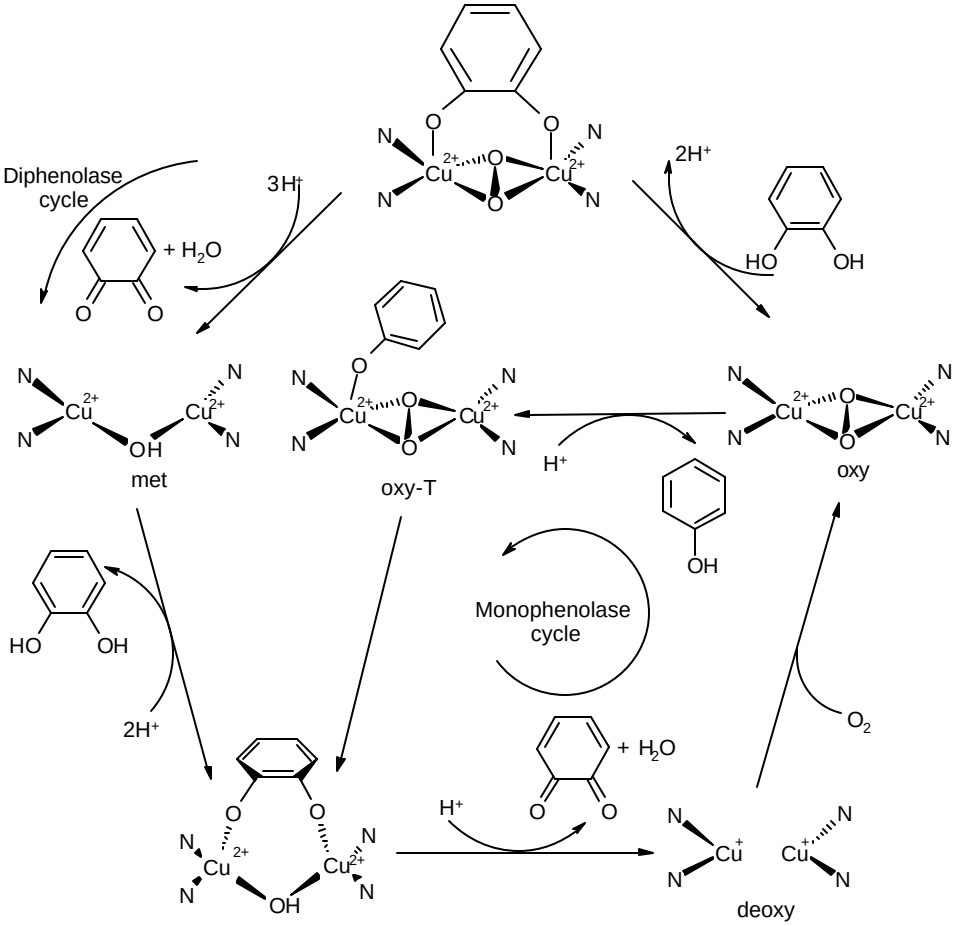

Fig. 1.3 Dioxygen activation by enzyme-tyrosinase (tyrosinase activity).

The EPR silent 'oxygenated' form of tyrosinase (oxy-Tyr) contains two tetragonal Cu atoms, each coordinated by two strong equatorial N_{HIS} ligands and one weak axial N_{HIS} ligand. The exogenous O_2 molecule is bound as peroxide in a side-on μ-η^2-η^2 mode of coordination and bridges the two Cu centers (119 - 121). A similar bridging mode observed in oxygen carrier protein "oxyhemocyanin" and corroborated through spectroscopic and X-ray

crystallography, reflects upon the electron delocalization between the two Cu atoms (122). This electronic side-on approach makes significant contributions to the biological function of oxy-Tyr. On the other hand, the met-tyrosinase form of the enzyme contains two endogenously bridged, antiferromagnetically coupled tetragonal Cu atoms. Deoxytyrosinase has a bicuprous [Cu^{I}-Cu^{I}] structure.

During hydroxylation, direct coordination of substrates, like phenols, to the Cu centers is followed by a transfer of electron density from the copper, which results in the weakening of O-O and Cu-O bonds. Oxygen is transferred to the *ortho*-position of the phenols and the resultant coordinated catecholate transfers two electrons to the binuclear Cu(II) site. Further dissociative elimination of the *ortho*-quinone product is accompanied by formation of the deoxy-site for further turnover. This monophenolase activity is the first stage in the melanization reaction pathway and results in the transformation of monophenol to diphenol. It is always accompanied by further oxidation of the resultant monophenol to quinone (diphenolase activity).

1.5.2 Activation of Dioxygen by Model Metal Complexes

In an attempt to understand coordination and binding of molecular oxygen to metalloenzymes and proteins, several model complexes have been synthesized and studied. Metal complexes coordinated to N- and O-donor acyclic and cyclic ligands were found to activate dioxygen. The cobalt(II) complexes of diethylenetriamine, propylenediamine, butylenediamine, tris(aminoethyl)amine, tris(aminopropyl)amine, chiral aminoethylbis(amino-propyl)amine, 1,5,9-triamino-5-methyl-3,7-diazanonane, 1,4,8,11-tetraaza-cyclotetradecane, hydridotris(pyrazolyl)borate, Schiff base, phthalocyanine and

porphyrin ligands activate dioxygen and form superoxide and peroxide complexes (59, 67, 123, 124). Because of the enforced dispersion of metal complexes in the zeolite, systems not readily observable in solution were investigated in zeolites. The mononuclear superoxo adduct of Co(III)-amine, $Co(NH_3)_4(O_2^-)^{2+}$, which would be expected to dimerize in solution was observed entrapped in zeolite-Y (125). Heterogenized Co(cyclam) complexes react with oxygen and form mononuclear superoxo-adducts (126). Mn(III) complexes of Salen, Br_2-Salen and (*tert*-butyl)$_4$Salen ligands encapsulated in zeolite-Y were investigated for the oxidation of styrene using molecular oxygen and *tert*-butylhydroperoxide as initiator (127). Woltinger et al (97) reported the efficient oxygen activation by zeolite-Y-encapsulated Co(Salophen) complexes in the palladium catalyzed 1,4-oxidation of 1,3-cyclohexadienes. Metal phthalocyanine complexes were realized to activate dioxygen and oxygenate organic compounds. Fe and Co phthalocyanine complexes exhibited remarkable rate enhancement on encapsulation in zeolite-Y, in the aerobic oxidation of hydroquinone (128). Metal phthalocyanine complexes encapsulated in NaY were also used for the dioxygen oxidation of *cis*-pinane (129). Balkus Jr. et al (130) reported the oxidation of cyclohexene with O_2 over encapsulated Ru(II)-hexadecafluorophthalocyanines. Dimeric copper acetate encapsulated in molecular sieves activates dioxygen in a similar manner to that of enzyme tyrosinase (112, 113).

1.6 Liquid Phase Aerial Oxidations

Several important liquid phase aerial oxidation processes were developed during 1950's and 1960's. Among them, prominent are the Wacker process for the oxidation of ethylene to acetaldehyde (Pd(II)/Cu(II) catalyst,

403 K, 3 bar) (131), the Celanese process for the oxidation of n-butane to acetic acid (Co(II) or Mn(II) ions, 423 – 498 K, 40 – 50 bar), the Amoco/Mid-Century process for the oxidation of *para*-xylene to terephthalic acid (Co(II)/Mn(II)/Br^-, acetic acid medium, 473 K, 30 bar) (132) and the oxidation of cyclohexane to KA oil (Mn or Co naphthenate catalyst, 398 – 438 K, 10 bar) (133).

1.6.1 Selective Oxidation of *Para*-Xylene

Terephthalic acid (TA) is a large volume commodity chemical, used mainly in the manufacture of polyester. More than 3.9 million tons of TA is produced worldwide by aerial autoxidation of *para*-xylene (PX) in the presence of a combination of cobalt and manganese salts and bromide ion promoter in acetic acid medium (Amoco-Mid Century process) (132, 134 –136). The process is optimized to yield TA purities of the order of 95 – 97% at PX conversion of 98 – 99%. Because of its industrial importance, the kinetics of the PX oxidation reaction was extensively studied. With cobalt alone in acetic acid, the reaction is much slower. In the presence of cobalt, bromide ion is oxidized to chain propagating bromine atoms. Unfortunately, the one-electron oxidation of acetic acid ligands leading to decarboxylation, seriously competes with the oxidation of PX. However, in the three component system Co/Mn/Br^-, Mn(II) is rapidly oxidized by Co(III) to yield Mn(III) which rapidly oxidizes Br^- to Br. The latter abstracts the hydrogen from the substrate to give the benzylic radical. Because Co(III) is readily removed from the reaction mixture by reaction with Mn(II), the steady-state concentration of Co(III) is maintained at a low-level, thus preventing undesirable decarboxylation of acetic acid by Co(III). Decomposition of acetic acid by Mn(III) is negligible under the

reaction conditions. Although much is explored about the reaction mechanism, the actual catalyst species in the Co/Mn/Br^- system is not yet understood. Spectroscopic studies on the reaction mixtures would help in this regard. Also several improvements are desirable in the existing commercial process for TA manufacture.

1.6.2. Preparation of Adipic Acid

Another industrially important chemical reaction is preparation of adipic acid from cyclohexanone. The commercial process of adipic acid preparation involves autoxidation of cyclohexane to a mixture of cyclohexanol and cyclohexanone (KA oil), followed by HNO_3 oxidation in the presence of a copper/vanadium catalyst (137). The drawbacks of this commercial process are low conversions and/or selectivities. The second-stage of the reaction (HNO_3 oxidation) produces significant toxic nitric oxide effluents and hence the process is not environmental friendly. The process is least efficient of all the major industrial processes. Methods to improve the selectivity have been the focus of the research in the area of adipic acid oxidation over the last decade (138 – 140). However, none of the alternative processes reported so far have the potential to replace the current commercial process due to low adipic acid selectivity and/or the use of expensive oxidants like H_2O_2 or alkylhydroperoxides.

The current trend in chemical manufacturing is towards processes that are more efficient in the use of raw materials and energy and more environmentally benign. In this context, heterogenization of the homogeneous catalysts would help overcome the drawbacks of the existing homogeneous processes.

1.7 Scope of the Work

So far the studies on encapsulated systems have been confined mostly to monomeric metal complexes. As described in the previous sections, multinuclearity is a common phenomenon in metalloenzymes (e.g., tyrosinase, hemocyanine, methane monoxygenase, hemerythrine, non-heme Mn catalases, water splitting Mn catalases etc). The multinuclear active sites are responsible for multi-electron redox transformations. It is, therefore, aimed to study in this thesis, multinuclear metal complexes encapsulated in porous inorganic solids such as zeolite-Y.

A majority of known metal complex catalysts utilize alkylhydroperoxides, iodosylbenzene (PhIO), NaOCl etc., as the source of oxygen. These oxidants are expensive and yield unwanted by-products, whose separation is formidable and an expensive task. Nature utilizes cheap, environmental-friendly oxidants like molecular oxygen in the oxidation reactions. Development of catalyst systems that can use dioxygen in oxidation reactions is highly desirable. The work presented in the thesis addresses this task.

The thesis describes synthesis, structure and catalytic properties of dinuclear Cu acetate and chloroacetate and trimeric (μ_3-oxo)(μ-acetato)-bridged Co and Mn cluster complexes. These multinuclear complexes are encapsulated, for the first time, in zeolite-Y. The copper complexes functionally mimic the copper containing monooxygenase enzyme, tyrosinase. The cobalt and manganese cluster complexes have some structural similarity to that of the active site of methane monooxygenase and manganese containing non-heme catalases. The formation and integrity of the encapsulated complexes

are confirmed by physicochemical characterization. The activities of these systems in three important multi-electron oxidation reactions, viz., hydroxylation of phenol (with Cu complexes) and oxidation of *para*-xylene and cyclohexanone (with Co and Mn complexes), are investigated. The reactions are carried out with dioxygen/air as oxidant. Comparative catalytic activities of "neat" and zeolite-Y-encapsulated multinuclear metal complexes are investigated. The encapsulated catalysts are more selective and in some cases, more efficient than the corresponding "neat" complexes. The causes for the enhanced activity of encapsulated metal complexes are probed into by spectroscopic methods. Briefly the objectives of the thesis are as follows:

1) Synthesis of multinuclear copper, cobalt and manganese complexes of acetates, inside the cages of zeolite-Y, as model systems.
2) Structural characterization of these zeolite-Y-encapsulated metal complexes.
3) Selective oxidation of organics using encapsulated multinuclear complexes:
   (i) Catalytic activity of encapsulated copper acetate and copper chloroacetate catalysts in hydroxylation of phenol.
   (ii) Catalytic activity of encapsulated (μ_3-oxo)(μ-acetato)-bridged Co and Mn acetate cluster catalysts in the selective oxidation of *para*-xylene to terephthalic acid.
   (iii) Catalytic activity of encapsulated (μ_3-oxo)(μ-acetato)-bridged Co and Mn cluster complexes in the selective oxidation of cyclohexanone to adipic acid.

4. Investigations of the mechanism of oxidation and to establish the structure-activity correlation in the zeolite-Y-encapsulated multinuclear metal complexes.

1.8 Plan of the Work

The thesis is divided into seven chapters including Chapter 1 on General Introduction.

Chapter 2 describes the syntheses of 'neat' and zeolite-Y-encapsulated multinuclear Cu, Co, Mn and Co/Mn complexes used in the study and the various experimental techniques of physicochemical characterization of the cluster complexes. The procedures of catalytic reactions and product analysis are also discussed.

Chapter 3 deals with the structures and catalytic properties of dinuclear copper acetate ($Cu(CH_3COO)_2.H_2O$; CuAc) and copper chloroacetate ($Cu(CH_2ClCOO)_2.2.5H_2O$; CuClAc) complexes encapsulated in zeolite-Y. The copper complexes mimic the enzymatic activity of the monooxygenase "tyrosinase" in the *ortho*-hydroxylation of phenol to catechol and additional oxidation to *ortho*-benzoquinone with dioxygen. Interestingly, the encapsulated complexes are superior and exhibited enhanced catalytic activities compared to the 'neat' complexes. The causes for the enhanced activities of the encapsulated dimer complexes are probed by detailed variable temperature EPR studies. The effect of chloro-substitution on the catalytic activity and structure is investigated.

Chapter 4 presents detailed electronic and EPR spectroscopic studies on the identity of the active catalyst species in the homogeneous system Co/Mn/Br^- in acetic acid, used for the commercial manufacture of terephthalic

acid (TA) by aerial oxidation of *para*-xylene (PX). The studies carried out on several homogeneous systems (Co/Br, Mn/Br, Co/Mn/Br, Co/Ce/Br, Co/Zr/Br, Co/Mn/Zr/Br, Co/Mn/Ce/Br, Ni/Mn/Br and Ni/Mn/Zr/Br in acetic acid) reveal formation of (μ_3-oxo)(μ-acetato)-bridged Co/Mn clusters, during the reaction. Various factors influencing the formation of the cluster complexes, and the effect on the rates of *para*-xylene oxidation and product distribution are investigated. The catalytic data are supplemented by the *in situ* electronic and EPR spectral measurements. The structural characterization of the active species and catalytic activity in homogeneous medium, under airflow reaction conditions are examined.

Chapter 5 describes characterization and catalytic activity studies of "neat" and zeolite-Y-encapsulated trinuclear (μ_3-oxo)(μ-acetato)-bridged Co and/or Mn cluster complexes viz., $[Co_3(O)(OOCCH_3)_6(C_5H_5N)_3](ClO_4)$, $[Mn_3(O)(OOCCH_3)_6(C_5H_5N)_3](ClO_4)$, and $[CoMn_2(O)(OOCCH_3)_6(C_5H_5N)_3]$. The cluster complexes are characterized by spectroscopic methods. The catalytic activity of the "neat" and encapsulated clusters in the aerial oxidation of *para*-xylene to terephthalic acid at high pressure and temperature are investigated. A comparative activity study of the commercial catalyst, and "neat" and encapsulated cluster complexes is made.

Chapter 6 deals with catalytic activity studies of "neat" and encapsulated (μ_3-oxo)(μ-acetato)-bridged Co/Mn cluster catalysts in the selective aerial oxidation of cyclohexanone, cyclohexanol and cyclohexane to adipic acid. The cluster catalysts are highly active and exhibited superior performance compared to individual Co and Mn acetate salts used commercially.

Chapter 7 presents an overall summary of the work presented in the thesis. The general conclusions are as follows: The present work reports for the first time, studies on the synthesis, structure and catalytic properties of oxo- and acetato-bridged metal cluster complexes encapsulated in zeolite-Y. The encapsulated multinuclear complexes are more selective and in some cases, more efficient than the "neat" complexes. Unlike the "neat" complexes, the solid cluster complexes can be easily separated and reused. Thus the catalytic processes involving the solid cluster complexes are cost effective, environmental-friendly and clean. The work provides deeper insight into the structure of the multinuclear cluster catalysts and contributes to the green chemistry and technology.

1.9 References

1. Likhtenshtein, G. I., "*Chemical Physics of Redox Metalloenzyme Catalysis*," Springer Verlag, Berlin (1988).

2. *"Principles of Bioinorganic Chemistry"* Lippard, S. J., and Berg, J. M., (Eds.), University Science Books, (1994).

3. Balkus Jr., K. J., and Gabrielov A. G., *J. Incl. Phenom. Mol. Recog. Chem.*, **21**, 159 (1995).

4. Herron, N., *CHEMTECH*, **19**, 542 (1989).

5. Parton, R., De Vos, D. and Jacobs, P. A., *"Enzyme Mimicking with Zeolites"* in *"Zeolite Microporous Solids: Synthesis, Structure and Reactivity,"* Derouane, E. G., Lemos, F., Naccache, E., and Ribeiro, F. R., (Eds.), Kluwer Academic Publishers: Dordrecht, 555 (1992).

6. Turro, N., *Acc. Chem. Res.*, **33**, 637 (2000).

7. Balkus Jr., K. J., Gabrielov, A. G., Bell, S. L., Bedioui, F., Roue, L., and Devynck, J., *Inorg. Chem.* **33**, 67 (1994).

8. Knops-Gerrits, P. P., and Jacobs, P. A., *"Catalytic Activation and Functionalization of Light Alkanes,"* in *NATO ASI Ser.* 3, 44, 413 (1998).

9. Balkus Jr., K. J., Eissa, M., and Levado, R., *J. Am. Chem. Soc.*, **117**, 10753 (1995).

10. Liu, C. J., Yu, W. Y., Li, S. G., and Che, C. M., *J. Org. Chem.* **63**, 7364 (1998).

11. "*Metal Clusters in Proteins*," Que Jr., L., and Comstock, M. J., (Eds.), ACS Symposium Series, 372 (1988).

12. Gunsalus, I. C., and Sligar, S. C., *Adv. Enzymol. Relat. Areas Mol. Biol.*, **47**, 1 (1978).

13. Eady, P., and Smith, B., *"Physicochemical Properties of Nitrogenases,"* Hardy, R. W. F., and Bottomley F., (Eds.), Wiley-Interscience, New York, 352 (1979).

14. Nelson, C. A., and Handler, P., *J. Biol. Chem.*, **243**, 5368 (1968).

15. Bray, R. C., *J. Less. Common Metals*, **54**, 527 (1977).

16. Yamada, H., Kumagai, H., Kawasaki, H., Matsui, H., and Koichi, O., *Biochem. Biophys. Res. Commun.*, **29**, 723 (1967).

17. Teixeira, M., Moura, I., Fauque, G., Czechowski, M., Berlier, X., Lespinat, P. A., LeGall, J., Xavier, A. V., and Moura J. J., *Biochimie*, **68**, 75 (1986).

18. Tanaka, M., Haniu, M., and Yasunobu, K. T., *Biochem. Biophys. Res. Commun.*, **76**, 1014 (1977).

19. Maelstrom, E. G., Andreasson, L. E., and Reinhammar, B., *"Copper containing Oxidases and Superoxide Dismutase"*, in Boyer, P. D. (Ed.) The Enzymes. 3rd edition, Academic Press, New York San Francisco, **12**, 507 (1975).

20. Reinhammar, B. R. M., *Biochem.Biophys. Acta*, **275,** 245 (1972).

21. Ulrich, V., and Duppel, W., *"Iron- and Copper- containing monooxygenases"* in Boyer, P. D. (Ed), The Enzymes, 3rd edition, Academic Press, New York San Francisco, **12,** 253 (1975).

22. Colman, P. M., Freeman, H. C., Guss, J. M., Murata, M., Norris, V. A., Ramshaw, J. A. M., and Venkatappa, M. P., *Nature* (London), **272,** 319 (1978).

23. Adman, E. T., Stenkamp, R. E., Sieker, L. C., and Jensen, L. H., *J. Mol. Biol.*, **123,** 35 (1978).

24. Govindjee, Kambara, T., and Coleman, W., *Photochem. Photobiol.* **42,** 187 (1985).

25. Dismukes, G. C., *Photochem. Photobiol.* **43,** 99 (1986).

26. Cheniae, G. M., *"Manganese Binding Sites and presumed Manganese Proteins in Chloroplasts"*, in San Pietro (Ed), Methods in Enzymology, Academic Press, New York, **69,** 349 (1980).

27. Breck, D. W., *"Zeolites and Molecular Sieves System"*, John Wiley & Sons Inc., New York, (1974).

28. Gates, B. C., *"Catalytic Chemistry "*, John Wiley & Sons Inc., New York, (1992).

29. Ribeiro, F. R., Rodrigues, A. E., Rollmann, L. D., and Naccache, C., (Eds.), *"Zeolites: Science and Technology"*, Martinius Nijhoff, The Hague, (1984).

30. Szostak, R., (Ed.), *"Molecular Sieves: Principles of Synthesis and Identification*", Van Nostrand Reinhold, New York, (1989).

31. Barrer, R. M., *"Hydrothermal Chemistry of Zeolites"*, Academic Press, London, (1982).

32. Vaarkamp, M., Von Grondelle, J., Miller, J. T., Sajkowski, D. J., Modica, F. S., Lane, G. S., Zajac, G. W., Gates, B. C., and Koningsbarger, D. C., *Catal. Lett.*, **6,** 369 (1990).

33. Zhou, P. –L., Maloney, S. D., and Gates, B. C., *J. Catal.* **129,** 315 (1991).

34. Bolton, A. P., in *"Experimental Methods in Chemical Research"* Vol. II, Anderson, R. B., and Dawson, P. T., (Eds.), Academic Press, New York, (1976).

35. Csissery, S. M., *Zeolites*, **4,** 202 (1984).

36. Carrott, P. J. M., and Sing, K. S. W., *Pure Appl. Chem.*, **61**, 1835 (1989).

37. Ramaswamy, A. V., *"Science and Technology*" in Chimica and Industria, (2000).

38. Ghosh, S. K., and Sharma, M. M., *Ind. Eng. Chem. Res.*, **31**, 445 (1992).

39. De Vos, D. E., Thibault-Starzyk, F., Knops-Gerrits, P. -P., Parton, R. F., and Jacobs, P. A., *"Macromol. Symp."*, **80**, 157 (1994).

40. Loewenstein, W., *"Am. Minerl."*, **39,** 92 (1954).

41. Ward, J. W., *"Molecular Sieve Catalysis, Applied Industrial Catalysis*", **3,** 271 (1984).

42. Herreros, B., *The X-ray Diffraction Zeolite Database* (on the web).

43. Bhatia, S., *"Zeolite Catalysis: Principles and Applications"*, CRC Press Inc., Boca Raton, Florida, (1990).

44. Olson, D. H., *J. Phys. Chem.*, **74,** 2758 (1970).

45. Price, G. L., and Kanazirev, V., *Zeolites,* **18**, 33 (1997).

46. Thomas, J. M., *"Advanced Catalysts: Interfaces in the Physical and Biological Sciences"* in *Angew. Chem. Adv. Mater.*, **101**, 1105 (1989).

47. Manassen, J., Basolo, F., and Burwell Jr., R. E., (Eds.); *"Catalysis, Progress and Research"*, Plenum, New York, 177 (1973).

48. Bailar Jr., J. C., *Catal. Rev. Sci. Eng.*, **10**, 17 (1974).

49. Candlin, J. P., and Thomas, H., *"Homogenous Catalysis – II"*, Forster, D., and Roth, J. F., (Eds.), American Chemical Society, Washington DC, 212 (1974).

50. Boehm, H. P., in *"Advances in Catalysis and Related Subjects"*, Eley, D. D., Pines, H., Weiss, P. B., and Boehm, H. P., (Eds.), **16**, 179 (1966).

51. Herron, N., Stucky, G. D., and Tolman, C. A., *J. Chem. Soc., Chem. Comm.*, 1521 (1986).

52. Bedioui, F., *Coord. Chem. Rev.*, **144,** 39 (1995).

53. Balkus Jr., K. J., Khanmamedova, A. K., Dixon, K. M., and Bedioui, F., *Appl. Catal. A,* **143,** 159 (1996).

54. Parton, R. F., Vankelecom, I. F. J., Tas, D., Janssen, K. B. M., Knops-Gerrits, P. -P., and Jacobs, P. A., *J. Mol. Cat. A,* **113,** 283 (1996).

55. Basset, J. –M., Lefebvre, F., and Santini, C., *Coord. Chem. Rev.*, **180**, 1703 (1998).

56. Corma, A., Fuerte, A., Iglesias, M., and Sanchez, F., *J. Mol. Cat. A.*, **107**, 225 (1996).

57. Thomas, J. M., *J. Mol. Cat. A*, **115**, 371 (1997).

58. Thomas, J. M., Maschmeyer, T., Johnson, B. F. G., and Shephard, D. S., *J. Mol. Cat. A.,* **141,** 139 (1999).

59. Corbin, D. R., and Herron, N., *J. Mol. Cat.,* **86,** 343 (1994).

60. Bowers, C., and Dutta, P. K., *J. Catal.*, **122,** 271 (1990).

61. Parton, R. F., Huybrechts, D. R., Buskens, Ph., and Jacobs, P. A. in *"Catalysis and Adsorption by Zeolites"*, Ohlmann, G., Pfeifer, R., and Fricke, R., (Eds.), *Stud. Sur. Sci. Catal.*, **65,** 47 (1991).

62. Mitchell, P. C. H., *Chem. Ind.*, 308 (1991).

63. Klier, K., and Ralek, M., *J. Phys. Chem. Solids*, **29,** 951 (1968).

64. Herron, N., *Inorg. Chem.*, **25,** 4714 (1986).

65. Raja, R., and Ratnasamy, P., *J. Catal.*, **170,** 244 (1997).

66. Rao, Y. V. S., De Vos, D. E., Bein, T., and Jacobs, P. A., *Chem. Comm.*, 355 (1997).

67. Jones, R. D., Summerville, D. A., and Basolo, F., *Chem. Rev.*, **79,** 139 (1979).

68. Bedioui, F., DeBoysson, E., Devynck, J., and Balkus Jr., K. J., *J. Chem. Soc., Faraday Trans.*, **87,** 3831 (1991).

69. Kowalak, S., Weiss, R. C., and Balkus Jr., K. J., *J. Chem. Soc., Chem. Comm.*, 57 (1991).

70. Herron, N., Stucky, G. D., and Tolman, C. A., *Inorg. Chem. Acta*, **100,** 135 (1985).

71. Knops-Gerrits, P. -P., De Vos, D. E., Thibault-Starzyk, F., and Jacobs, P. A., *Nature*, **369**, 543 (1994).

72. Knops-Gerrits, P. -P., Thibault-Starzyk, F., and Jacobs, P. A., XIVth International Conference on Raman Spectroscopy in Yu, N. –I., and Li, X. –Y., (Eds.), Hong Kong, John Wiley & Sons, A 165.

73. De Vos, D. E., Meinershagen, J. L., and Bein, T., *Angew. Chem. Intl. Ed. Engl.*, 35, No. **19**, 2211 (1996).

74. Berezin, B. D., *Coordination Compounds of Porphyrins and Phthalocyanins*, Wiley, New York, (1981).

75. Zakharov, V. Y., and Romanovsky, B. V., *Sov. Mosc. Univ. Bull.*, **32,** 16 (1977).

76. Zakharov, V. Y., Zakharova, O. M., Romanovsky, B. V., and Mardalishvili, P. E., *React. Kinet. Catal. Lett.*, **6,** 133 (1977).

77. Rankel, L. A., and Valyocsik, E. W., U. S. Patent, US 4 500 503 (1985).

78. Rankel, L. A., and Valyocsik, E. W., U. S. Patent, US 4 388 285 (1983).

79. Balkus Jr., K. J., and Kowalak, S., U. S. Patent, US 5 167 942 (1992).

80. Balkus Jr., K. J., Kowalak, S., Ly, K. T., and Hargis, D. C., *Stud. Surf. Sci. Catal.,* **69,** 93 (1991).

81. Gabrielov, A. G., Balkus Jr., K. J., Bedioui, F., Bell, S. L., and Devynck, J., *Microporous Materials,* **2,** 119 (1994).

82. Balkus Jr., K. J., and Gabrielov, A. G., *J. Inclusion Phenom. Mol. Recognit. Chem.,* **21,** 159 (1995).

83. Balkus Jr., K. J., *Phthalocyanins,* **4,** 285 (1996).

84. Knops-Gerrits, P. -P., and Jacobs, P. A., *NATO ASI Ser., Ser.3,* **44,** 413 (1998).

85. Schulz-Ekloff, G., and Ernst, S., *Fachbereich 2, Prep. Solid Catal.,* Ertl, G., Knoezinger, H., and Weitkamp, J., (Eds.), Wiley-VCH Verlag Gm bH: Weinheim, Germany, 405 (1999).

86. Sheldon, R. A., *Stud. Surf. Sci. Catal.,* **110,** 151 (1997).

87. Sheldon, R. A., Arends, I. W. C. E., and Lempers, H. E. B., *Catal. Today,* **41,** 387 (1998).

88. Van de Velde, F., Arends, I. W. C. E., and Sheldon, R. A., *J. Inorg. Biochem.,* **80,** 81 (2000).

89. Arends, I. W. C. E., and Sheldon, R. A., *Appl. Catal. A,* **212,** 175 (2001).

90. Fieters, M. C., *Met. Ions Biol. Syst.,* **38,** 461 (2001).

91. Herron, N., and Tolman, C. A., *J. Am. Chem. Soc.,* **109,** 2837 (1987).

92. Collman, J. P., Gagne, R. R., Halbert, T. R., Marchon, J. C., and Reed, C. A., *J. Am. Chem.Soc.,* **95,** 7868 (1973).

93. Parton, R. F., Vankelecom, I. F. J., Casselman, M. J. A., Bezoukhanova, C. P., Uytterhoeven, J. B., and Jacobs, P. A., *Nature,* **370,** 541 (1994).

94. Raja, R., and Ratnasamy, P., *Appl. Catal. A: General,* **158**, L7 (1997).

95. Neys, P. E. F., Vankelecom, I. F. J., Parton, R. F., Dahaen, W., L'abbe, G., and Jacobs, P. A., *J. Mol. Cat A: Chem.,* **126,** L9 – L12 (1997).

96. Jacob, C. R., Varkey, S. P., and Ratnasamy, P., *Appl. Catal. A,* **182,** 91 (1999).

97. Woltinger, J., Backvall, J.–E., and Zsigmond, A., *Chem.–Eur. J.,* **5,** 1460 (1999).

98. Diegruber, H., Plath, P. J., and Schulz-Ekloff, G., *J. Mol. Catal.*, **24**, 115 (1984).

99. Murphy, B. P., *Coord. Chem. Rev.*, **124,** 63 (1993).

100. Beinert, H., *Coord. Chem. Rev.*, **23,** 119 (1977).

101. Weckhuysen, B. M., Verberckmoes, A. A., Fu, L., and Schoonheydt, R. A., *J. Phys. Chem.*, **100,** 9456 (1996).

102. Ogunwumi, S. B., and Bein, T., *Chem. Commun*., 901**,** (1997).

103. Sabater, M. J., Corma, A., Domenech, A., Fornes, V., and Garcia, H., *Chem. Commun.*,1285 (1997).

104. Piaggio, P., McMorn, P., Langham, C., Bethell, D., Bulman-Page, P. C., Hancock, F. E., and Hutchings, G. J., *New J. Chem.*, 1167 (1998).

105. Kimura, T., Fukuoka, A., and Ichikawa, M., *Catal. Lett.*, **4,** 279 (1990).

106. Zakharov, A. N., *Mendeleev Commun*. 80 (1991).

107. Ernst, S., Fuchs, E., and Yang, X., *Microporous and Mesoporous Materials*, **35 – 36,** 137 (2000).

108. Sheu, L. L., Knoezinger, H., and Sachtler, W. M. H., *Catal. Lett.*, **2,** 129 (1989).

109. Ichikawa, M., Rao, L. F., and Fukuoka, A., *Catal. Sci.. Technol.,Proc., Tokyo Conf.*, Yoshida, S., Takezawa, N., and Ono, T.,(Eds.), 111 (1991).

110. Hubelkova, L., Vylita, J., Brabec, L., Drozdova, L., Bolom, T., Novakova, J., Schulz-Ekloff, G., and Jaeger, N. I., *J. Chem. Soc., Faraday Trans.*, **92,** 2035 (1996).

111. Yamamoto, T., Shido, T., Inagaki, S., Fukushima, Y., and Ichikawa, M., *J. Am. Chem. Soc.*, **118,** 5810 (1996).

112. Raja, R., and Ratnasamy, P., *Stud. Surf. Sci. Catal.*, **101,** 181 (1996).

113. Eswaramoorthy, M., Neeraj, and Rao, C. N. R., *Chem. Commun.*, **5,** 615 (1998).

114. Sulikowski, B., Haber, J., Kubacka, A., Pamin, K., Olejniczak, Z., and Ptaszynski, J., *Catal. Lett.*, **39,** 27 (1996).

115. Deshpande, S., Srinivas, D., and Ratnasamy, P., *J. Catal.*, **188,** 261 (1999).

116. Seelan, S., Sinha, A. K., Srinivas, D., and Sivasanker, S., *J. Mol. Cat. A*,

157, 163 (2000).

117. Sheldon, R. A., and Kochi, J. K., *"Metal Catalyzed Oxidations of Organic Compounds"*, Academic Press, New York, (1981).

118. Vanneste, W. H., and Zuberbuhler, A., *"Molecular Mechanism of Oxygen Activation"*, Nayashi, O., (Ed.), Academic Press, New York, 371 (1974).

119. Solomon, E. I., and Lowery, M. D., *Science,* **259,** 1575 (1993).

120. Eickman, N. C., Himmelwright, R. S., and Solomon, E. I., *Proc. Natl. Acad. Sci., USA*, **76,** 2094 (1979).

121. Solomon, E. I., in *"Copper Proteins"*, Spiro, T. G. (Ed.), Wiley Interscience, New York, Vol. III, 41 (1981).

122. Kitajima, N., Fujisawa, K., Moro-oka, Y., and Toriumi, K., *JACS*, **111**, 8975 (1989).

123. Kim, S.–Y, Jung, I. –S., Lee, E., Kim, J., Sakamoto, S., Yamaguchi, K., and Kim, K., *Angew. Chem. Int. Ed.*, **40,** 2119 (2001).

124. Hassanein, M., Selim, A., and El-Hamshary, H., *Macromol. Chem Phys.*, **195,** 3845 (1994).

125. Frostin-Rio, M., Pujol, D., Bied-Charreton, C., Perree-Fauvet, M., and Gaudemer, A., *J. Chem. Soc., Perkin Trans.*, **1,** 1971 (1984).

126. Dubois, G., Corriu, R. J. P., Reye, C., Brandes, S., Denat, F., and Guilard, R., *Chem. Commun*., **22**, 2283 (1999).

127. Zsigmond, A., Horvath, A., and Notheisz, F., *J. Mol. Cat. A,* **171,** 95 (2001).

128. Zsigmond, A., Notheisz, F., and Backvall, J. -E., *Catal. Lett.,* **65,** 135 (2000).

129. Valente, A. A., and Vital, J., *J. Mol. Cat. A,* **156,** 163 (2000).

130. Balkus Jr., K. J., Eissa, M., and Levado, R., *Chem. Ind.,* **69,** 363 (1997).

131. Stanley, H. M., *Chem. Ind.,* 681, (1979).

132. Partenheimer, W., and Gipe, R. K., *Catalytic Selective Oxidation,* Oyama, S. T., and Highower, J. W., (Eds.), *ACS Symp. Ser.,* **523,** 81 (1993).

133. Davis, D. D., and Kemp, D. R., in *"Kirk-Othmer Encyclopaedia of Chemical Technology"*, Kroschwitz, J. I., and Howe-Grant, M., (Eds.),

Wiley, New York, Vol. I, 466 (1991).

134. Partenheimer, W., *Catal. Today*, **23,** 69 (1995).

135. Sheldon, R. A., *"Dioxygen Activation and Homogenous Catalytic Oxidation"*, Simandi, L. I., (Ed.), Elsevier, Amsterdam, Vol. **66,** 573 (1991).

136. Parshall, G. W., and Ittel, S. D., *"Homogenous Catalysis: The Applications and Chemistry of Catalysis by Soluble Transition Metal Complexes"*, John Wiley & Sons Inc., New York, (1992).

137. Danly, D. E., and Campbell, C. R., in *"Kirk-Othmer Encyclopaedia of Chemical Technology"*, Mark H. F., (Ed.), Wiley, New York, Vol. I, 510 (1979).

138. Raja, R., and Ratnasamy, P., *Catal. Lett.*, **48**, 1 (1997).

139. De Vos, D. E., and Jacobs, P. A., *Catal. Today*, **57,** 105 (2000).

140. Dugal, M., Sankar, G., Raja, R., and Thomas, J. M., *Angew. Chem., Int. Ed.*, **39,** 2310 (2000).

Chapter-2

Experimental Methodology

2.1 Introduction

The "neat" and zeolite-Y-encapsulated metal complexes studied in the present work are generalized into two categories: (a) μ-acetato-bridged dinuclear Cu complexes, and (b) (μ_3-oxo)(μ-acetato)-bridged trinuclear Co/Mn complexes. A bridging acetato group is the commonality of these complexes. It is to be noted that such oxo- and carboxylato-bridged metal complexes have been identified as active sites of several metalloenzymes *ca.*, hemocyanin, hemerythrin, methane monooxygenase, Mn catalases, and Mn enzymes involved in photosynthetic water-splitting reaction (1 – 6). Zeolite-Y-encapsulated complexes can be prepared by (a) flexible ligand synthesis method (b) template synthesis or *in situ* synthesis method and (c) zeolite synthesis method (7, 8). But, the "flexible ligand synthesis method" is ideal for the preparation of encapsulated complexes studied in this work. The formation and purity of the "neat" and encapsulated complexes were confirmed by chemical analysis (C, H & N, atomic absorption spectroscopy (AAS), and inductively coupled plasma atomic emission spectroscopy (ICP-AES)), thermogravimetric and differential thermal analyses (TG-DTA), X-ray diffraction (XRD), Fourier transform infrared (FT-IR), UV-visible and electron paramagnetic resonance (EPR) techniques. The structures of the active catalyst species were determined from the detailed EPR and UV-visible spectroscopic studies. The synthesis of the metal complex catalysts and characterization methodologies are described in the following sections.

2.2 Synthesis

This section describes the synthesis of the "neat" and zeolite-Y-encapsulated metal complex catalysts. The preparation of metal ion-exchanged zeolites is also summarized.

2.2.1 Acetato-Bridged Dimeric Cu Complexes

2.2.1.1 Preparation of $Cu(CH_3COO)_2.H_2O$ and $Cu(CH_2ClCOO)_2.2.5H_2O$

"Neat" $Cu(CH_3COO)_2.H_2O$ obtained from LOBA Chem., India was used as received. Copper chloroacetate ($Cu(CH_2ClCOO)_2.2.5H_2O$) was prepared as follows. An aqueous solution (10 ml) of monochloroacetic acid ($CH_2ClCOOH$; 1.89 g; LOBA Chem., India) was neutralized with NaOH (extrapure LOBA Chem., India; 0.82 g) dissolved in 5 ml distilled water. To this, 1.71 g of $CuCl_2.2H_2O$ (LOBA Chem., India) in 10 ml water was added drop-wise. The resultant mixture was refluxed for 2 h. Good quality single crystals (greenish-blue in color) were obtained in 4 - 5 days on slow evaporation of the reaction solution at 298 K. The purities of the "neat" acetate complexes were confirmed by elemental analysis. Anal. Calcd. for $Cu(CH_3COO)_2.H_2O$: C, 24.06%, H, 4.01%. Found: C, 23.91%, H, 4.09%. Anal. Calcd. for $Cu(CH_2ClCOO)_2.2.5H_2O$: C, 17.88%, H, 2.23%. Found: C, 17.53%, H, 2.24%.

2.2.1.2 Preparation of Cu(II)-Exchanged Zeolite-HY

Zeolite-HY (Si/Al = 2.4) was obtained by calcining zeolite-NH_4Y at 753 K for 24 h in a static air-oven. The Cu(II)-exchanged zeolite-HY (Cu-Y), was prepared by the ion exchange of zeolite-HY with Cu(II) ions. In a typical ion

exchange method, 3.5 g of zeolite-HY was added to 1.8 g of copper acetate monohydrate dissolved in 20 ml distilled water. The mixture was stirred gently at 323 K for a period of 3 - 4 h. Later, the sky-blue biphasic system was allowed to stand undisturbed overnight, after which it was filtered off. The solid product, Cu(II)-exchanged zeolite-HY (Cu-Y), was washed copiously with warm, distilled water until the extract contained no copper ions. The solid was dried at 373 K in a static air-oven for 8 h. The above exchange procedure was repeated two more times. The sky-blue Cu-Y was stored in a dry desiccator containing $CaCl_2$ (S. D. Fine Chem., India). The amount of Cu loading was estimated (by AAS) to be 0.11 wt %.

2.2.1.3 Preparation of $Cu(CH_3COO)_2$-Encapsulated in Zeolite-Y

The zeolite-Y-encapsulated copper acetate was prepared as follows. 3.5 g of Cu-Y was evacuated at 383 K for 2 h. It was then exposed to vapours of acetic acid in a BET adsorption apparatus at 333 K for 90 min, until the color of the copper exchanged zeolite changed from sky-blue to bluish green. The material (designated as CuAc-Y) was then stored in a dry desiccator containing $CaCl_2$.

2.2.1.4 Preparation of $Cu(CH_2ClCOO)_2$-Encapsulated in Zeolite-Y

The zeolite-Y-encapsulated copper chloroacetate (designated as CuClAc-Y) was prepared in a similar manner as that of CuAc-Y, except that the copper exchanged zeolite-HY was exposed to the vapors of monochloroacetic acid.

2.2.2 (μ_3-Oxo)(μ-Acetato)-Bridged Trinuclear Co/Mn Complexes

2.2.2.1 Preparation of "Neat" $[Co_3(O)(CH_3COO)_6(py)_3]ClO_4$

The cobalt cluster complex $[Co_3(O)(CH_3COO)_6(py)_3]ClO_4$, where py = pyridine, was prepared by a method analogous to that of Sumner and Steinmetz (9).

In a typical synthesis, 1.25 g of $Co(CH_3COO)_2.4H_2O$ (S. D. Fine Chem., India) was taken in a solution of glacial acetic acid (12.5 ml; S. D. Fine Chem., India) and py (0.4 ml; S. D. Fine Chem., India), which was then warmed to 323 K with constant stirring until all the solid dissolved. Later, the purple colored solution was cooled to 298 K and a freshly prepared peracetic acid solution was added drop-wise over a period of 30 min while stirring. During the addition of peracetic acid, the color of the solution changed to dark brown. Then to this, was added 3 ml of distilled water and the resultant solution was refluxed for 1 h at 353 K. The reaction mixture was cooled to 298 K and to it was added 0.4 g of $NaClO_4$ (Aldrich Co., USA) dissolved in 20 ml distilled water. Good quality micro-crystals of $[Co_3(O)(CH_3COO)_6(py)_3]ClO_4$ (hereafter designated as $Co_3(O)$) were obtained on keeping the solution at 278 K for one week. Peracetic acid used in the synthesis was prepared by the addition of 0.7 ml of aqueous H_2O_2 (30%) to 0.4 ml of glacial acetic acid. Elemental analysis of $Co_3(O)$: Calcd.: C, 35.66%, H, 3.69%, N, 4.99%. Found: C, 35.07%, H, 3.74%, N, 4.85%.

2.2.2.2 Preparation of "Neat" $[Mn_3(O)(CH_3COO)_6(py)_3](ClO_4)$

The manganese cluster complex $[Mn_3(O)(CH_3COO)_6(py)_3]ClO_4$ was prepared according to the procedure of Vincent et al (10). In a typical synthesis, 2.7 g of $Mn(CH_3COO)_2.4H_2O$ (S. D. Fine Chem., India) was dissolved in a solution comprising of 25 ml of ethanol (MERCK, India), 12 ml of glacial acetic acid and 3 ml of pyridine while stirring at 298 K. To this was added a freshly prepared ethanolic solution (10 ml; MERCK, India) of $N\text{-}n\text{-}Bu_4MnO_4$ (1.14 g), drop-wise, over a period of 45 min. The resultant brown solution was stirred for 30 min, after which

0.695 g of $NaClO_4$ was added to it. The mixture was stirred for another 15 - 20 min. The brown crystalline product $[Mn_3(O)(CH_3COO)_6(py)_3]ClO_4$ (hereafter designated as $Mn_3(O)$) was obtained overnight on slow evaporation at 298 K. The product was filtered out, washed with ethanol and dried in vacuum. Elemental analysis: Calcd.; C, 37.12%, H, 3.99%, N, 4.56%. Found; C, 37.04%, H, 4.28%, N, 4.48%.

N-n-Butyl manganese oxide (N-n-Bu_4MnO_4) used in the above synthesis was prepared as follows: 12 g of N-n-Bu_4Br (Aldrich Co., USA) was dissolved in 100 ml distilled water and the colorless solution was filtered. To it was added an aqueous solution (100 ml) of $KMnO_4$ (5 g; LOBA Chem., India) slowly with constant stirring. Purple colored, microcrystalline precipitate of N-n-Bu_4MnO_4, which was obtained almost immediately, was filtered under vacuum, washed copiously with distilled water and diethyl ether and dried in a desiccator containing $CaCl_2$.

2.2.2.3 Preparation of "Neat" $CoMn_2(O)(CH_3COO)_6(py)_3$

In the preparation of "neat" $CoMn_2(O)(CH_3COO)_6(py)_3$ (hereafter designated as $CoMn_2(O)$), 2.7 g of freshly prepared manganic acetate (11) was taken in a solution comprising of 25 ml of ethanol and 4.2 ml of glacial acetic acid and stirred for 10 - 15 min till all the manganic acetate dissolved. To this brown solution, 2.5 g of $Co(CH_3COO)_2.4H_2O$ dissolved in pyridine (4 g) was added with continuous stirring. The solution was then allowed to stand at 298 K from which shiny, black microcrystals of $CoMn_2(O)$, were obtained. Elemental analysis: Calcd.; C, 43.39%, H, 4.41%, N,1.87%. Found; C,43.53%, H, 4.77%, N,1.87.

Manganic acetate used in the above synthesis was prepared by the method of Christensen (11) as follows: $Mn(CH_3COO)_2.4H_2O$ (19.6 g) was added to 200 ml of glacial acetic acid at the boiling temperature of the latter and stirred until completely dissolved. To it, 3.1 g of $KMnO_4$ was added in small amounts and the mixture was further heated for a short time with constant stirring. The dark brown solution thus obtained, was filtered and to it was added 3 ml of distilled water. The resultant mixture was allowed to stand overnight. The brown microcrystalline product was filtered out under vacuum, washed copiously with glacial acetic acid and dried in a desiccator containing $CaCl_2$.

2.2.2.4 Preparation of Co(II)-Exchanged Zeolite-HY

In the preparation of Co(II)-exchanged zeolite-HY (hereafter designated as Co-Y), 7 g of zeolite-HY was added to 4.3 g of $Co(CH_3COO)_2.4H_2O$ dissolved in 100 ml distilled water. The slurry was stirred for 4 - 5 h at 333 K and then allowed to stand overnight at 298 K. The solid, pink Co-Y was filtered, washed with warm, deionized water (500 ml) and dried at 393 K. The Co content in Co-Y was estimated to be 10.21 wt.% (ICP-AES).

2.2.2.5 Preparation of Mn(II)-Exchanged Zeolite-HY

Mn(II)-exchanged zeolite-HY (hereafter designated as Mn-Y) was prepared in a similar manner as that of Co-Y, except that $Mn(CH_3COO)_2.4H_2O$ (4.3 g) was used in place of $Co(CH_3COO)_2.4H_2O$. The Mn content was estimated to be 3.08 wt% (ICP-AES).

2.2.2.6 Preparation of Co/Mn(II)-Exchanged Zeolite-HY

In the preparation of Co/Mn(II)-exchanged zeolite-HY (hereafter designated as CoMn-Y), 1.43 g of $Co(CH_3COO)_2.4H_2O$ and 4.3 g of $Mn(CH_3COO)_2.4H_2O$ were used for ion exchanging 7 g of zeolite-HY. Zeolite-HY was initially exchanged with Mn ions, as described above. The Mn-Y thus formed was then used for further exchange with Co ions to form finally the CoMn-Y. The Co and Mn contents in CoMn-Y were estimated to be 1.02 and 2.01 wt%, respectively (ICP-AES).

2.2.2.7 Preparation of $Co_3(O)(CH_3COO)_6(py)_3$-Encapsulated in Zeolite-Y

The Co-Y (1.5 g) was suspended in 15 ml of glacial acetic acid taken in a double-necked, round-bottom flask fitted with an air condenser and an inlet for air. The suspension was stirred gently for 30 min while passing air. To this was added 3 ml of pyridine, drop-wise with stirring for 15 min. Then 0.5 g of NaBr (S.D. Fine Chem., India), and 5 ml of distilled water were added and the solution was stirred for another 30 min. To this, 10 ml of aqueous H_2O_2 (50%; LOBA, Chem., India) was added drop-wise and the slurry was stirred for another 2 – 3 h, at 298 K, while passing air. The pink solid, $Co_3(O)(CH_3COO)_6(py)_3$-Y (hereafter designated as $Co_3(O)$-Y), was filtered, washed with glacial acetic acid until all the metal complexes adsorbed on the external surface were removed, and then dried at 298 K, under vacuum. The Co content in $Co_3(O)$-Y was estimated to be 0.70 wt% (ICP-AES).

2.2.2.8 Preparation of $Mn_3(O)(CH_3COO)_6(py)_3$-Encapsulated in Zeolite-Y

$Mn_3(O)(CH_3COO)_6(py)_3$ encapsulated in zeolite-HY (hereafter designated as $Mn_3(O)$-Y; pale brown) was prepared in a similar manner to that of $Co_3(O)$-Y described above, except that 1.5 g of Mn-Y was used instead of Co-Y. The Mn content in $Mn_3(O)$-Y was estimated to be 1.38 wt% (ICP-AES).

2.2.2.9 Preparation of $CoMn_2(O)(CH_3COO)_6(py)_3$-Encapsulated in Zeolite-Y

$CoMn_2(O)(CH_3COO)_6(py)_3$ encapsulated in zeolite-HY (hereafter designated as $CoMn_2(O)$-Y) was prepared in a similar manner described for $Co_3(O)$-Y, except that, CoMn-Y was used in the place of Co-Y. The Co and Mn contents in the purple solid $CoMn_2(O)$-Y were estimated to be 0.38 wt % and 1.31 wt %, respectively (ICP-AES).

It may be mentioned that all the Co/Mn complexes and clusters are highly soluble in acetic acid.

2.3 Characterization Procedures

This section describes the various physicochemical procedures employed for the characterization of the metal-exchanged zeolites and the "neat" and encapsulated metal complexes.

2.3.1 Chemical Composition (C, H & N; AAS; ICP-AES)

The C, H & N analyses of the samples were done on a Carlo Erba EA 1108 elemental analyzer. In a typical analysis, 5 mg of the sample was used to estimate the percentage carbon, hydrogen and nitrogen contents. The results have enabled estimation of the molecular formula of the metal complex.

The metal ion contents (Cu, Co and Mn) in the ion exchanged zeolites and encapsulated metal complexes were determined using a Hitachi (Z 8000) or a Varian Spectr SF-220 atomic absorption spectrometer. The sample solutions required for AAS measurements were prepared by dissolving 100 mg of the solid zeolite in 10 ml conc. H_2SO_4. The homogenous solutions were then transferred to a 100 ml volumetric flask and made up to the mark with deionized water. The sample

solutions, thus prepared, were injected into the sample port of the spectrometer. The metal ion content (in ppm) was estimated from the optical absorption values and calibration plot (made using standard solutions of different concentrations).

The metal ion content in zeolite samples was determined simultaneously by inductively coupled plasma-atomic emission spectroscopy. In a typical sample preparation for ICP-AES analysis, 50 mg of solid zeolite material was dissolved in a 1:1 mixture of conc. HNO_3 (3 ml) and 40% HF (3 ml) taken in a polypropylene beaker. The resultant homogenous solution was transferred to a 100 ml polypropylene volumetric flask and made up to the mark using deionized water. The ICP-AES analysis was done on a Perkin Elmer PE-1000 system in Ar atmosphere.

2.3.2 Powder X-ray Diffraction (XRD)

The phase purity and crystallinity of the "neat" and zeolite-Y-encapsulated complexes were determined using a computer-controlled automatic Rigaku RINT 2000 and a Rigaku Miniflex X-ray diffractometers. The Ni-filtered Cu-Kα radiation (λ = 1.5404 Å) was used with a curved graphite crystal monochromator and a NaI scintillator. XRD data at 298 K were collected in the 2θ range 5 - 50° at a scan rate of 4 deg/min or lower. After the background correction, the peak positions were marked and the d-values and relative intensities (I/I_o) of the peaks were estimated. Finely powdered and sieved (170 mesh) solid catalysts were used for the XRD analysis. The samples were prepared as thin layers on metal or glass slides. The relative peak intensities of (331), (311) and (220) reflections of zeolite-Y samples indicated the cation distribution in the lattice (12).

2.3.3 Thermal Analysis (TG-DTA-DTG)

The thermal stabilities of "neat" and encapsulated metal complexes were examined using thermogravimetric and differential thermal analyses (TG-DTA). Thermogravimetry (TG) involves recording the weight of a substance in the presence of controlled heating or cooling as a function of time or temperature. The TG curve is characterized by two prominent features viz., the flat portions, which indicate temperature ranges, wherein the thermal stability of the compound is assured and the curved portions, which indicate weight loss. From the weight loss observed, it is possible to determine the chemical composition of the compound. In differential thermal analysis (DTA) the temperature difference of the material of interest and a reference material under identical controlled conditions of heating or cooling with respect to either time or temperature are recorded. A DTA curve constitutes exothermic peaks, arising due to chemical reactions, especially of an oxidative nature and endotherms relating to physical changes. In derivative thermogravimetry (DTG), the derivative of mass change with respect to time (dm/dt) is continuously recorded as a function of time or temperature. Simultaneous TG-DTA-DTG analyses of the "neat" and zeolite-Y-encapsulated complexes were recorded on an automatic Setaram TG-DTA 92 derivatograph. Preheated and finely powdered α-alumina was used as the reference material. The thermograms of the samples were recorded with the following experimental conditions: weight of the sample = 30 mg ; heating rate = 10 $K.min^{-1}$; atmosphere = air; sensitivity: TG = 25 mg; DTG = 0.2 mV; DTA = 0.1 mV.

2.3.4 Fourier Transform Infrared Spectroscopy (FT-IR)

This is a most important "fingerprint" technique for the determination of molecular structure of metal complexes (both "neat" and encapsulated forms), by analyzing the characteristic vibrational bands corresponding to different functional groups and bonds present in the system. The FT-IR spectra were recorded on a Shimadzu FT-COM 1 spectrophotometer in the range of 4000-400 cm^{-1}. The samples were made as Nujol mulls or KBr pellets (1% w/w). The spectra were recorded in transmittance (%T) mode. In a typical IR sample preparation procedure, 10 - 25 mg of the sample was mulled in Nujol. The mull was evenly spread over an oval quartz plate and then subjected to FT-IR analyses. Characteristic vibrational bands of Nujol were observed at 2925, 2854, and 1377 cm^{-1}.

2.3.5 UV-Visible Spectroscopy

The UV-visible spectra of the "neat" and encapsulated complexes were recorded using the Shimadzu UV-2101 and UV-2550 spectrophotometers in the range 200 - 800 nm. The spectra for the liquid samples were recorded in the normal mode and for the solid samples in the diffuse reflectance (DRUV-visible) mode. The UV-visible bands provide information about the changes in the electronic structure of metal complexes after they are encapsulated in zeolites.

2.3.6 Electron Paramagnetic Resonance Spectroscopy (EPR)

The EPR spin Hamiltonian parameters provide information about the molecular and electronic structure of the metal complexes. EPR spectroscopy in ideal cases can differentiate the encapsulated metal complexes from the surface adsorbed species. It provides information about the electron spin density distribution and any structural changes, which may have taken place after the complex is encapsulated

inside the zeolite pores. The EPR spectra of the "neat" and zeolite-Y-encapsulated complexes were recorded using a Bruker EMX X-band spectrometer with 100 kHz field modulation. Frequency calibration was done using a microwave frequency counter fitted in an ER 041 XG-D microwave bridge. The variable temperature EPR experiments in the temperature range 80 - 380 K were performed using a Bruker BVT 3000 temperature controller. The spectra at liquid nitrogen temperature (77 K) were recorded using a quartz insert Dewar. The spectral simulations and manipulations were done using the Bruker Simfonia and WINEPR software packages. The measurements for liquid samples were done in a quartz aqueous cell.

2.3.7 Molecular Modeling

The molecular modeling studies enabled (1) the understanding of encapsulation of a complex in zeolitic cages, (2) the structure of the encapsulated complex and (3) the interaction between the encapsulated complex and the zeolite. This information was derived from the strain energy calculations. Modeling studies were done using a Silicon Graphics, Octane workstation and the INSIGHT II software supplied by Molecular Simulation Inc. (MSI), USA.

2.3.8 Cyclic Voltammetry (CV)

The redox behavior of complexes was investigated using a three-electrode BAS CV-50 electrochemical system. Platinum as a working electrode, Pt-wire as an auxiliary electrode and saturated calomel as a reference electrode were used. Tetraethyl ammonium perchlorate (TEAP; 0.1 M) was used as a supporting electrolyte. Cyclic voltammetric studies provide knowledge about the redox behavior

of the metal centers and any changes in the redox properties of the metal ion after they are supported or encapsulated in porous inorganic solids.

2.4 Catalytic Activity Studies

This section describes the oxidation reactions investigated over the "neat" and zeolite-Y-encapsulated metal complex catalysts, the reaction conditions and the methods of product analysis.

2.4.1 Hydroxylation of Phenol

The liquid phase hydroxylation of phenol was carried out over the "neat" and zeolite-Y-encapsulated copper acetate and chloroacetate complexes with molecular oxygen as oxidant. In a typical reaction, crystalline phenol (1.88 g; S. D. Fine Chem., India) and the catalyst (0.073 g in the case of "neat complexes and an equivalent amount of encapsulated complexes) in 20 ml phosphate buffer (pH = 6.5; S. D. Fine Chem., India) were taken in a 100 ml double-necked glass reactor equipped with a water cooled condenser and a rubber septum (Fig. 2.1). Stirring was effected by a magnetic needle of 2 cm length. The reactions were conducted at pH = 6.5 (the dimeric structure of copper acetate and copper chloroacetate complexes is stable at this pH condition). The hydroxylation reactions were carried out at 298 K while

passing oxygen (1 atm) continuously through the reaction mixture. The reaction was conducted for 19 - 24 h. At the end of the reaction, the solid catalyst was separated by centrifuging. The liquid portion was subjected to product analysis. No indication of copper leaching into the reaction mixture was observed (AAS).

The supernant liquid (2 ml) was extracted with 5 ml of diethyl ether. The organic phase containing the products and unreacted phenol and the aqueous phase were separated. The organic layer (0.2 μL) was injected into a Shimadzu GC 14-B gas chromatograph equipped with a SE-52 packed column (length 2 m and diameter 0.125 inches) and a flame ionization detector (FID). In the program used for GC analysis, the column temperature was initially maintained at 368 K for 2 min and then raised at a rate of 10 deg/min to 498 K. Prior to the sample analysis, the response factors of the substrate and products were estimated.

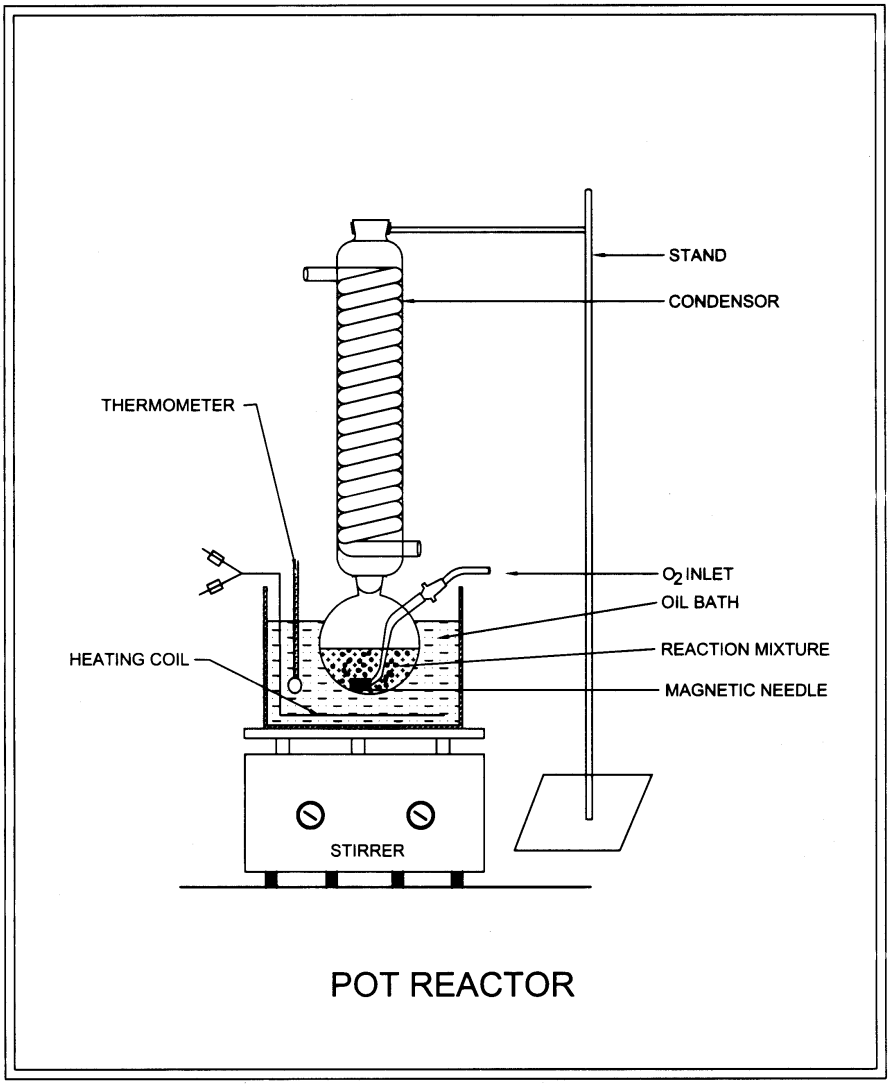

Fig. 2.1 Reaction set-up for phenol hydroxylation

2.4.2 Oxidation of *Para*-Xylene (Continuous Flow System)

The liquid phase oxidation of *para*-xylene (PX) was done using air (1 atm) as oxidant in the presence of "neat" cobalt and manganese acetates. The role of the metals (Co, Mn and Ni), promoter (Br^-) and additives like Ce and Zr in the oxidation of PX was investigated. Nickel acetate, cerium nitrate and zirconium hydroxide

(freshly prepared by interacting $ZrOCl_2$ with NH_4OH) were used as sources of Ni, Ce and Zr, respectively. PX was obtained from Aldrich Co.

The catalytic runs were performed in a specially designed U-shaped, tubular, continuous flow glass reactor (Fig. 2.2; height 18 inches and volume 100 ml) fitted with a sintered disc at the bottom of the reactor for efficient dispersion of air. The reactor was placed in an appropriate bath and the temperature was maintained at around 363 K. The glass reactor was fitted with a condenser through which chilled water (280 K) was continuously circulated.

In a typical flow reaction, known amounts of PX (5 ml), distilled water (5.6 ml), glacial acetic acid (purity 97%, 38 ml), metal acetate catalysts (0.35 - 1.03 mmol) and NaBr (1.35 - 10.2 mmol) were taken in the glass reactor. The temperature of the reactor was maintained at around 363 K. Air was passed through the reaction mixture (50 ml/min) using a compressor. The reactions were conducted for 4.5 to 16 h. Then the reaction mixture was rapidly cooled to 298 K and the products were analyzed. The weights of the reaction mixture before and after the reaction were noted for the mass balance studies.

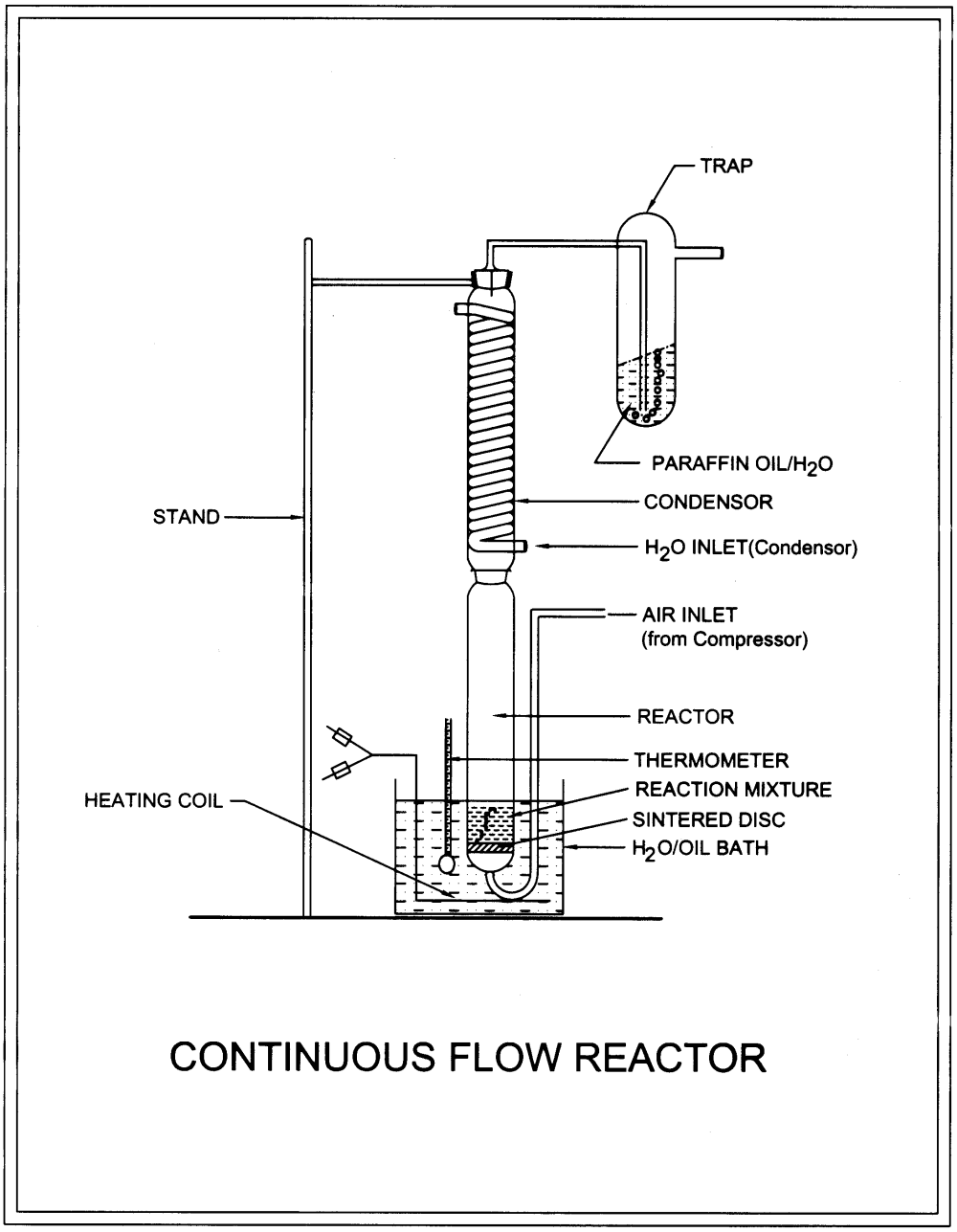

Fig. 2.2 Reaction set-up for *para*-xylene oxidation

From the final reaction mixture 0.2 μL of the liquid portion was subjected for GC analysis (Shimadzu GC-14B; 6 ft 10 % SE-30 S.S. packed column, 1/8 in. O. D.; FID). The starting column temperature was maintained at 373 K for 3 min and

then raised at a rate of 10 deg/min to 523 K. The total reaction mixture was distilled under vacuum to remove acetic acid, unreacted PX, water, *p*-tolyl alcohol and *p*-tolualdehyde. The solid containing *p*-toluic acid, 4-carboxybenzaldehyde and terephthalic acid was thoroughly washed with distilled water to remove the water-soluble catalysts. This solid product was dried in an oven at 363 K and the weight was recorded. The solid product was then esterified in the following manner: 100 mg of the solid product was taken in 5 ml of methanol. To this 2 ml of BF_3 in methanol (14%; Merck, India) was added and the mixture was refluxed at 373 K for 6 - 8 h till a homogenous clear solution was obtained. The esterified products were extracted in diethyl ether, which were later dried off at 313 K over a water bath. The dried extract was then dissolved in 1,2-dichloromethane and analyzed by GC. The products were identified by GCMS (Shimadzu QP 5000).

2.4.3 Oxidation of *Para*-Xylene (Under Pressurised Conditions)

The oxidation of PX was performed in a 300 ml titanium lined Parr 4833 pressure reactor over "neat" and zeolite-Y-encapsulated (μ_3-oxo)(μ-acetato)-bridged Co/Mn cluster complexes and a physical mixture of cobalt and manganese acetates (3 : 1 mmol). The reactions were conducted at 473 K with air as the source of oxygen.

In a typical batch reaction, 2 ml of PX, 5.6 ml of distilled water, 38 ml of glacial acetic acid (97%), 0.0865 g of NaBr, and 0.0342 g of "neat" or 0.2995 g of encapsulated (μ_3-oxo)(μ-acetato)-bridged cluster catalysts, were taken in the Parr autoclave. The reactor was pressurized with air to 200 - 550 psig at 298 K. Then

the temperature was raised to 473 K, in steps of 50° in about 20 min. At 473 K, the pressure in the reactor went up to about 400 - 900 psig depending on the initial pressure at cold conditions. The reactions were conducted for 15 min to 4 h. Subsequently the temperature was quenched to 298 K with ice. A pressure drop of 40 - 60 psig (depending on the initial pressure) was noted. The remainder gas in the reactor was released and the reaction mixture was carefully transferred to a clean, dry beaker and the weight of the final reaction mixture was noted.

The reaction mixture was then transferred to a 100 ml round bottom flask; 0.2 μL of the liquid portion was subjected to GC for the analysis of *p*-tolyl alcohol, *p*-tolualdehyde, *p*-toluic acid and unreacted PX. The total reaction mixture was then distilled under vacuum, at 418 K, to remove all the glacial acetic acid, unreacted PX, water and *p*-tolyl alcohol and *p*-tolualdehyde, if any. The solid product containing *p*-toluic acid, 4-carboxybenzaldehyde, benzoic acid and terephthalic acid was thoroughly washed with distilled water and dried in an air-oven at 363 K. The weight of the solid product was recorded. The products were converted into water-soluble sodium salts and analyzed by HPLC.

The water-soluble sodium salts were prepared as follows: To 100 mg of the solid product taken in a 50 ml beaker, were added 15 ml of distilled water and 6 ml of 2 N NaOH with constant stirring, till a clear homogenous solution (pH = 10) was obtained. Then, the pH of the solution was adjusted to about 7 using glacial acetic acid. The solution was then transferred to a 100 ml volumetric flask and diluted up to the mark with distilled water. The solution was then analyzed by HPLC (Shimadzu

LC 9A; mobile phase comprised of 57% deionized water, 40% methanol and 3% sodium acetate buffer (pH = 3.9)). All reagents used for the analysis were of HPLC grade (MERCK, India); 20 μL of sample solution was injected each time. The HPLC C18 column was flushed thoroughly with acetonitrile (HPLC grade) and deionized water before and after the sample injections. All solvents and the mobile phase were filtered over a 0.5 micron filter paper prior to use. Using the standards (*p*-toluic acid, 4-carboxybenzaldehyde, benzoic acid and terephthalic acid (Aldrich Co.)) calibrations were made and response factors were determined before the actual sample analysis.

2.4.4 Oxidation of Cyclohexane, Cyclohexanone and Cyclohexanol

2.4.4.l Oxidation of Cyclohexanone

The oxidation of cyclohexanone was performed in a 300 ml titanium lined Parr 4833 pressure reactor over the "neat" and encapsulated (μ_3-oxo)(μ-acetato)-bridged Co and/or Mn cluster complexes in acetic acid and water medium. Air was used as the source of oxygen and methylethyl ketone (MEK) as oxidation initiator. The oxidations were performed at 373 K and air pressures of 550 - 700 psig.

In a typical batch reaction, 4.21 ml of cyclohexanone was taken in 38 ml of glacial acetic acid (97%) and 1.9 ml of distilled water contained in the Parr reactor. To it, MEK (0.114 ml; 0.0917 g) and catalyst ("neat" complexes: 7.5 - 354 mg and encapsulated complexes: 74.9 - 299.5 mg) were added. In reactions over the "neat" complex catalysts, the reaction mixture was pressurized with air (550 psig) at the reaction temperature. In reactions over encapsulated cluster complexes, the reaction

mixture was pressurized at room temperature and then heated to the desired temperature (353 - 393 K). The reactions were conducted for 45 min to 8 h. A pressure drop of 10 - 100 psig depending upon the catalyst system and reaction conditions was noticed. After cooling, the reaction mixture was carefully transferred to a clean, dry beaker. In case of solid, encapsulated complexes, the catalyst was separated by filtration; 0.2 μL of the liquid sample was subjected to GC analysis (Shimadzu GC-14B; 6 ft 10 % SE-30 S.S. packed column, 1/8 in. O. D.; FID) to estimate the unreacted cyclohexanone. Later, a portion of the liquid sample was esterified as described below to identify the acid products formed: 2 ml of the reaction mixture was taken in 5 ml of methanol. To this, 2 ml of BF_3 in methanol (14%; Merck, India) was added and the mixture was refluxed at 373 K for 6 - 8 h till a homogenous clear solution was obtained. The esterified acids were extracted in diethyl ether, which was later dried off at 313 K over a water bath. The dried extract was then dissolved in 1,2-dichloromethane and analyzed by GC. The products were identified by GC-MS (Shimadzu QP 5000).

The yields of acid products were independently estimated as follows: The liquid sample was distilled out under vacuum and most of the glacial acetic acid, unreacted cyclohexanone, and water were removed. The concentrated reaction mixture was then cooled to 273 K and the solid product containing adipic acid and other impurities like succinic acid, valeric acid and glutaric acid were recovered by filtration. The solid products were then washed thoroughly with ice-cold distilled water, dried in an air-oven at 333 K and the weight of the solid products (yield) was

noted. The weight of the reaction mixture was recorded at different stages of manipulations for the mass balance studies.

2.4.4.2 Oxidation of Cyclohexane

The oxidation of cyclohexane was performed in a similar manner as that described for cyclohexanone, except that 4.4 ml of cyclohexane was taken in place of cyclohexanone.

2.4.4.3 Oxidation of a Mixture of Cyclohexanone-Cyclohexanol

The oxidation of a mixture of cyclohexanone and cyclohexanol (90:10, 80:20, 50:50 volume%) was performed in a similar manner as that of cyclohexanone.

2.5 References

1. Liu, K. E., and Lippard, S. J., "*Studies of the Soluble Methane Monooxygenase Protein System: Structure, Component Interactions and Hydroxylation Mechanism*," in *Adv. Inorg. Chem.*, Sykes, A. G., (Ed.), Academic Press, New York, Vol. **42**, 263 (1995).

2. Andersson, K. K., and Gräslund, A., "*Diiron-Oxygen Proteins*" in *Adv. Inorg. Chem.*, Sykes, A. G., (Ed.), Academic Press, New York, Vol. **43**, 359 (1995).

3. Law, N. A., Caudle, M. T., and Pecoraro, V. L., "*Manganese Redox Enzymes and Model Systems: Properties, Structures and Reactivity*" in *Adv. Inorg. Chem.*, Sykes, A. G., (Ed.), Academic Press, New York Vol. **46**, 305 (1999).

4. Brudvig, G. W., and Crabtree, R. H., "*Bioinorganic Chemistry of Manganese Related to Photosynthetic Oxygen Evolution*," in *Prog. Inorg. Chem.*, Lippard, S. J., (Ed.), John Wiley & Sons, New York, Vol. **37**, 99 (1989).

5. Vincent, J. B., and Christou, G., "*Higher Oxidation State Manganese Biomolecules*," in *Adv. Inorg. Chem.*, Sykes, A. G., (Ed.), Academic Press, New York, Vol. **33**, 197 (1989).

6. Karlin, K. D., and Gultneh, Y., *"Binding and Activation of Molecular Oxygen by Copper Complexes*," in *Prog. Inorg. Chem*., Lippard, S. J., (Ed.), John-Wiley & Sons, New York, Vol. **35**, 219.

7. Balkus Jr., K. J., and Gabrielov, A. G., *J. Incl. Phenom. Mol. Recog. Chem*., **21**, 159 (1995).

8. Balkus Jr., K. J., Gabrielov, A. G., Bell, S. L., Bedioui, F., Roue, L., and Devynck, J., *Inorg. Chem.*, **33**, 67 (1994).

9. Sumner Jr., C. E., and Steinmetz, G. R., *J. Am. Chem. Soc*. **107**, 6124 (1985).

10. Vincent, J. B., Chang, H.-R., Folting, K., Huffman, J. C., Christou, G., and Hendrickson, D. N., *J. Am. Chem. Soc*.**109**, 5704 (1987).

11. Christensen, O. T., *Z. Anorg. Chem.* **27,** 325 (1901).

12. Quayle, W. H., and Lunsford, J. H., *Inorg. Chem.* **21**, 97 (1982).

Chapter-3

Structure and Tyrosinase Activity of Zeolite-Y-Encapsulated Dimeric Copper Acetato and Chloroacetato Complexes

3.1 Introduction

Copper complexes with varying nuclearity are constituents of the active sites of a number of important proteins and enzymes (1 – 6). These copper-protein complexes catalyze many biological functions including oxygen transport and activation, electron transfer, iron metabolism and superoxide metabolism (6). Due to the unusual geometric and electronic structures induced at the active site by the protein ligand, the copper enzymes exhibit spectral features that differ from those of "neat" copper complexes with smaller ligands (1, 7).

Tyrosinase (EC 1.14.18.1), a dinuclear Cu-containing monooxygenase enzyme, is responsible for the formation of melanin in mammals and the browning of fruits and vegetables (7). It catalyses the selective oxidation of L-tyrosine to L-DOPA and the *ortho*-hydroxylation of phenols to *ortho*-diphenols (monophenolase activity) and *ortho*-quinones (diphenolase activity). In an attempt to understand the mechanism of dioxygen activation, several structural and functional models of the enzyme tyrosinase have been developed (8 – 12). Catalysis researchers have, in the past decade, encapsulated various transition metal complexes in the cavities of zeolites and studied the physicochemical and catalytic properties of such "zeozymes" (13 – 17). However, in a majority of the reports on phenol hydroxylation over "neat" and zeolite-encapsulated complexes, catechol, hydroquinone and *para*-benzoquinone were obtained as the major products. Raja and Ratnasamy (18) reported, for the first time, that copper acetate encapsulated in molecular sieves Y, MCM-22, and VPI-5, uses atmospheric dioxygen, to regioselectively *ortho*-hydroxylate L-tyrosine to L-DOPA, phenol to catechol and *ortho*-benzoquinone

and cresols to the corresponding *ortho*-dihydroxy and *ortho*-quinone compounds. The zeolite-encapsulated copper acetate exhibited higher catalytic activity than the "neat" complex in the homogeneous medium (18). Later, Eswaramoorthy et al reported that copper acetate encapsulated in cubic Al-MCM-48 also exhibits enhanced catalytic activity in the oxidation of phenol to catechol by dioxygen (19). This zeozyme, hence, mimics functionally the copper monooxygenase enzyme, tyrosinase (7). *Why do the intrinsic catalytic activities (turnover frequencies) of such complexes increase upon encapsulation in zeolites?* The present work probes the origin of enhancement in the oxidation activity of copper acetates upon encapsulation in zeolite-Y using FT-IR, UV-visible and especially, EPR spectroscopies.

Copper acetate monohydrate was one of the smallest clusters studied by EPR, as early as 1952, by Bleaney and Bowers (20) and subsequently by Abe and Shimada (21). The single crystal X-ray structure of copper acetate monohydrate (22, 23) revealed the presence of isolated dimeric units in the solid state with an unusually short Cu-Cu separation of 2.61 Å (which is only slightly longer than the separation in copper metal, i.e., 2.54 Å). The X-band EPR spectra correspond to that of a thermally populated excited triplet (S = 1) state (20). Copper acetate exhibits an unusual magnetic behavior due to the antiferromagnetic interaction between the Cu atoms in the dimer. The exchange coupling constant (-J) was determined from EPR measurements and was found to be 259 cm^{-1} (20), which was in close agreement with that found from magnetic susceptibility studies (286 cm^{-1}) (24, 25). The δ-overlap of magnetic $d_{x^2-y^2}$ orbitals and carboxylato-bridges were attributed to the

pathways for exchange interaction. Depending upon the mode of coordination and the strength of the carboxylato-bridge, the exchange coupling between the Cu atoms in carboxylato-bridged complexes varies from –217 to –575 cm^{-1} (26, 27). It is known that encapsulation of metal ions in zeolites could result in unusual oxidation states/electronic configuration and consequent catalytic activity. The present EPR study throws light on the consequences of encapsulation on the structure, magnetic properties and catalytic activity of copper acetato complexes. The effect of electron withdrawing Cl-substitution on the structural and catalytic properties of copper acetate is also investigated.

3.2 Materials and Procedures

The materials $Cu(CH_3COO)_2.H_2O$ (CuAc), $Cu(CH_2ClCOO)_2.2.5H_2O$ (CuClAc), copper acetate encapsulated in zeolite-Y (CuAc-Y), copper chloroacetate encapsulated in zeolite-Y (CuClAc-Y) and copper exchanged zeolite-HY (Cu-Y) were prepared as described in Chapter 2. The catalytic activities of these materials in phenol hydroxylation with molecular oxygen were evaluated as described in Chapter 2.

3.3 Results and Discussion

3.3.1 Structural Characterization

3.3.1.1 X-ray Diffraction Studies

No major changes except a marginal reduction in the XRD peak intensity were observed indicating that encapsulation of copper acetato and chloroacetato complexes did not alter the framework structure of zeolite-Y. Representative XRD patters of Cu-Y and CuAc-Y are shown in Fig. 3.1.

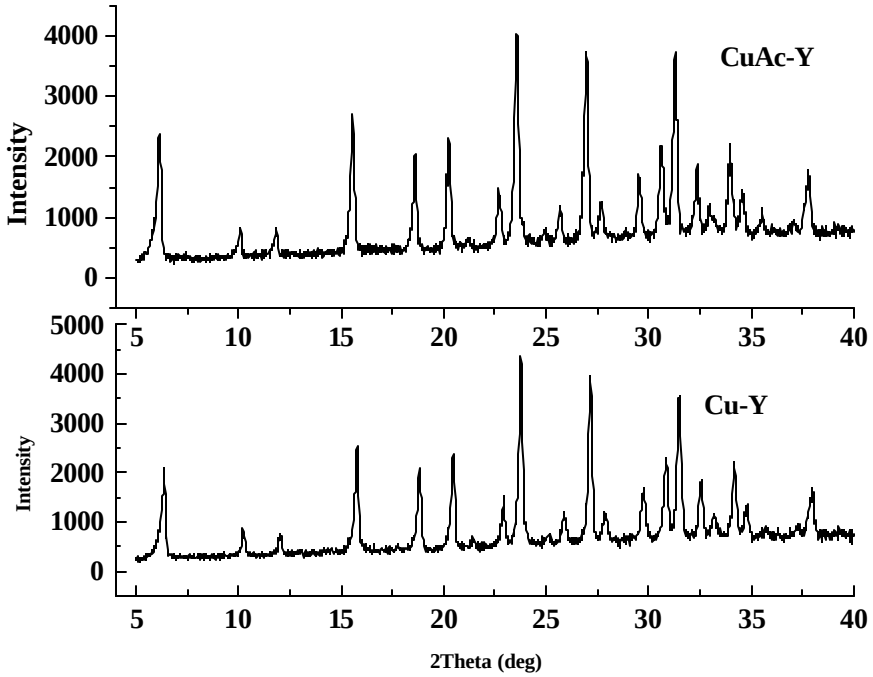

Fig. 3.1 XRD patterns of Cu-Y(0.11%) and CuAc-Y.

3.3.1.2 Chemical and Thermal Analyses

The %C and %H contents estimated from the elemental analysis confirm the formation and purity of the copper complexes (see Chapter 2). The Cu content in Cu-Y was estimated to be 0.11 wt.% (AAS).

The thermogravimetric analyses of "neat" and encapsulated CuAc and CuClAc complexes, measured in flowing dry air, are shown in Fig. 3.2. "Neat" CuAc exhibited two stages of weight loss in the range 349 – 410 K (peak maximum = 388 K; weight loss = 9.02 wt%) and 438 – 558 K (peak maximum = 534 K;

weight loss = 59.1 wt%), due to decomposition of hydrated water and acetate ligands, respectively (Fig. 3.2a). "Neat" CuClAc, on the other hand, showed three stages of weight loss in the range 315 – 356 K (peak maximum = 334 K) due to decomposition of hydrated water and 433 – 545 K (peak maximum = 495 K) and 545 – 666 K (peak maximum = 571 K) due to combustion of chloroacetate ligand (Fig. 3.2b). The chloro-substitution lowered the combustion temperature of acetate.

CuAc-Y and CuClAc-Y, on the other hand, showed several stages of endothermic weight losses, in the range 313 - 493 K, attributable to desorption of condensed, physically adsorbed and chemisorbed (in the form of OH groups) water in the zeolite channels or cavities as well as the water coordinated to the copper complexes (Fig. 3.2c and Fig. 3.2d). The exothermic weight losses in the temperature range 523 - 663 K correspond to the decomposition and combustion of the acetato and chloroacetato ligands with different modes of coordination. The combustion of acetato ligand bridging the two Cu(II) ions in CuAc-Y takes place at higher temperature (593 K) compared to that in "neat" CuAc (~534 K) (compare Fig. 3.2c and Fig. 3.2a). This indicates that the thermal stability of CuAc increases upon encapsulation in zeolite-Y. The exothermic weight loss (~4.5 wt.%) around 663 K is due to the combustion of acetato groups with a chelate mode of coordination to the zeolite framework or to monomeric Cu(II) complexes.

An increased thermal stability (by ~ 40 K) was observed also for encapsulated CuClAc. CuClAc-Y decomposes at 538 K as compared to 495 K in the "neat" complex (compare Fig. 3.2d and Fig. 3.2b). Further, CuClAc-Y

decomposes at lower temperature (538 K) compared CuAc-Y (593 K) due to chloro-substitution (compare Fig. 3.2d and Fig. 3.2c).

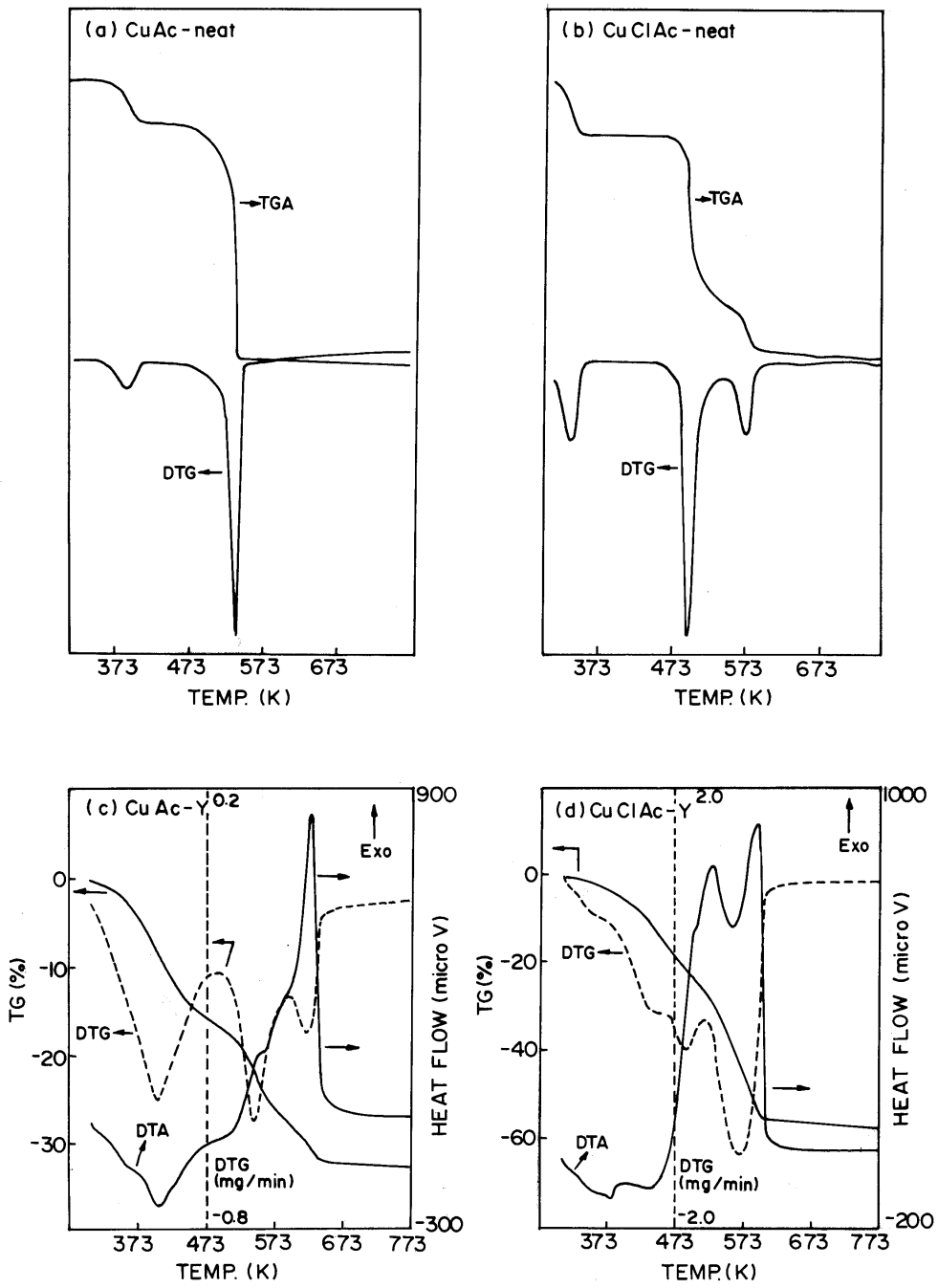

Fig. 3.2 Thermal analyses (TGA, DTA & DTG) of (a) "neat" CuAc, (b) "neat" CuClAc, (c) CuAc-Y and (d) CuClAc-Y.

The chemical and thermal analyses together confirm the formation and stoichiometric integrity of CuAc-Y and CuClAc-Y. Additionally, the thermal analysis reveals an increased thermal stability of CuAc and CuClAc encapsulated in zeolite-Y compared to the corresponding "neat" complexes. Electron withdrawing chloro-substitution exhibits a marked effect on the thermal stability of CuClAc.

3.3.1.3 FT-IR Spectroscopy

The FT-IR spectra indicated the formation of dimeric Cu(II) acetato and chloroacetato complexes in the supercages of zeolite-Y (Fig. 3.3) The assignments of selected vibrational band positions of "neat" and zeolite-Y-encapsulated CuAc and CuClAc are listed in Table 3.1.

As is evident from Table 3.1, significant shifts in band positions of CuAc and CuClAc are observed on encapsulation. The band for $\nu_{as}(COO^-)$ shifts by ~ 13 cm^{-1} toward higher energy for CuAc-Y and by ~ 19 cm^{-1} for CuClAc–Y, as compared to the corresponding "neat" complexes. Similarly, $\nu_s(COO^-)$ shifts towards lower energy by ~ 19 cm^{-1} for CuAc-Y, as compared to CuAc. The position of this band is unaltered for CuClAc on encapsulation. Similarly, the band at 692 cm^{-1} corresponding to deformation of COO^- is unaltered for CuAc-Y. For CuClAc-Y, it shifts by 10 cm^{-1}. The separation ($\Delta\nu$) between $\nu_s(COO^-)$ and $\nu_{as}(COO^-)$ bands, indicative of the type of coordination of the carboxylato group falls well within the range reported for the *syn-syn* mode of coordination (28). But its value increases

upon encapsulation (from 182 to 213 cm^{-1} for CuAc and from 185 to 205 cm^{-1} for CuClAc). The FT-IR spectra, thus, indicate

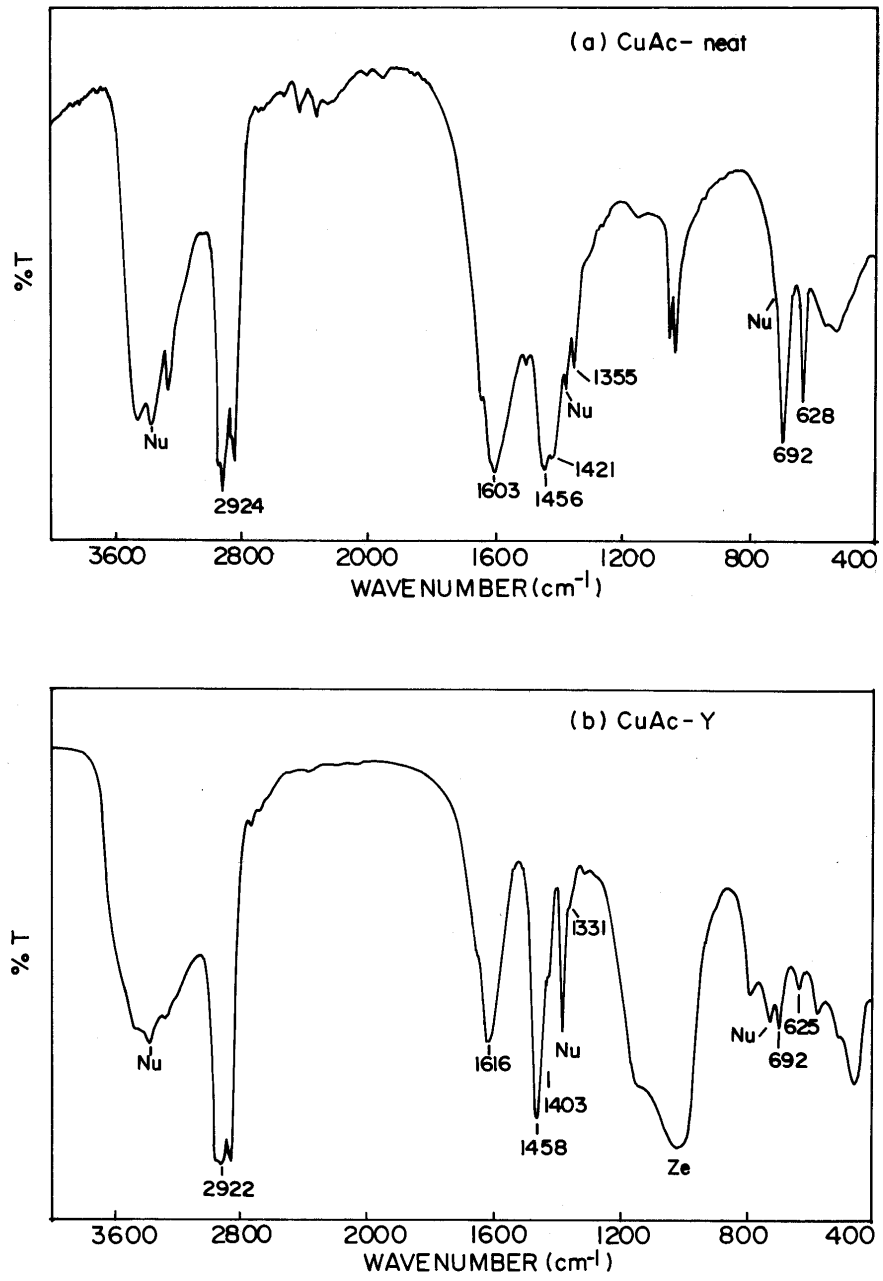

Fig. 3.3 FT-IR spectra of (a) "neat" CuAc, (b) CuAc-Y, (c) "neat" CuClAc and (d) CuClAc-Y. The band positions of the dimeric complexes are numbered. Asterisk (*) = the bands due to the organics in the zeolite; Nu = bands due to Nujol; Ze = bands due to zeolite-Y

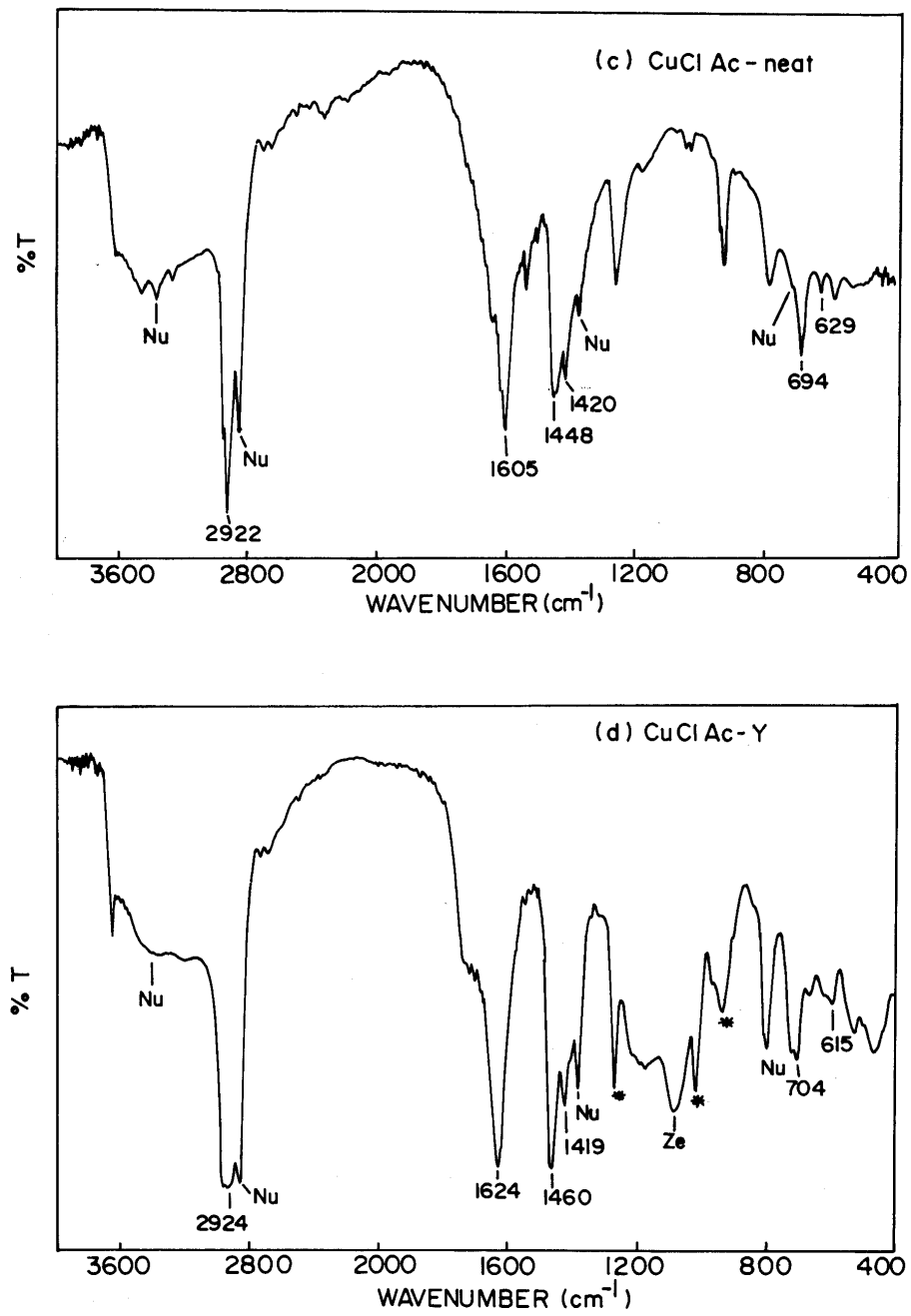

Fig. 3.3 (contd…) FT-IR spectra of (a) "neat" CuAc, (b) CuAc-Y, (c) "neat" CuClAc and (d) CuClAc-Y. The band positions of the dimeric complexes are numbered. Asterisk (*) = the bands due to the organics in the zeolite; Nu = bands due to Nujol; Ze = bands due to zeolite-Y.

that encapsulation causes structural and electronic changes in copper complexes.

EPR studies (*vide infra*) indicate that the amount of encapsulated dimeric copper ions is lower in the case of CuClAc than in CuAc. However, the large amount of organic content in CuClAc-Y, as seen from the FT-IR spectra (Fig. 3.3d) as well as the decomposition profiles in the thermographs (Fig. 3.2d), indicate the presence of additional acetato or chloroacetato ligands / acetic acid molecules in the zeolite. These are presumably chemisorbed on the zeolite surface.

Table 3.1 FT-IR Assignments for "Neat" and Encapsulated CuAc and CuClAc Dimers

Assignment	CuAc (cm^{-1})		CuClAc (cm^{-1})	
	"Neat"	Encapsulated	"Neat"	Encapsulated
C-H stretch (Asym. and sym.)	2924	2922	2922	2924
COO^- asym. stretch	1603	1616	1605	1624
COO^- sym. stretch	1421	1403	1420	1419
C-H bending (CH_3, CH_2Cl)	1355, 1456	1331, 1458	1448	1460
COO^- deform.	628, 692	629, 692	628, 694	615, 704

3.3.1.4 Electronic Spectroscopy

Diffuse reflectance UV-visible spectra of "neat" and zeolite-Y-encapsulated CuAc (Fig. 3.4) showed two characteristic bands, one in the ultraviolet region (designated as band I) and the other in the visible and near IR region (designated as band II). Band I for "neat" CuAc and CuClAc occurs at 386 and 377 nm, respectively. For encapsulated complexes, this band shifts to 373 nm for CuAc-Y

and 387 nm for CuClAc-Y, respectively. Band II is in general broad and unresolved. It occurs in the region of 600 to 900 nm with maxima at 713 and 856 nm for "neat" CuAc and CuClAc complexes, respectively. Upon encapsulation, this band shifts to 717 nm (CuAc-Y) and 710 nm (CuClAc-Y), respectively. Also, an additional band due to acetate ligands is observed at around 250 nm. These bands are characteristic of dimeric CuAc complexes and are not seen in copper exchanged zeolite-Y samples (Fig. 3.4).

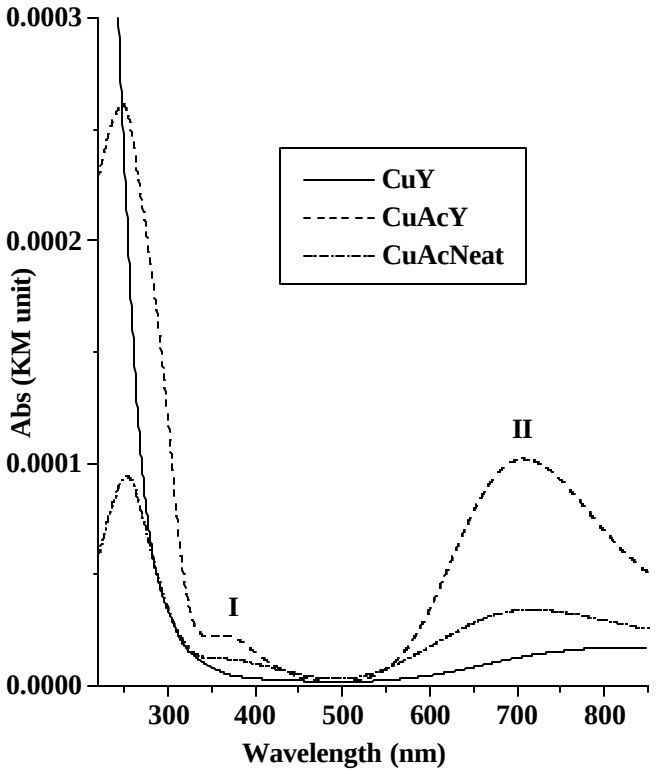

Fig. 3.4 Diffuse reflectance UV-visible spectra of CuY, CuAc and CuAc-Y.

Thermal analysis, and FT-IR and UV-visible spectroscopies indicate that the copper complexes undergo significant structural changes upon encapsulation. These changes are investigated in some detail by EPR spectroscopy.

3.3.1.5 EPR Spectroscopy

3.3.1.5.1 EPR of Cu-Y

0.11% Cu-Y showed a symmetric, isotropic signal in the temperature range 280 – 380 K. The g_{iso} value of the signal changed from 2.194 to 2.166 and the peak to peak line width (ΔH) reduced from 175 to 158 G as the temperature was lowered. Below 275 K, the spectrum was anisotropic and characterized by axial g and copper hyperfine (A) tensors. The anisotropic spin Hamiltonian parameters are $g_{||} = 2.392$, $g_{\perp} = 2.093$, $A_{||} = 132.2$ G and $A_{\perp} = 25.0$ G. Representative spectra of Cu-Y at different temperatures are shown in the Fig. 3.5. The spectra, when the Cu-loading is 10 times lower (0.01% Cu-Y), are described by a rhombic g and A tensors (Fig. 3.6), with spin Hamiltonian parameters being $g_z = 2.376$, $g_x = 2.083$, $g_y = 2.095$ and $A_{zz} = 119$ G, $A_{xx} = A_{yy} = 10.0$ G. This indicates that Cu(II) occupies two different locations in zeolite-Y. In samples with lower Cu concentrations (say 0.01% Cu), the Cu(II) ions occupy the sodalite cages (cation exchangeable positions) and in those samples with higher concentrations (0.11% Cu), they are located in the supercage in addition to the sodalite cages. The EPR spin Hamiltonian parameters, obtained after spectral simulation, are in close agreement with previous reports (29, 30).

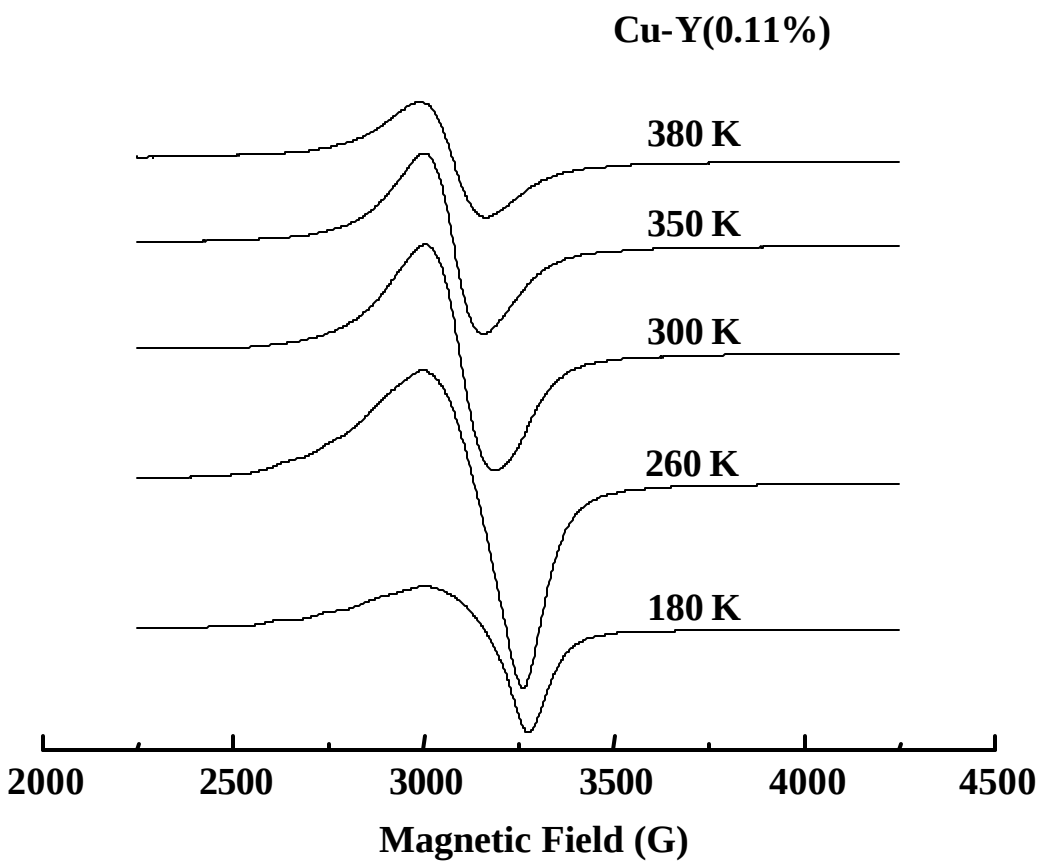

Fig. 3.5 Variable temperature EPR spectra of Cu-Y(0.11%).

In the sodalite cage, the geometry around the Cu(II) ion is distorted octahedral with three coordination sites being the oxygens from the zeolite framework (S_{II}) and the remaining three being water molecules. The Cu(II) ion in the supercages possesses O_h symmetry with water molecules occupying all the six coordination sites. The Cu(II) ions with $t_{2g}^6 e_g^3$ electronic configuration in the O_h symmetry are conformationally unstable and prone to the Jahn-Teller (JT) distortion (31). This distortion is usually an elongation along the coordination axis x, y or z. When the thermal energy is more than the JT stabilization energy ($kT > E_{JT}$), the system undergoes a dynamic JT distortion (31). As the temperature is lowered, it

undergoes a transition from dynamic to static JT distortion. For $[Cu(H_2O)_6]^{2+}$ located in the supercages of zeolite-Y, this transition occurs at 275 K, corresponding to JT stabilization energy of 412 cm^{-1}. Interestingly, $Cu(H_2O)_6^{2+}$ ions in Tuttons' salts exhibit this transition at lower temperatures corresponding to JT stabilization energy of ~160 cm^{-1} (32). Hence, the JT transition temperature (from dynamic to static distortion), occurs at an elevated temperature when $[Cu(H_2O)_6]^{2+}$ ion is encapsulated and constrained within the geometric confines of the zeolite supercages.

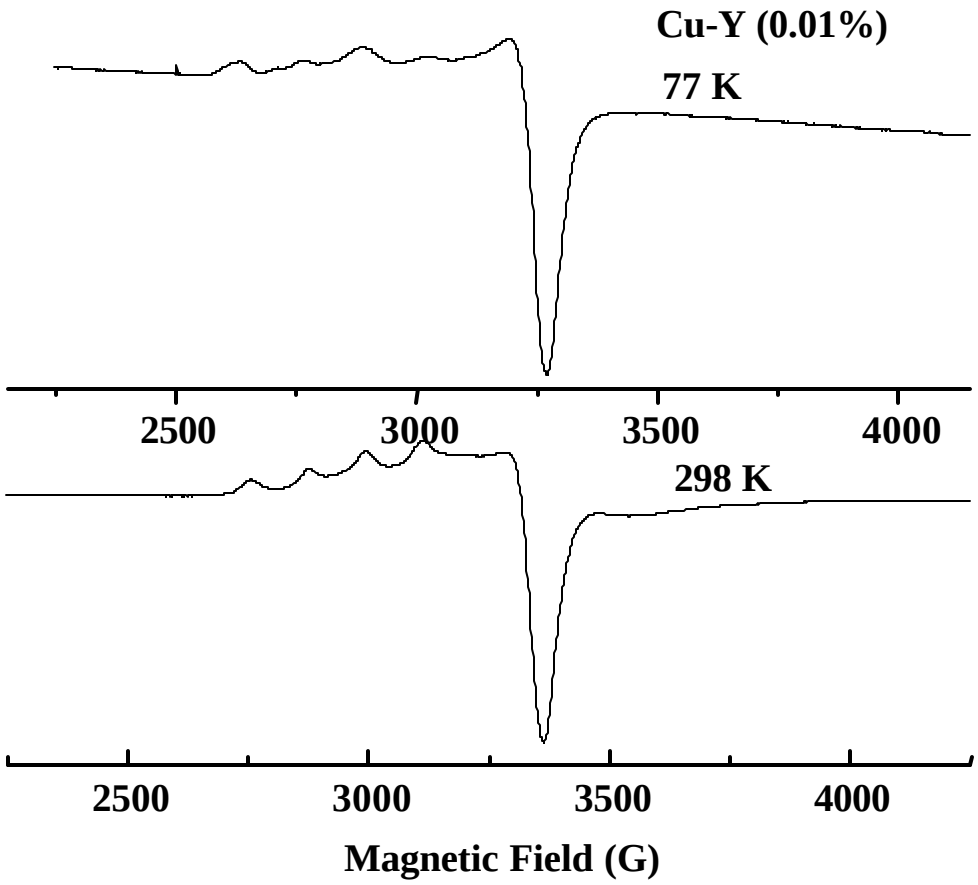

Fig. 3.6 X-band EPR spectra of Cu-Y(0.01%) at 298 K (bottom) and 77 K (top).

3.3.1.5.2 EPR of "Neat" CuAc and CuClAc Complexes

CuAc in the solid state exists as isolated dimers as shown in Fig. 3.7 (22, 23). The spins on the two Cu centers (S = ½) couple antiferromagnetically resulting in a ground state singlet (S = 0) and a low lying excited triplet (S = 1). At ambient temperatures, the excited triplet state is populated and the complex exhibits paramagnetism (1.4 B.M.). As the temperature is lowered, the excited triplet states are depopulated and as a consequence, the magnetic moment and EPR signal intensity decreases. Around 20 K the complex becomes diamagnetic and EPR silent (20, 21). In the following, the EPR studies reveal the marked effects of chloro-substitution and encapsulation on the structural properties.

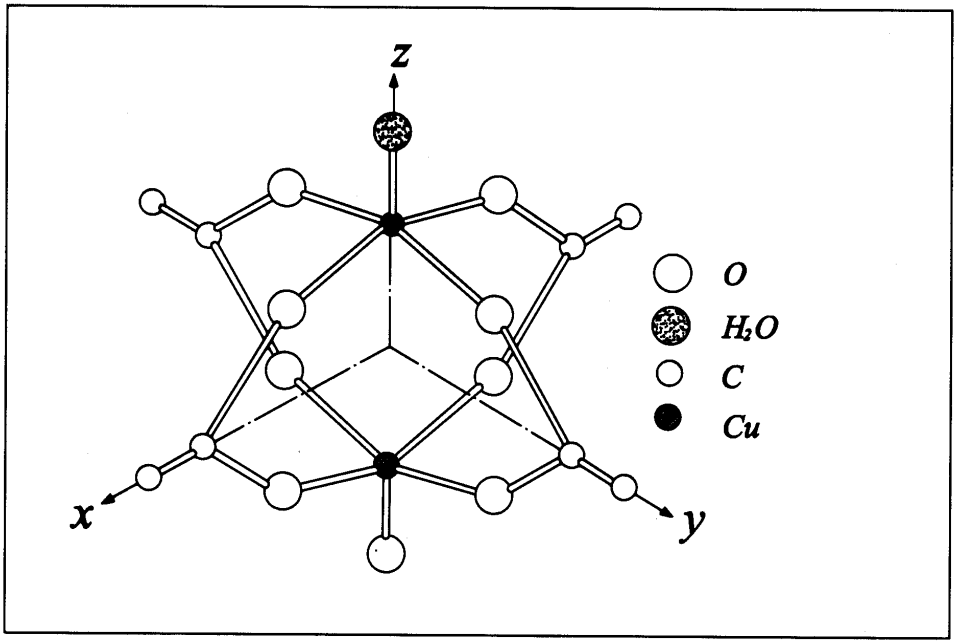

Fig. 3.7 Dimeric Structure of $Cu(CH_3COO)_2.H_2O$ (22, 23).

The powder samples of CuAc and CuClAc showed three EPR signals, at X-band frequency (λ = 3 cm), near 240, 4600 and 5900 G, respectively.

Representative spectra of "neat" CuAc and CuClAc are shown in Figs. 3.8 and 3.9, respectively. At ambient temperatures the spectra were more intense and broader (Figs. 3.8 and 3.9). As the temperature was lowered, the intensity decreased and the signals became narrower. Seven copper hyperfine features, with relative intensity ratio of 1:2:3:4:3:2:1, due to two interacting Cu(II) ions (2nI + 1; number of Cu ions (n) = 2 and nuclear spin (I) = 3/2), were observed on the low field signal (Figs. 3.8 and 3.9). An expanded portion of the spectrum in the low field region revealing the septet Cu hyperfine pattern is shown in Fig. 3.10.

The spectra of CuAc could be fitted satisfactorily using the interactive spin Hamiltonian (27, 33) for isolated Cu(II) dimers (S = 1).

$$H = DS_z^2 + E(S_x^2 - S_y^2) + \beta(g_z H_z S_z + g_x H_x S_x + g_y H_y S_y) \qquad [1]$$

where, D and E are the zero-field splitting parameters, β is the Bohr magneton and x, y and z are the principal axes coordinating system, fixed with respect to the Cu-Cu bond (Fig. 3.7). When the external magnetic field is in an arbitrary direction with respect to x, y and z axes, we expect in general three transitions: two $\Delta M_S = \pm 1$ transitions and one $\Delta M_S = \pm 2$ transition. When the magnetic field is along the x, y and z directions, respectively, we obtain from eq. [1] the six allowed $\Delta M_S = \pm 1$ resonance fields.

$$H_{x1}^2 = (g_e / g_x)^2[(H_o - D' + E')(H_o + 2E')]$$

$$H_{x2}^2 = (g_e / g_x)^2[(H_o + D' - E')(H_o - 2E')]$$

$$H_{y1}^2 = (g_e / g_y)^2[(H_o - D' - E')(H_o - 2E')] \qquad [2]$$

$$H_{y2}^2 = (g_e / g_y)^2[(H_o + D' + E')(H_o + 2E')]$$

$$H_{z1}^2 = (g_e / g_z)^2[(H_o - D')^2 - E'^2)]$$

$$H_{z2}^2 = (g_e / g_z)^2[(H_o + D')^2 - E'^2)],$$

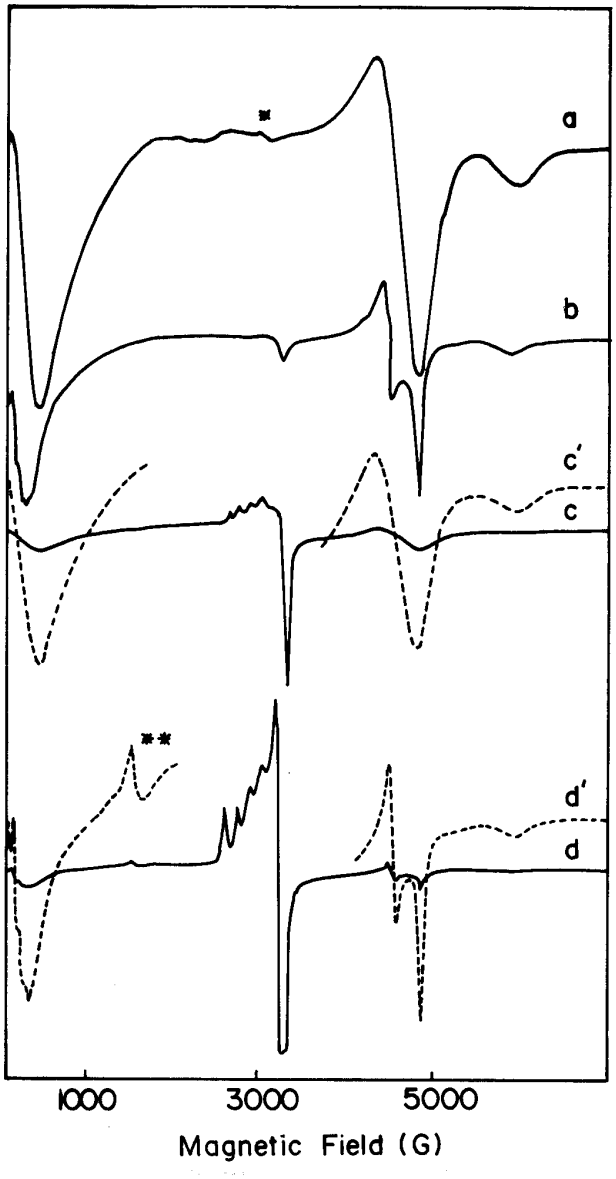

Fig. 3.8 X-band EPR spectra of "neat" CuAc at (a) 298 K and (b) 95 K and CuAc-encapsulated in zeolite-Y at (c) 298 K and (d) 86 K. Signals in dotted lines (c') and (d') are the dimer signals at high spectroscopic gain. Asterisk (*) indicates signals due to monomeric Cu impurity and ** indicates the Fe(III) impurity in zeolite-Y.

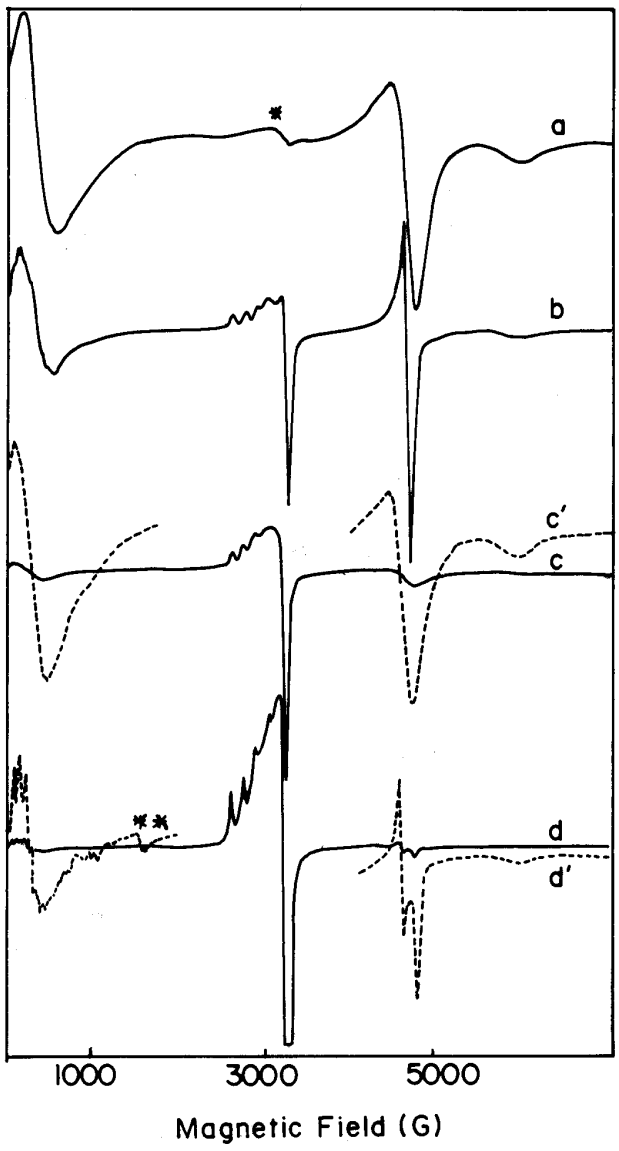

Fig. 3.9 X-band EPR spectra of "neat" CuClAc at (a) 298 K and (b) 80 K and CuClAc-encapsulated in zeolite-Y at (c) 298 K and (d) 80 K. Signals in dotted lines (c') and (d') are the dimer signals at the higher spectrometer gain. Asterisk (*) indicates the signals due to monomeric impurity and ** indicates Fe(III) impurity in zeolite-Y.

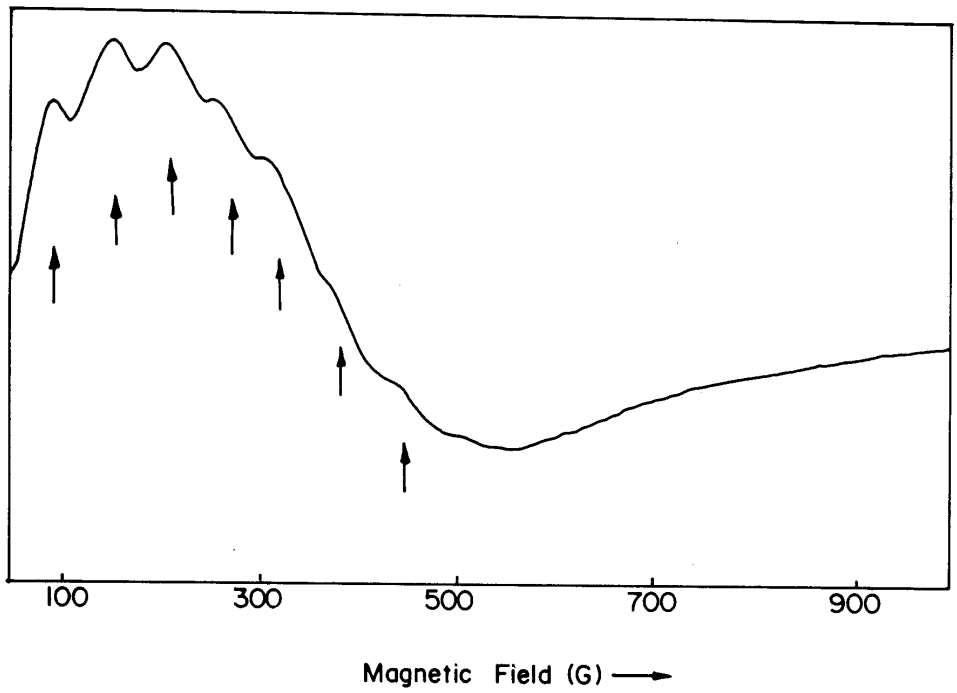

Fig. 3.10 Expanded portion of the dimer signal near zero-magnetic field showing the hyperfine resolution due to two interacting copper ions in "neat" CuClAc.

where $H_o = h\nu/g_e\beta$, $D' = D/g_e\beta$ and $E' = E/g_e\beta$; H_{z1} and H_{z2} are, for example, the two $\Delta M_S = \pm 1$ transitions when the magnetic field is along the z-axis and g_e is the free electron g-value (2.0023). However, for powder samples, the spectrum is an average of the spectra corresponding to several possible orientations. Six allowed $\Delta M_S = \pm 1$ transitions along with a half-field ($\Delta M_S = \pm 2$) transition are observed for a rhombic symmetry ($E \neq 0$). When $D < h\nu$, four $\Delta M_S = \pm 1$ transitions along with a half-field ($\Delta M_S = \pm 2$) transition are allowed for an axial symmetry ($E = 0$). When $D > h\nu$, as in the case of the present copper dimers at X-band frequency, H_{x1} and H_{y1} and the half-field $\Delta M_S = \pm 2$ transition lines can no longer be observed. Hence the powder spectrum consists of only four lines. If, in addition, $E = 0$, only three EPR lines are observed and the eq. [2] can be rewritten as follows.

$$H_{\perp}^{2} = (g_e / g_{\perp})^2[\, H_o(H_o + D')\,],$$

$$H_{z1} = -(g_e / g_z)(H_o - D') \qquad [3]$$

$$H_{z2} = (g_e / g_z)(H_o + D')$$

The effect of substitution (by Cl) is more evident in the low temperature spectra around 4800 G (compare Figs. 3.8 and 3.9). While the spectra of CuAc could be fitted with a rhombic spin Hamiltonian ($E \neq 0$ and $g_x \neq g_y$), that of CuClAc could be fitted to an axial spin Hamiltonian ($E \approx 0$). In other words, the symmetry around Cu is C_{4v} for "neat" CuClAc and C_{2v} for CuAc. This difference in the molecular symmetry of "neat" CuClAc and CuAc is attributed to a difference in the carboxylato ion binding. This inference from the EPR study agrees well with the X-ray structure of "neat" CuAc (22, 23). According to the latter, the *cis*-carboxylato groups bind differently to the central metal ion Cu(II), the average *cis*-C-O bond distances are 1.990 and 1.948 Å, respectively, and the basal CuO_4 is non-planar and results in an overall C_{2v} symmetry at the individual Cu atoms of the dimer (22, 23). The EPR parameters for "neat" CuAc and CuClAc, obtained after least squares fitting to the eqs. [2] and [3], respectively, are listed in Table 3.2.

3.3.1.5.3 EPR of CuAc-Y and CuClAc-Y

Representative EPR spectra of zeolite-Y-encapsulated CuAc and CuClAc complexes are shown along with the corresponding "neat" complexes, in Figs. 3.8 and 3.9, respectively. The spin Hamiltonian parameters obtained after fitting the spectra to eq. [2] are listed in Table 3.2, along with the values for the "neat" complexes. Curves b in Figs. 3.8 and 3.9 represent the EPR spectra at 95 K of "neat" CuAc and CuClAc, respectively. They are different because of the different

symmetries of the Cu(II) ions in the two cases (C_{2v} for CuAc and C_{4v} for CuClAc). The EPR spin Hamiltonian and structural parameters are hence, different (see Table 3.2). Curves d in Figs. 3.8 and 3.9 represent the EPR spectra at 80 – 86 K of CuAc and CuClAc encapsulated in zeolite-Y, respectively. The differences between curves b and d in Fig. 3.8 compared to similar differences in Fig. 3.9 arise primarily because of changes in the symmetry of the Cu(II) ions responsible for curve b in Fig. 3.8 and curve b in Fig. 3.9. There are significant differences between CuAc-Y (curve d in Fig. 3.8) and CuClAc-Y (curve d in Fig. 3.9). This may be seen from the different values of their spin Hamiltonian and structural parameters (see Table 3.2).

Table 3.2 EPR Spin Hamiltonian and Structural Parameters of "Neat" and Encapsulated CuAc and CuClAc Complexes

Complex	g_z	g_x	g_y	A(Cu) (cm^{-1})	D (cm^{-1})	E (cm^{-1})	–J (cm^{-1})	Cu-Cu r (Å)
CuClAc ("neat")	2.348	2.068	2.068	0.0054	0.34	0.0	247	2.92
CuClAc-Y	2.353	2.064	2.070	0.0066	0.34	0.03	132	2.73
CuAc ("neat")	2.358	2.055	2.095	0.0073	0.34	0.07	259	2.64
CuAc-Y	2.358	2.055	2.095	0.0073	0.34	0.07	310	2.40

The spectra reveal the presence of two types of encapsulated Cu(II) species; species I is the encapsulated dimeric copper acetato or chloroacetato complex and species II (marked by the asterisk, *) corresponds to monomeric Cu(II) ion. A

comparison of the spectrum of species II with that of Cu-Y containing a lower amount of Cu (0.01 wt%) indicates that the Cu(II) ions of species II are located in the sodalite cages of zeolite-Y (Fig. 3.11). The Cu(II) ions in the sodalite cages (species II) do not form Cu-Cu dimeric complexes with acetic acid and chloroacetic acid due to the geometric constrains in the sodalite cages.

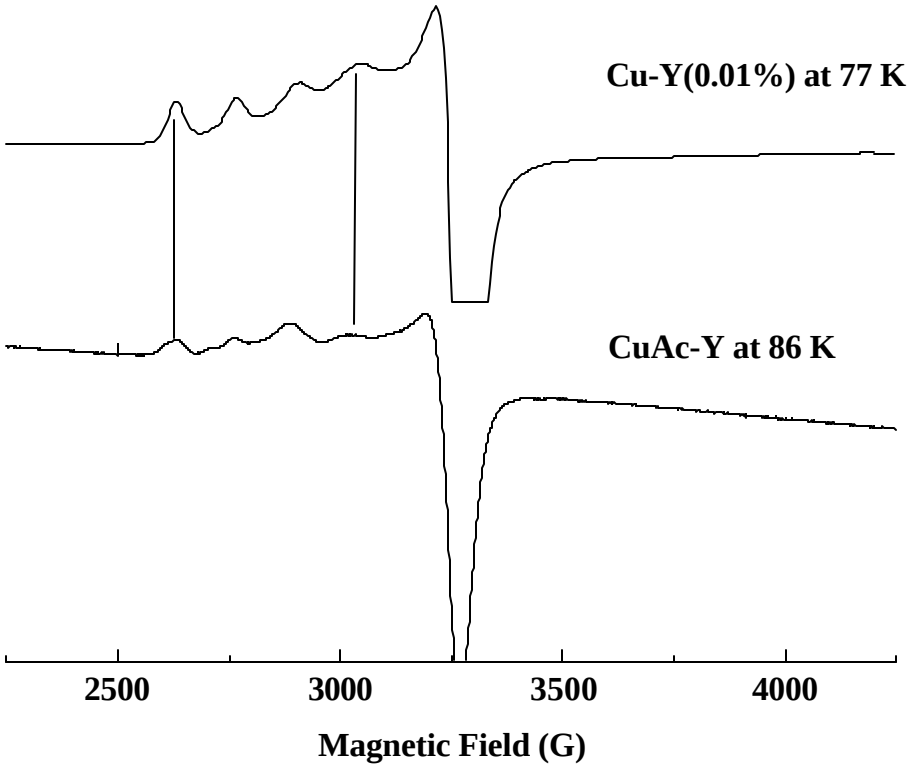

Fig. 3.11 Comparative EPR spectra of the monomeric species in CuAc-Y and the Cu(II) ions situated in the sodalite cages of zeolite-Y.

No apparent difference is observed in the spectra of CuAc upon encapsulation (see curves a and c, and curves b and d of Fig. 3.8). CuClAc, on the other hand, shows marked changes upon encapsulation (see curves a and c, and curves b and d of Fig. 3.9). CuClAc which exhibits an axial spectrum in the "neat"

state, corresponding to C_{4v} symmetry (Fig. 3.9b) exhibits a rhombic-type spectrum corresponding to a C_{2v} symmetry after encapsulation (Fig. 3.9d; see the splitting of the signal around 4800 G upon encapsulation). A higher resolution of the copper hyperfine features is also observed in the signal near 240 G (Fig. 3.9d).

From the comparison of the signal intensities of the dimeric "neat" and encapsulated complexes, the amounts of acetato and chloroacetato complexes encapsulated in supercages were estimated to be 65% and 20% (of the total copper) for CuAc and CuClAc, respectively. The remaining copper is located mostly in the sodalite cages.

As described in the previous section, in Cu-Y, the copper ions in the sodalite cage show rhombic EPR spectra at 298 K (g_z = 2.376, g_x = 2.083, g_y = 2.095 and A_{zz} = 119 G, A_{xx} = 10.0 G and A_{yy} = 10.0 G). Above 275 K, the Cu(II) ions in the supercages and those near the hexagonal prism (in Cu-Y) exhibit a broad isotropic spectrum (g_{iso} = 2.194, ΔH_{pp} = 175 G). Below 275 K, the spectrum becomes axial ($g_{||}$ = 2.392, $g_{\perp}$ = 2.093, $A_{||}$ = 132.2 G and $A_{\perp}$ = 25.0 G). The reason for this transition is the Jahn-Teller distortion of the Cu(II) ions in the supercages or those near the hexagonal prism with O_h/D_{3h} symmetry. These signals due to Cu(II) ions in the supercage and near the hexagonal prism are not present in CuAc-Y and CuClAc-Y; instead, new signals due to dimeric acetato and chloroacetato complexes appear (Fig. 3.8 and 3.9, respectively), confirming the formation of the dimeric complexes and their location in the supercages. From the EPR signal intensity and thermogravimetric data, it was estimated that, on an average, the

copper dimers occupy one in two (CuAc-Y) or one in eight (CuClAc-Y) of the supercages of the Faujasite lattice.

3.3.1.5.4 Magnetic Exchange Coupling Constant

At high temperatures, the triplet states are relatively more populated and the dimer signals are broader due to short, electron spin-lattice relaxation times (T_{1e}) and intermolecular interactions. As the temperature is lowered, the excited triplet levels are depopulated and the copper hyperfine features are better resolved. The intensity of the signal of a monomeric paramagnetic ion, obeying the Curie-Weiss law, is inversely proportional to the temperature. The ratio (R) of the intensity of the dimer (I_{dimer}) to that of the monomer ($I_{monomer}$) signals is

$$R = I_{dimer} / I_{monomer} = 2 \exp(-J/kT)/ [1 + 3\exp(-J/kT)]. \qquad [4]$$

The signal of Cu-Y was taken as the reference paramagnetic ion signal In eq. [4], J is the exchange coupling constant or singlet-triplet separation. Its sign is negative for antiferromagnetic interaction and positive for ferromagnetic interaction. The plots of relative intensities (R) of dimer to monomer signals for "neat" and encapsulated CuAc and CuClAc complexes are shown in Fig. 3.12.

If the triplet levels are not very much higher in energy than the singlet or if the magnitude of J is small, then –log(R) should increase linearly with T^{-1}. Such behavior is indeed observed for CuClAc complexes (Fig. 3.12, curve b). The plots for CuAc and CuAc-Y, on the other hand, are linear only up to a certain temperature (210 and 160 K, for the "neat" and encapsulated complexes, respectively, Fig. 3.12, curve a). The relative intensity values (R) were fitted to eq. [4] and the exchange coupling constants (J) were obtained for both the "neat" and the encapsulated complexes (see

Table 3.2). The value of J for CuAc (–259 cm^{-1}) compares well with that reported by Bleaney and Bowers (20, 21) and to that obtained by bulk susceptibility measurements (–286 cm^{-1}) (24, 25). From Table 3.2, we may infer the following consequences of substitution and encapsulation.

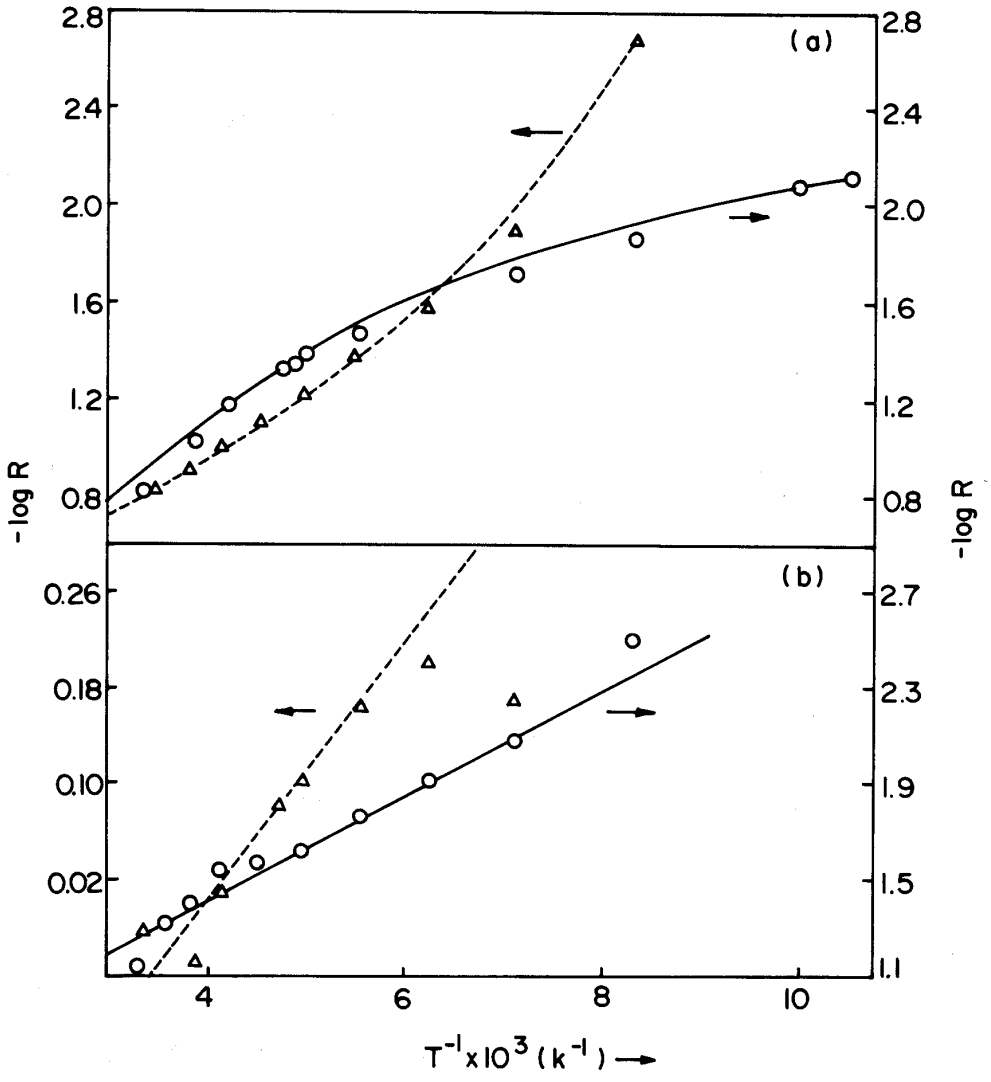

Fig. 3.12 Plot of –log R versus T^{-1} for "neat" (—) and encapsulated (-----) complexes of (a) CuAc and (b) CuClAc.

1) The g values ($g_z > g_x$ and g_y) reveal a tetragonal distortion of the molecular geometry around Cu(II) and indicate that the unpaired electron occupies a "formal" $3d_{x^2-y^2}$ orbital of Cu(II).

2) The electron withdrawing Cl substitution significantly influences the symmetry of the g and zero-field tensors. Their values are characteristic of a rhombic symmetry for the "neat" CuAc and an axial symmetry for the "neat" CuClAc complex. Chlorine substitution alters the magnitude of the exchange coupling constant (J), which changes from -259 cm^{-1} for CuAc to -247 cm^{-1} for "neat" CuClAc.

3) The value of A(Cu) is smaller for CuClAc (54×10^{-4} cm^{-1}) than for CuAc (73×10^{-4} cm^{-1}), consistent with a depletion of electron density from Cu orbitals on chlorine substitution.

4) The molecular symmetry at copper in CuClAc reduces from C_{4v} to a lower symmetry (C_{2v}) as a consequence of encapsulation. CuAc has a lower symmetry in both the "neat" and encapsulated complexes.

5) An increase in the value of the copper hyperfine coupling constant (from 54×10^{-4} cm^{-1} to 66×10^{-4} cm^{-1}) is observed for CuClAc upon encapsulation, probably due to changes in the molecular geometry of CuClAc, caused by the confinement and consequent host-guest interactions in the supercages. Such a change (in A values) is not observed for the CuAc complex, probably due to its smaller size.

6) The value of J is negative for both the CuAc and CuClAc indicating that the Cu-Cu interactions are antiferromagnetic. Interestingly, the exchange coupling constant (-J) increases from 259 to 310 cm^{-1} upon encapsulation for CuAc. But it decreases from 247 to 132 cm^{-1} for CuClAc upon encapsulation.

3.3.1.5.5 Cu-Cu Distance in Dimeric CuAc and CuClAc

The zero-field splitting parameter, (D_{total}), obtained from experiment, has contributions from exchange as well as direct dipole-dipole interactions (27, 33).

$$D_{total} = D_{ex} + D_{dip} \qquad [5]$$

Considering, for the sake of simplicity, an axial symmetry for both CuAc and CuClAc, the D_{ex} and D_{dip} terms can be related to the exchange coupling constant (J) and internuclear Cu-Cu distance (r) as follows:

$$D_{ex} = -J / 8 [(g_{||} - 2)^2 / 4 - (g_{\perp} - 2)^2] \qquad [6]$$

$$D_{dip} = - [(g_{||}^2 + (1 / 2) g_{\perp}^2] \beta^2 / r^3 \qquad [7]$$

Here, $g_{||} = g_z$ and $g_{\perp} = (g_x + g_y)/2$. Interestingly, electron withdrawing substituents and encapsulation have only a minor effect on D_{total} values, while marked changes are observed in the values of J, the exchange-coupling constant. The intramolecular Cu-Cu separation (r) estimated from eqs. [5] – [7], by substituting the values of g and J, are given in Table 3.2. This value for r is larger for CuClAc than for CuAc and it decreases upon encapsulation for both CuAc and CuClAc from 2.64 to 2.40 Å and 2.92 to 2.73 Å, respectively. The value of 2.64 Å for "neat" CuAc matches well

with that reported from X-ray diffraction (2.61 Å) (22, 23) and validates the Cu-Cu distances estimated from EPR spectroscopy. Conventional X-ray diffraction methods cannot be used to estimate such intermolecular distances in encapsulated complexes. Although there may be some error in the estimation of the Cu-Cu separation, arising from the assumption of axial instead of rhombic symmetry, the reduction of r by about 0.2 Å, due to encapsulation, is a significant feature and indicates changes in the coordination/conformation of the carboxylato group. The shift upon encapsulation in the IR band positions of $\nu_{as}(COO^-)$ and $\nu_s(COO^-)$ and the UV band near 375 nm, all characteristic of the carboxylato bridge, also support such an inference.

To summarize, the spectroscopic and thermogravimetric studies reveal that the dimeric acetato and chloroacetato complexes of Cu(II) are encapsulated in the supercages of zeolite-Y. The dimensions of these dimeric Cu(II) complexes are more than 8.5×10 Å, while the size of the window of the supercage is only about 7.4 Å. Hence, these complexes, once formed, are truly encapsulated and cannot come out of the supercages of zeolite-Y easily. Molecular modeling studies revealed that the dimeric copper acetato complexes fit well within the supercages of zeolite-Y and possess some rotational degree of freedom (Fig. 3.13). Encapsulation has a significant effect on the molecular and electronic structure of CuAc and CuClAc as revealed by EPR. The CuAc has a lower symmetry (C_{2v}) in both the "neat" and encapsulated complexes. On the other hand, the symmetry of Cu(II) ions in CuClAc changes from C_{4v} to C_{2v} upon encapsulation. In addition to the changes in molecular symmetry, the Cu-

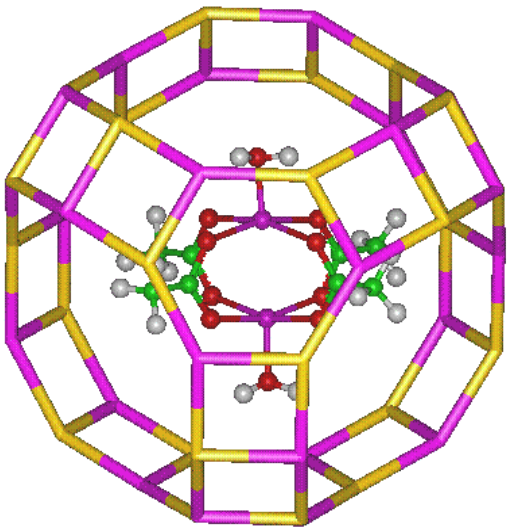

Fig. 3.13 Structure of CuAc encapsulated in zeolite-Y (molecular model).

Cu separation decreases by about 0.2 Å, for both the complexes, as a consequence of encapsulation.

3.3.1.5.6 Adsorption Studies

Zeolite-Y-encapsulated CuAc samples were exposed to phenol, DMF and pyridine. The color of the samples changed from bluish green to brown or green after the adsorption. The EPR spectra of the exposed samples (Fig. 3.14) reveal marked changes in the position of the dimer signals confirming that the dimer is accessible to the solvent molecules and is hence located in the supercages of zeolite-Y. The spectra reveal that the D and J values increase in the series: phenol > DMF > pyridine. The $g_{\|}$ and $g_{\perp}$ values decrease in the order: phenol (2.367, 2.096) > DMF (2.363, 2.092) > pyridine (2.252, 2.084), while $A_{\|}^{Cu}$ vary in the order: DMF (126.5 G) < phenol (132.4 G) < pyridine (188.5 G).

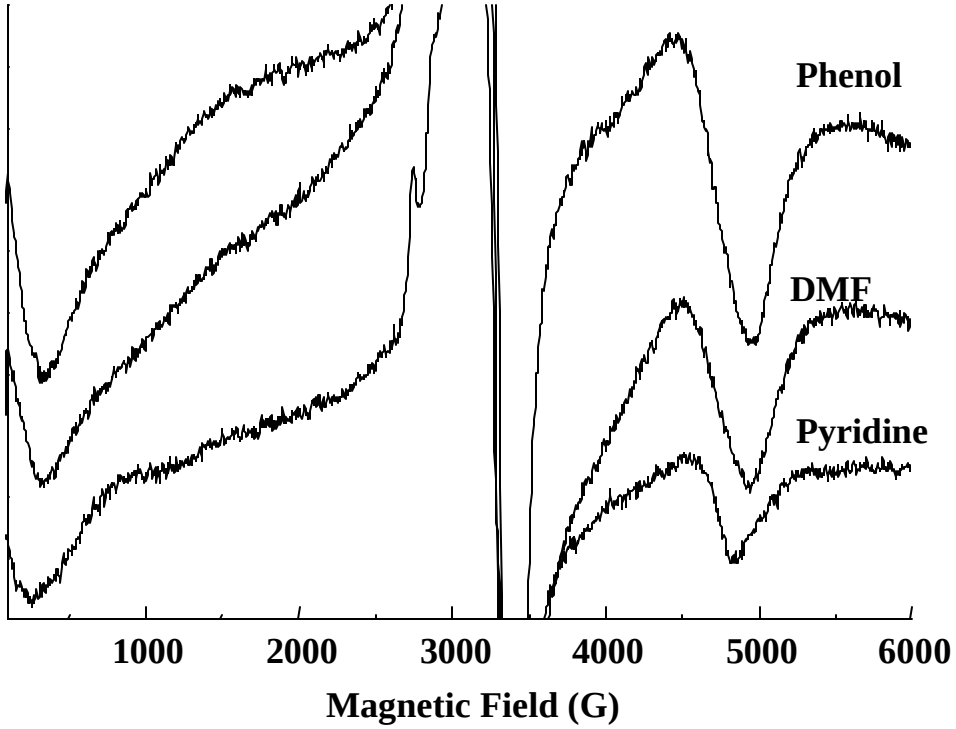

Fig. 3.14 Effect of solvent adsorption on the EPR spectra of dimeric CuAc-encapsulated in zeolite-Y.

3.3.2 Catalytic Activity Studies: Hydroxylation of Phenol

The catalytic activities of "neat" and zeolite-Y-encapsulated CuAc and CuClAc in the oxidation of phenol with molecular oxygen at 298 K were investigated. The reaction was conducted at pH = 6.5 (phosphate buffer). *ortho*-Benzoquinone was the major selective product of the reaction. The catalytic activity data for both the "neat" and encapsulated CuAc and CuClAc complexes are listed in Table 3.3.

Table 3.3 Hydroxylation of Phenol Using Molecular Oxygen (pH = 6.5, Temp. = 298 K, Contact Time = 19 h)

Catalyst	Phenol conv. (mol %)	TOF (h^{-1})	*Ortho*-benzoquinone (mol %)	Others (mol %)
CuAc - "neat"	5.1	3.6	4.9	0.2
CuAc-Y	11.5	60.9	11.5	-
CuClAc -"neat"	1.0	0.9	1.0	-
CuClAc-Y	12.0	227.1	11.9	0.1

TOF = turnover frequency (moles of phenol converted per mole of Cu per hour).

Hydroxylation did not occur in the absence of catalyst suggesting that the dimeric copper unit in CuAc and CuClAc as the active site. Both CuAc and CuClAc oxidize phenol selectively to *ortho*-benzoquinone. The turnover frequency (TOF) for oxidation is enhanced significantly upon encapsulation of the complexes in zeolite-Y for both CuAc and CuClAc (Fig. 3.15 and Table 3.3). This enhancement in TOF upon encapsulation of complexes is about 17 times in the case of CuAc and about 250 times in the case of CuClAc. Chloro-substitution has a marked effect on the activity. The specific catalytic activity (TOF) of CuClAc-Y is higher than that of CuAc-Y at similar levels of phenol conversion. In other words, the catalytic activity studies reveal that the dimeric copper acetato and chloroacetato complexes mimic the enzymatic activity of tyrosinase. The zeolite mantle (as noted from the detailed EPR studies) imparts certain steric restrictions on the metal complexes. These

structural changes occurring upon encapsulation are perhaps responsible the enhanced activity of the encapsulated complexes. A detailed structure-activity correlation is discussed in the following section.

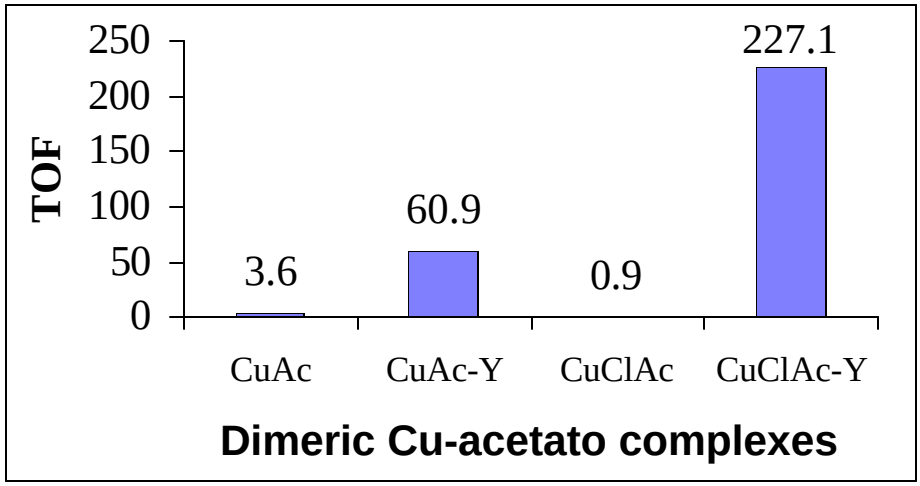

Fig. 3.15 Catalytic activities of "neat" and encapsulated CuAc and CuClAc.

3.3.3 Structure -Activity Correlations

Copper acetate complexes mimic, functionally, the enzymatic activity of the copper monooxygenase, tyrosinase, in the regiospecific *ortho*-hydroxylation of phenols to catechols and further the oxidation of catechol to *ortho*-benzoquinone (7). Interestingly, the enzyme also contains a dicopper site as the active center. The proposed mechanism for tyrosinase involves dioxygen binding to the Cu_2 sites to generate a Cu_2-O_2 side-on bound oxygen adduct (η^2 - η^2 type of peroxide coordination) (7, 34). During the hydroxylation reaction, the tyrosine phenolate group coordinates directly to the Cu(II) ion, leading to donation of electron density from the substrate tyrosine to the LUMO of the complex, which is antibonding with

respect to both the O-O and Cu-O bonds. This electron transfer, in turn, initiates the transfer of one of the two peroxide oxygens to the position *ortho* to the OH group in the tyrosine molecule. The resultant coordinated catecholate ion transfers two electrons to the binuclear cupric ion, leading to the dissociative elimination of the product and the regeneration of the deoxy- site for further turnover (7, 34).

It is pertinent to note that the EPR spectra (Fig. 3.14) of the phenol adsorbed on the encapsulated CuAc complexes in the presence of O_2 give clear evidence for the formation of an axially coordinated copper-phenol adduct, an intermediate identified during the oxidation of phenols by tyrosinase. The labile coordination of the axial ligand (phenol in this case) and the enhanced catalytic activity of the encapsulated dimeric CuAc and CuClAc could both be attributed, perhaps, to the shorter Cu-Cu distance and consequent greater interaction between the two copper ions in the encapsulated state compared to the "neat" complex. The short Cu-Cu distance and the consequent greater, lateral overlap of the copper orbitals would facilitate the transfer of electron density from the phenolate ligand to the antibonding LUMO of the complex, thereby weakening the O-O and the Cu-O bonds. Weakening of these bonds would, in turn, make it easier for the cleavage and the transfer of one of the two oxygens of the peroxide ligand to the position *ortho* to the phenolate bond.

Analogous rhodium complexes having direct overlap of the metal orbitals also exhibit such a *trans*-axial lability and consequent enhanced catalytic activity

(35). In quadruply-bridged dinuclear platinum clusters, with a "lantern-type" structure similar to copper acetate, a strengthening of the metal-

metal bond often leads to a decrease in the strength of the metal-axial ligand bond (36).

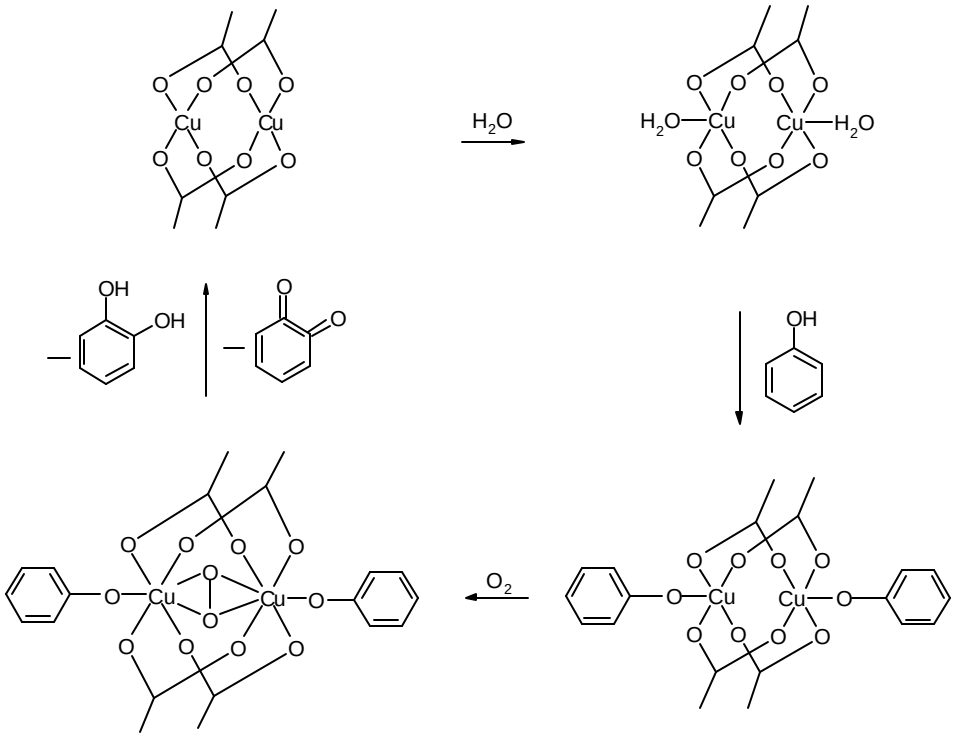

Fig. 3.16 Mechanism for the *ortho*-hydroxylation of phenol by dimeric copper acetato complexes.

A qualitative and preliminary picture of the mechanism of oxidation that emerges from this study is shown in Fig. 3.16. Under the reaction conditions (pH = 6.5), the phenols exist in the phenolate form. Two phenolate ions coordinate to the two Cu(II) ions of the copper acetate dimer, reducing them to the Cu(I) oxidation state. Next, dioxygen reacts with the copper-phenolate complex forming Cu_2-O_2-

phenolate adduct. The latter undergoes an O-O bond scission concomitant with the hydroxylation of substrate. The acetate group can change its mode of coordination from a bidentate to a monodentate type as consequences of forming the dioxygen adduct. Such a coordination lability is common in the enzymatic reactions.

3.4 Conclusions

The cause of enhancement in the catalytic activity of dimeric copper acetate and copper chloroacetate complexes in the *ortho*-hydroxylation of phenols when encapsulated in zeolite-Y are investigated. EPR spectra confirm the location of these complexes in the supercages of zeolite-Y. Even though, the stoichiometric integrity of the complex is conserved upon encapsulation, the shift in the vibrational and electronic band positions clearly reveal changes in the carboxylato-bridge coordination. The variation in EPR spectral intensities in the range of 77 – 298 K indicates that the Cu-Cu antiferromagnetic exchange interaction increases upon encapsulation due to the compression of the Cu-Cu separation to 2.40 Å from 2.64 Å for the "neat" CuAc complex. The corresponding decrease for CuClAc is from 2.92 Å ("neat") to 2.73 Å (encapsulated). The steric constraints imposed by the cavities of the zeolite probably cause the changes in the structure of these encapsulated complexes. Due to the greater Cu-Cu bonding, the strength and the lability of the Cu-phenolate and Cu-dioxygen bonds are modified by a *trans*-axial ligand effect, leading to enhanced reactivity of the encapsulated complex. There is, hence, a direct, causal relationship between the shortening of the internuclear Cu-Cu distance upon encapsulation and the enhanced reactivity of the resultant, structurally

modified complex. The geometric (and the consequent electronic) changes are probably at the origin of the enhanced catalytic activity of the encapsulated complexes. Hence, by varying the substituent groups on the acetate ligand and the shape and size of the zeolite cavity, one should be able, at least in principle, to design suitable solid catalysts for selective oxidation reactions at low temperatures in the liquid phase.

3.5 References

1. Solomon, E. I., Penfield, K. W., and Wilcox, D. E., *Struct. Bonding*, **53**, 1 (1983).
2. Messerschmidt, A., *Strut. Bonding*, **90**, 37 (1998).
3. Abolmaali, B., Taylor, H. V., and Weser, U., *Struct. Bonding,* **91**, 91 (1998).
4. Sykes, A.G., *"Active-site Properties of the Blue Copper Proteins," Adv. Inorg. Chem.*, **36**, 377 (1991).
5. Messerschmidt, A., *"Blue Copper Oxidases," Adv. Inorg. Chem.*, **40**, 121 (1994).
6. Wolfgang, K., and Jochen, R., *Angew. Chem. Int. Ed. Engl.*, **35**, 43 (1996).
7. Solomon, E. I., Tuczek, F., Root, D. E., and Brown, C. A., *Chem Rev.*, **94,** 827 (1994).
8. Holland, P. L., and Tolman, W. B., *Coord. Chem. Rev.*, **190 – 192,** 855 (1999).
9. Mukherjee, R. N., *Curr. Sci.*, **72,** 802 (1997).
10. Sorrell, T. N., *Tetrahedron,* **45,** 3 (1989).
11. Kitajima, N., and Moro-Oka, Y., *J. Chem. Soc. Dalton Trans.*, **18,** 2665 (1993).
12. Kitajima, N., *Bioinorg. Chem. Copper,* **251.**
13. Corma, A., Navarro, M. T., and Pariente, J. P., *J. Chem. Soc., Chem.*

Commun., 147 (1994).

14. Jacob, C. R., Varkey, S. P., and Ratnasamy, P., *Appl. Catal. A,* **182,** 91 (1999).

15. Deshpande, S., Srinivas, D., and Ratnasamy, P., *J. Catal.,* **188,** 261 (1999).

16. Herron, N., *CHEMTECH,* 543 (1989).

17. Gao, J., and Zhong, S. –H., *J. Mol. Cat.A,* **168,** 1 (2001).

18. Raja, R., and Ratnasamy, P., *J. Mol. Catal. A,* **100,** 93 (1995).

19. Eswaramoorthy, M., Neeraj, and Rao, C. N. R., *J. Chem. Soc., Chem Commun.,* 615 (1998).

20. Bleaney, B., and Bowers, K. D., *Proc. Roy. Soc. London,* **214A,** 451 (1952).

21. Abe, H., and Shimada, J., *Phys. Rev.,* **90,** 316 (1953).

22. Van Niekerk, J. N., and Schoening, F. R. L., *Acta Crystallogr.,* **6,** 227 (1953).

23. De Meester, P., Fletcher, R., and Skapski, A. C., *J. Chem. Soc., Dalton Trans.,* 2575 (1973).

24. Guha, B. C., *Proc. Roy. Soc. London,* **206,** 353 (1951).

25. Figgis, B. N., and Martin, R. L., *J. Chem. Soc.,* 3837 (1956).

26. Kato, M., and Muto, Y., *Coord. Chem.Rev.,* **92,** 45 (1988).

27. Smith, T. D., and Pilbrow, J. R., *Coord. Chem.Rev.,* **13,** 173 (1974).

28. Mehrotra, R. C., and Bohra, R., *"Metal Carboxylates,"* Academic Press, New York (1983).

29. Naccache, C., and Ben Taarit, Y., *Chem. Phys. Lett.,* **11**, 11 (1971).

30. Herman, R. G., and Flentge, D. R., *J. Phys. Chem.,* **82,** 720 (1978).

31. Bersuker, I. B., *The Jahn-Teller Effect and Vibrionic Interactions in Modern Chemistry,* Plenum, New York, 1984.

32. Riley, M. J., Hitchman, M. A., and Mohammed, A.W., *J. Chem. Phys.,* **87**, 3766 (1987).

33. Bertini, A., and Gatteschi, D., *EPR of Exchange Coupled Systems,* Chap. 10, Springer Verlag, Berlin (1990).

34. Solomon, E. I., and Lowery, M. D., *Science,* **259,** 1575 (1993).

35. Felthouse, T. R., *Prog, Inorg. Chem.*, **29,** 73 (1982).

36. Umakoshi, K., and Sasaki, Y., in: *"Advances in Inorganic Chemistry"*, Vol. **40**, p. 187, Sykes A. G (Ed..), Academic Press, New York (1993).

Chapter-4

Structure of the Active Catalyst in the Liquid Phase Oxidation of *Para*-Xylene to Terephthalic Acid by Co/Mn/Br- System

4.1 Introduction

Selective oxidation of petroleum hydrocarbon feed-stocks such as alkanes, olefins and aromatics in the liquid phase, using air/oxygen, is an important reaction. Some notable examples are the oxidation of *para*-xylene to terephthalic acid, of cyclohexane to cyclohexyl hydroperoxide and cyclohexanone/cyclohexanol, of cumene to cumene hydroperoxide and of *iso*-butane to *tert*-butyl hydroperoxide and *tert*-butyl alcohol. These reactions belong to the class of "autoxidations" wherein molecular oxygen is activated via., a free-radical chain mechanism process. They are also classified as homolytic processes, as they originate from the homolytic breakage of the C-H bond.

Terephthalic acid (TA), one of the largest volume commodity chemicals, is commercially manufactured by the selective dioxygen oxidation of *para*-xylene (PX), using a catalyst combination of cobalt and manganese salts and a bromide ion promoter, in acetic acid (HOAc) medium, at 443 – 483 K (1, 2). TA is principally used as raw material for the manufacture of polyesters. The commercial process has been optimized to the point where typical crude TA purities of 98 – 99.5% are produced, in yields of 96 – 97 mol% based on PX feed, at an oxidizer contact time of 45 – 90 min. However, the following three improvements are desirable in the existing process:

(i) reduction or elimination of significant HOAc oxidation to CO or CO_2 (5 – 10 wt.% of TA); this can perhaps be achieved by the use of more efficient radical promoters, which allow oxidizer temperatures to be lowered without reduction of the reaction rates,

(ii) alternatives to the highly corrosive HOAc and Br^- promoter, which require the use of expensive titanium steel, and

(iii) reduction or elimination of 4-carboxybenzaldehyde (4-CBA) and other impurities from crude TA, which necessitate elaborate hydrogenation and recrystallization procedures in the manufacture of purified TA, required for the polyester industry.

A better understanding of the *chemistry* of the catalyst system is essential to achieve the above process improvements. Surprisingly, even though the kinetics of the reaction network and the process engineering aspects of the manufacture of TA have been thoroughly investigated (3 – 17), there are comparatively fewer studies devoted to the identity and the role of the catalytically active cobalt and manganese species involved in the complex series of reactions in the conversion of PX to TA (18 – 20). Similarly, the roles of the promoter Br^-, the solvent HOAc and other additives used in the industrial process, are also not well understood. The mechanism of PX oxidation is believed to begin with a hydrogen atom abstraction from the methyl group by the bromine atom. The resultant benzyl radical adds to O_2 and proceeds through the hydroperoxide to *p*-tolyl alcohol, *p*-tolualdehyde and *p*-toluic acid. Hydrogen atom abstraction from the methyl group in *p*-toluic acid generates a secondary benzyl radical, which follows the same pathway to yield eventually, TA (Scheme 4.1).

The transition metals (Co and Mn) are found to be responsible for the chain initiation, propagation and decomposition of the various peroxides formed during the reaction, as well as the conversion of Br^- to $Br^\bullet$ (8, 9). The active forms of cobalt and manganese in the systems, however, are still not

established with certainty, although several mononuclear, Co(OAc)Br (9, 15), binuclear, $[Co_2(OH)_2(OAc)_4]$ (20, 21) and trinuclear, $[Co_3O(OAc)_5(OH)(OAc)_3]$ and $[Co_3O(OAc)_5(HOAc)_3]$ (22 – 25) complexes have been proposed. It is probable that the identity, concentrations and role of these complexes depend upon the Co/Mn, Br^-/Co and Co/HOAc ratios, presence of additives like Zr and Ce (2), as well as the conditions like temperature, pressure, concentration of dioxygen etc.

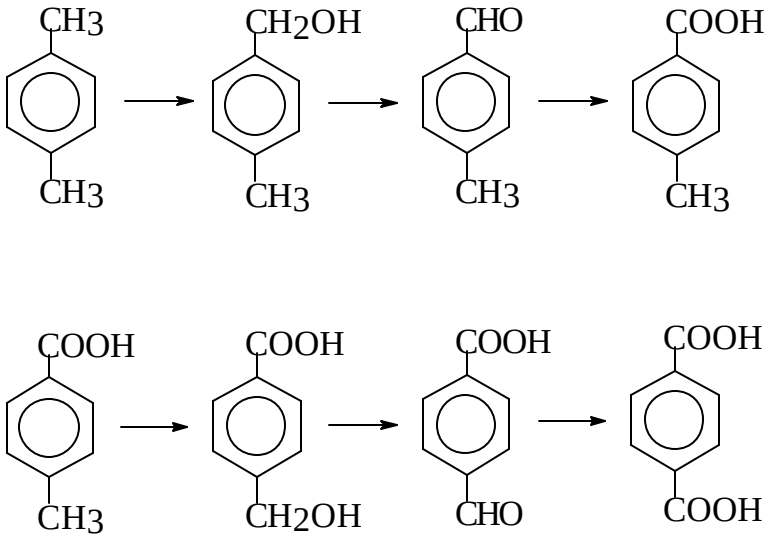

Scheme 4.1

The major objectives of the study in the present chapter are (1) to investigate, using electronic and electron paramagnetic resonance (EPR) spectroscopies, the cobalt and manganese species that are formed during the dioxygen oxidation of PX over the Co and Mn acetate catalyst system, and (2) the influence of additives like Zr, Ce and Ni, on the rates of the oxidation, product distribution and EPR spectra. The catalysis data are supplemented by performing *in situ* electronic and EPR spectral measurements. These spectroscopic techniques are complimentary and powerful to detect even trace

quantities of various species present in the reaction medium and provide a deeper insight into the structure of the catalytically active species (26, 29).

Mn(II) is paramagnetic ($3d^5$, S = 5/2) and shows a resolved hyperfine pattern in the EPR spectrum, even at room temperature. The hyperfine splitting and the other spin Hamiltonian parameters are sensitive to the symmetry and the molecular environment. However, Mn(II) does not show any d-d bands in the electronic spectrum due to the $^6A_{1g}$ ground state and transition to the excited states is spin-forbidden (27). Mn(III), on the other hand, shows characteristic electronic spectral features but is EPR silent due to very high zero-field splitting. The Co(II) ion is also paramagnetic ($3d^7$, S = 3/2), but due to the short spin lattice relaxation times, it's EPR signals cannot be detected at ambient temperatures and the measurements need to be performed below liquid nitrogen or at liquid helium temperatures (28). However, both Co(II) and Co(III) exhibit distinct electronic spectra even at room temperature (12, 15). Thus, a combined study using both electronic and EPR spectroscopies can yield significant insight into the identity and role of Co and Mn species formed during the oxidation reaction. A detailed EPR spectroscopic study of this catalyst system and the influence of Zr and Ni and bromide ion promoter have not been published so far.

4.2 Experimental

4.2.1 Materials and Reaction Methodology

The materials $Co(OAc)_2.4H_2O$, $Mn(OAc)_2.4H_2O$, $Ni(OAc)_2.4H_2O$, $Ce(NO_3)_3$, NaBr, glacial HOAc, PX and others were used as received. The preparation of $Zr(OH)_4$ and reaction methodology are described in Chapter 2.

4.3 Results and Discussion

4.3.1 *In Situ* Spectroscopic Studies

4.3.1. 1 Electronic Spectroscopy

In situ electronic spectral studies were carried out on the following homogenous solutions:

(a) $Co(OAc)_2.4H_2O$ (1.03 mmol) / NaBr (1.35 mmol) / HOAc (587 mmol) / H_2O (311 mmol) / air.

(b) $Co(OAc)_2.4H_2O$ (1.03 mmol) / NaBr (1.35 mmol) / HOAc (587 mmol) / H_2O (311 mmol) / PX (44.3 mmol) / air.

(c) $Co(OAc)_2.4H_2O$ (1.03 mmol) / $Mn(OAc)_2.4H_2O$ (0.35 mmol) / NaBr (1.35 mmol) / HOAc (587 mmol) / H_2O (311 mmol) / PX (44.3 mmol) / air.

(d) $Co(OAc)_2.4H_2O$ (1.03 mmol) / $Mn(OAc)_2.4H_2O$ (0.35 mmol) / NaBr (1.35 mmol) / HOAc (587 mmol) / PX (44.3 mmol) / H_2O (311 mmol) / H_2O_2.

(e) $Mn(OAc)_2.4H_2O$ (1.03 mmol) / NaBr (1.35 mmol) / HOAc (587 mmol) / H_2O (311 mmol) / PX (44.3 mmol) / air.

A known amount of solution was taken out from the reaction vessel (maintained at 363 K), at specified times, quenched quickly and the electronic spectrum was recorded at 298 K, in the wavelength range 200 – 900 nm. The solution containing $Co(OAc)_2.4H_2O$ / NaBr / HOAc / H_2O showed a broad asymmetric band, with a band maximum at 520 nm and two shoulders at 470 and 450 nm. These bands correspond to d-d transitions of an octahedrally coordinated Co(II)-acetato complex (12, 25). The solution on contact with oxygen (air) (solution (a)) showed marked changes in the electronic spectrum. Representative spectra of $Co(OAc)_2.4H_2O$ / NaBr / HOAc / H_2O / air solutions are shown in Fig. 4.1(a). The optical density of the band, at 520 nm, increased

gradually on interaction with oxygen and a new, weak band, characteristic of the Co(III)-acetato complex appeared at 630 nm (12). The enhanced optical density of the band at 520 nm suggests the formation of yet another Co(II) complex, Co(OAc)Br having a symmetry lower than that of $Co(OAc)_2.4H_2O$. The lower symmetry of Co(OAc)Br admixes the molecular orbitals and allows the d-d transitions. As a consequence, the intensity of the d-d transitions for Co(OAc)Br are higher than that of $Co(OAc)_2.4H_2O$ (Fig 4.1(a)).

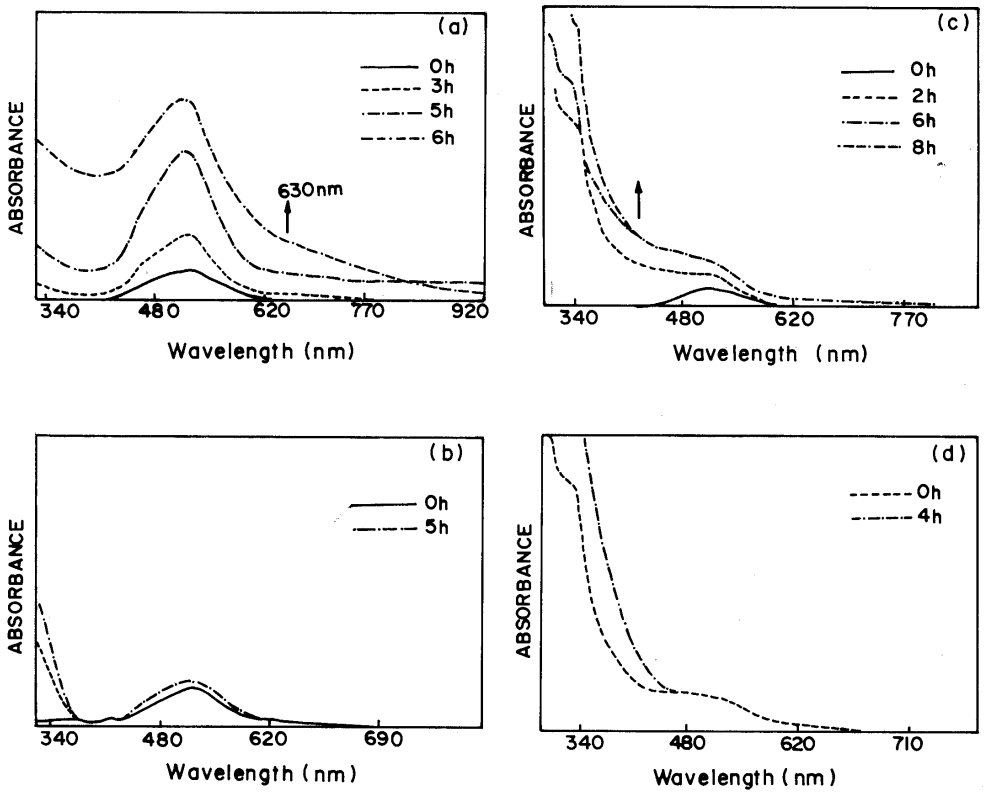

Fig. 4.1 Electronic spectra as a function of time: (a) $Co(OAc)_2.4H_2O$ (1.03 mmol) / NaBr (1.35 mmol) / HOAc (587 mmol) / H_2O (311 mmol) / air; (b) $Co(OAc)_2.4H_2O$ (1.03 mmol) / NaBr (1.35 mmol) / HOAc (587 mmol) / H_2O (311 mmol) / PX (44.3 mmol) / air; (c) $Co(OAc)_2.4H_2O$ (1.03 mmol) / $Mn(OAc)_2.4H_2O$ (0.35 mmol) / NaBr (1.35 mmol) / HOAc (587 mmol) / H_2O (311 mmol) / PX (44.3 mmol) / air; (d) $Co(OAc)_2.4H_2O$ (1.03 mmol) / $Mn(OAc)_2.4H_2O$ (0.35 mmol) / NaBr (1.35 mmol) / HOAc (587 mmol) / H_2O (311 mmol) / PX (44.3 mmol) / H_2O_2.

Interestingly, solution (b), containing the substrate PX, (Fig. 4.1(b)) did not show the above spectral changes even after several hours, on interaction

with air. This difference in the spectral behavior in the presence of PX, indicates that Co(III)-acetato and Co(OAc)Br species, formed during the dioxygen (air) oxidation are highly reactive towards the substrate PX and, hence, have very short lifetimes.

To elucidate the role of $Mn(OAc)_2.4H_2O$ in the homogeneous catalyst combination, spectral studies were carried on the system $Co(OAc)_2.4H_2O$ / $Mn(OAc)_2.4H_2O$ / NaBr / HOAc / H_2O / PX (solution (c)). $Mn(OAc)_2.4H_2O$ does not exhibit any band due to metal-centered, d-d transitions. However, on interaction with oxygen (air), new features characteristic of an oxo-bridged Mn(III) cluster complex (30 – 32) appeared at 460 and 350 nm, in addition to the band at 520 nm. The latter is characteristic of $Co(OAc)_2.4H_2O$. The band at 460 nm corresponds to the d-d transition while that at 350 nm is attributed to the ligand-to-metal charge transfer (LMCT) transition (30 – 32). Co(III)-acetato complexes (630 nm), could not be detected in the spectrum for $Co(OAc)_2.4H_2O$ / $Mn(OAc).4H_2O$ / NaBr / HOAc / H_2O / PX / air. The intensity of the bands at 460 and 350 nm, due to the Mn(III) cluster complex increased during the course of the reaction. Typical spectra for solution (c) are shown in Fig. 4.1(c).

The Mn(III)-oxo cluster complexes are also seen when H_2O_2 is substituted for oxygen (air) (solution (d), Fig. 4.1(d)). In the oxidation with air, the reaction had to be carried out for a minimum period of 3 – 5 h, before Mn(III)-oxo cluster complexes could be detected. They are, however, formed instantaneously on the addition of H_2O_2 (compare Fig. 4.1(d) with Fig. 4.1(c)). In the absence of cobalt, solutions containing only manganese, like solution (e), $Mn(OAc)_2.4H_2O$ / NaBr / HOAc / H_2O / PX / air, did not reveal the formation

of Mn(III)-oxo cluster complexes. When Co(II) is present, it is probably oxidized initially to a Co(III) complex, which promotes the oxidation of Mn(II) to a Mn(III)-oxo cluster complex. When H_2O_2 was used as the oxidant, both Co(II) and Mn(II), are oxidized simultaneously to their corresponding +3 oxidation states.

4.3.1.2 EPR Spectroscopy

EPR investigations were carried out on the following reaction mixtures:

(i) $Co(OAc)_2.4H_2O$ (1.03 mmol) / NaBr (1.35 mmol) / HOAc (587 mmol) / H_2O (311 mmol); ($Co : Br^- = 3 : 4$ mmol).

(ii) $Co(OAc)_2.4H_2O$ (1.03 mmol) / NaBr (1.35 mmol) / HOAc (587 mmol) / H_2O (311 mmol) / pyridine (25 mmol) / H_2O_2; ($Co : Br^- = 3 : 4$ mmol).

(iii) $Co(OAc)_2.4H_2O$ (1.03 mmol) / $Mn(OAc)_2.4H_2O$ (0.35 mmol) / NaBr (1.35 mmol) / HOAc (587 mmol) / H_2O (311 mmol) / PX (44.3 mmol) / air; ($Co : Mn : Br^- = 3 : 1 : 4$ mmol).

(iv) $Co(OAc)_2.4H_2O$ (0.35 mmol) / $Mn(OAc)_2.4H_2O$ (1.03 mmol) / NaBr (1.35 mmol) / HOAc (587 mmol) / H_2O (311 mmol) / PX (44.3 mmol) / air; ($Co : Mn : Br^- = 1 : 3 : 4$ mmol).

(v) $Mn(OAc)_2.4H_2O$ (1.03 mmol) / NaBr (1.35 mmol) / HOAc (587 mmol) / H_2O (311 mmol) / PX (44.3 mmol) / air; ($Mn : Br^- = 3 : 4$ mmol).

(vi) $Co(OAc)_2.4H_2O$ (1.03 mmol) / $Mn(OAc)_2.4H_2O$ (0.35 mmol) / $Zr(OH)_4$ (0.1 mmol) / NaBr (1.35 mmol) / HOAc (587 mmol) / H_2O (311 mmol) / PX (44.3 mmol) / air; ($Co : Mn : Zr : Br^- = 3 : 1 : 0.3 : 4$ mmol).

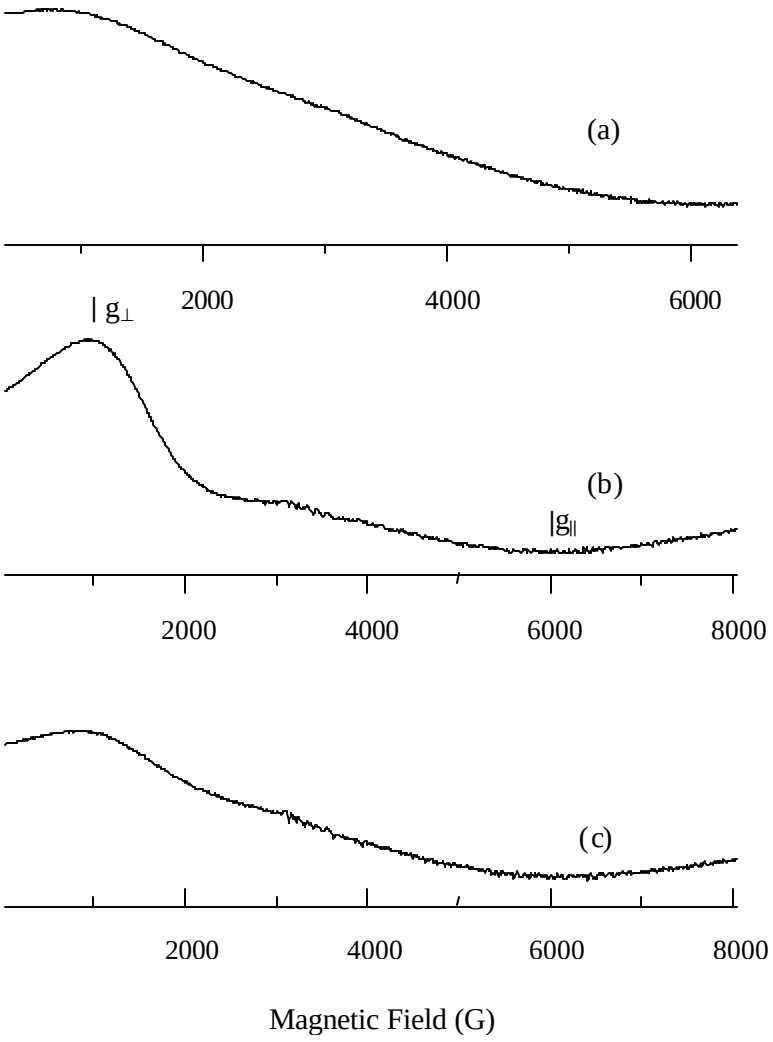

Fig. 4.2 X-band EPR spectra at 77 K: (a) $Co(OAc)_2.4H_2O$ (1.03 mmol) / NaBr (1.35 mmol) / HOAc (587 mmol) / H_2O (311 mmol); (b) $Co(OAc)_2.4H_2O$ (1.03 mmol) / NaBr (1.35 mmol) / HOAc (587 mmol) / H_2O (311 mmol) / pyridine (25 mmol); (c) $Co(OAc)_2.4H_2O$ (1.03 mmol) / NaBr (1.35 mmol) / HOAc (587 mmol) / H_2O (311 mmol) / pyridine (25 mmol) / H_2O_2.

Solution (i) did not show any EPR signal at 298 K, but at 77 K a broad symmetric signal with a width of about 5500G was observed (Fig. 4.2 (a)). The broad feature is due to the short electron spin lattice relaxation time of Co(II) ions in HOAc. However, upon adding pyridine (py), the purple colored

solution (ii) showed a spectrum characterized by an axially symmetric g tensor ($g_{\perp}$ = 7.02 and $g_{||}$ = 1.11) (Fig. 4.2(b)). The signals are attributed to the $Co(OAc)_2(py)_x$ complex (33). Upon interaction with H_2O_2, the overall spectral intensity decreased by about 30% and the signal was further broadened (Fig.4.2 (c)). The reduction in spectral intensity reveals the formation of Co(III) acetato/oxo-bridged Co(III) cluster complexes. It may be noted that oxo-bridged cluster complexes of the composition $[Co_3O(OAc)_6(py)_3]^+$ and $[Co_3O(OAc)_5(OH)(py)_3]^+$ have been isolated and structurally characterized by Sumner and Steinmetz (23, 24) and Beattie et al (34).

Narrow signals due to Mn(II) dominated those of high spin Co(II) in solutions (iii), (iv) and (vi). Solution (iii) showed a resolved sextet, hyperfine pattern due to Mn(II) at 298 K (Fig. 4.3(a)). The spin Hamiltonian parameters (g_{iso} = 2.0012 and A_{iso} = 93.8 G) indicate an octahedral geometry for the Mn(II) ion (35). On passing air through the reaction mixture for 3 h, the overall intensity of the spectrum decreased by about 35% (Fig 4.3 (b)) suggesting oxidation of part of Mn(II) to Mn(III) ions. The spectra at 77 K consist of an unresolved central zero-field signal (m_S: -1/2 $\leftrightarrow$ +1/2), typical for weakly interacting Mn(II) ions in linear, trimeric $Mn(OAc)_2.4H_2O$ complex (Figs. 4.3(c) and (d)). At 77 K, interaction with air showed improved resolution of manganese hyperfine features (Fig. 4.3(d)).

Solution (iv) containing 0.35 mmol of cobalt and 1.03 mmol of manganese salts showed similar spectral behavior as that of solution (iii) (Fig. 4.4(a)). The overall intensity of the sextet pattern at 298 K, decreased during air oxidation (Fig. 4.4(a) – 4.4(c)). The outermost hyperfine signals became more intense than the inner ones. The linewidth increased from 45 to 72 G on

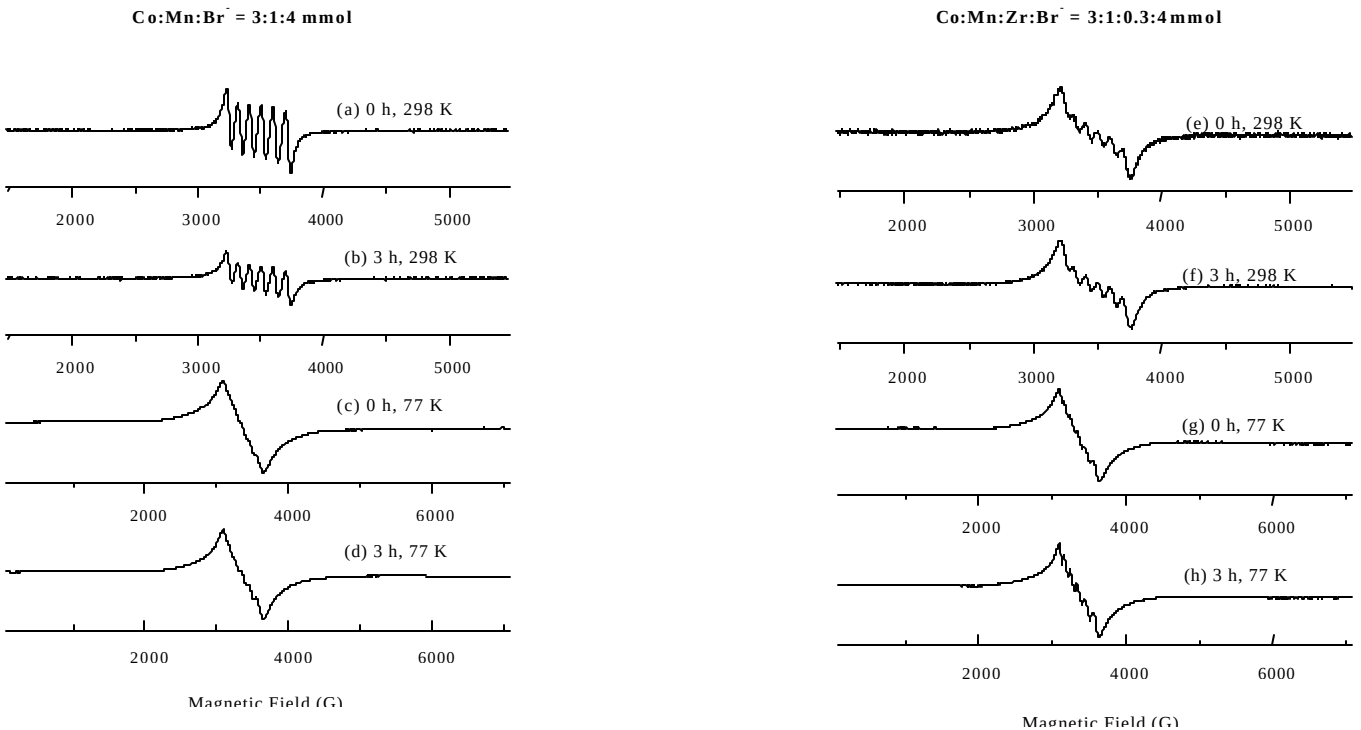

Fig. 4.3 EPR spectra of $Co(OAc)_2.4H_2O$ (1.03 mmol) / $Mn(OAc)_2.4H_2O$ (0.35 mmol) / NaBr (1.35 mmol) / HOAc (587 mmol) / H_2O (311 mmol) / PX (44.3 mmol) / air at: (a) 0 h, 298 K; (b) 3 h, 298 K; (c) 0 h, 77 K; (d) 3 h, 77 K, respectively, and $Co(OAc)_2.4H_2O$ (1.03 mmol) / $Mn(OAc)_2.4H_2O$ (0.35 mmol) / $Zr(OH)_4$ (0.1 mmol) / NaBr (1.35 mmol) / HOAc (587 mmol) / H_2O (311 mmol) / PX (44.3 mmol) / air at: (e) 0 h, 298 K; (f) 3 h, 298 K; (g) 0 h, 77 K; (h) 3 h, 77 K, respectively.

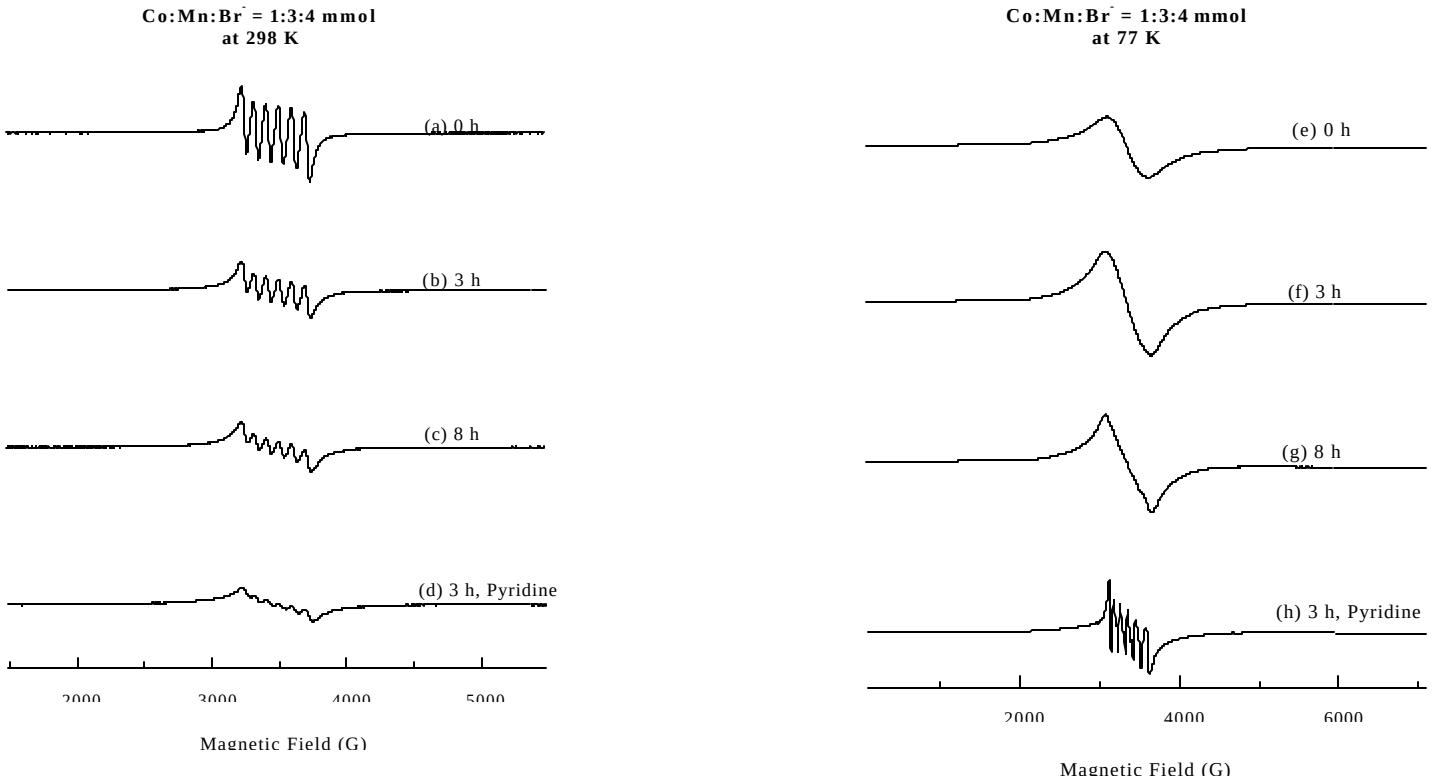

Fig. 4.4 EPR spectra, as a function of time, of $Co(OAc)_2.4H_2O$ (0.35 mmol) / $Mn(OAc)_2.4H_2O$ (1.03 mmol) / NaBr (1.35 mmol) / HOAc (587 mmol) / H_2O (311 mmol) / PX (44.3 mmol) / air. Curves (a) – (d) refer to (a) 0 h; (b) 3 h; (c) 8 h and (d) 3 h with pyridine at 298 K an curves (e) – (f) refer to (e) 0 h; (f) 3 h; (g) 8 h and (h) 3 h with pyridine at 77 K, respectively.

interaction with oxygen (air) (Table 4.1). Moreover, changes in spin Hamiltonian parameters (g_{iso} = 2.0005 and A_{iso} = 94.6 G) were also noticed during the course of reaction. Addition of pyridine to the reaction mixture showed marked changes in the overall spectral intensity as well as the intensity of outer and innermost hyperfine signals (compare Fig. 4.4(b) with 4.4(d)). The spectrum could be fitted to the presence of two types of signals overlapping with each other, one with a sextet pattern corresponding to monomeric Mn(II) in $Mn(OAc)_2(py)_4$ complex (g_{iso} = 2.000 and A_{iso} = 92 G) (35) and the other, a broad signal at g_{iso} = 1.992, due to the Mn cluster complex $Mn_3O(OAc)_6(py)_3$ (30, 32). The spectra for solution (iv) recorded at 77 K, are depicted in Fig. 4.4 (e) – 4.4(h). Addition of pyridine enhanced the formation of oxo-bridged Mn cluster complexes. The resolved Mn hyperfine features at 77 K in pyridine–containing solutions are typical of non-interacting Mn(II) ions (Fig. 4.4(h)); the Mn(III) cluster complexes were EPR silent at 77 K due to the intermolecular antiferromagnetic interactions. The broad signal for the cluster complex at 298 K arises, perhaps, due to population of low lying paramagnetic excited triplet states (S′ = 1) (30).

Solution (vi) is similar to solution (iii) except that the former contains a small quantity of $Zr(OH)_4$ (0.1 mmol) as an additive. Their spectra are, however, markedly different (compare Figs. 4.3(e) – 4.3(h) with Figs. 4.3(a) – 4.3(d)). The manganese hyperfine pattern is well resolved in solution (iii) without Zr(IV) ion, while solution (vi) containing Zr(IV) additive showed a partially resolved hyperfine pattern (similar to that observed for (iii) and (iv) after interacting with air for several hours; see Figs. 4.4(c) and 4.4(d) for comparison). Surprisingly, unlike solutions (iii) and (iv), the solution

containing Zr(IV) ion showed no change in overall spectral intensity even after 8 h of interaction with air (see Figs. 4.3(e) and 4.3(f)). The spectra at 77 K (Figs. 4.3(g) and 4.3(h)) resemble those of solution (iii) at 77 K (Figs. 3(c) and (d)). However, they are significantly different from those of solution (iv) (Figs. 4.4(e) and 4.4(g)). This difference in spectral behavior is due to the following reasons: The presence of Zr(IV) enhances the oxidation of Co(II) to Co(III) and subsequently, Mn(II) to Mn(III). This enhancement enables the formation of Mn(III) cluster complexes. These cluster complexes are different in composition in solutions (iii), (iv) and (vi). From the spectral differences, it may be concluded that solution (iv) contains homonuclear $Mn_3(O)(OAc)_x$ type clusters characterized by g_{iso} = 2.0005 and spectral width = 525 G as the major species with a minor component being $CoMn_2(O)(OAc)_x$ clusters; solutions (iii) and (vi) contain the heteronuclear clusters of the type $Co_2Mn(O)(OAc)_x$ as predominant species and $Co_3(O)(OAc)_x$ and $CoMn_2(O)(OAc)_x$ as minor species (characterized by g_{iso} = 2.0012 and spectral width = 516 G for solution (iii) and g_{iso} = 1.998 and spectral width = 547 G for solution (vi)).

Solution (v) containing $Mn(OAc)_2.4H_2O$ (1.03 mmol) / NaBr (1.35 mmol) / HOAc (587 mmol) / H_2O (311 mmol) / PX (44.3 mmol) shows resolved hyperfine pattern as observed for solution (iv) (Fig. 4.4(a)). The changes are only marginal on interaction with air. This result is in agreement with the electronic spectral studies. Both the spectral techniques suggest that the oxidation of Mn(II) to Mn(III) species is difficult in the absence of cobalt or zirconium salts. Table 4.1 gives a summary of the EPR spin Hamiltonian parameters at 298 K.

Table 4.1 EPR Spin Hamiltonian Parameters of Mn in Co/Mn/Zr/Br System at 298 K

Catalyst[a]	Conditions[b]	g_{iso}	A_{Mn} (G)	ΔH_{pp} (G)	Spectral width (G)	Remarks
Co(1.03)+Mn(0.35)+Br(1.35)	without O_2, 0 h	2.0012	93.8	45	511	resolved sextet
	with O_2, 3 h	2.0012	92.0	45	516	resolved sextet
	with O_2, 3h + py	1.9960	92.0	85	526	interacting Mn clusters
Co(1.03)+Mn(0.35)+Br (1.35)	without O_2, 0 h	2.0014	93.8	45	511	resolved sextet
	with O_2, 3h	2.0012	93.6	60	516	small amounts of interacting Mn clusters
	with O_2, 8h	2.0005	94.6	72	525	interacting Mn clusters
	with O_2, 8h + py	1.9920	92.0	85	530	high amounts of interacting Mn clusters
Co(1.03)+Mn(0.35)+Zr(0.1)+ Br(1.35)	without O_2, 0 h	2.0015	94.6	95	546	interacting Mn clusters
	with O_2, 3 h	2.0000	94.6	95	547	interacting Mn clusters
	with O_2, 5 h	1.9980	94.6	95	547	high amounts of interacting Mn clusters
Co(1.03)+Mn(0.35)+Br(2.03)	without O_2, 0 h	2.0000	93.0	70	548	Interacting Mn clusters
	with O_2, 1 – 7 h	2.0000	92.0	75	544	interacting Mn clusters
Co(1.03)+Mn(0.35)+Br(6.09)	without O_2, 0 h	2.0025	93.8	55	527	resolved sextet
	with O_2,1 – 5 h	2.0025	93.8	55	527	resolved sextet
Co(1.03)+Mn(0.35)+Br(10.2)	without O_2, 0 h	2.0025	93.8	58	528	resolved sextet
	with O_2, 1 - 5 h	2.0025	93.8	58	528	resolved sextet

[a]Values in the parentheses refer to the number of mmol of catalyst in AcOH.
[b]Air was the source of O_2.

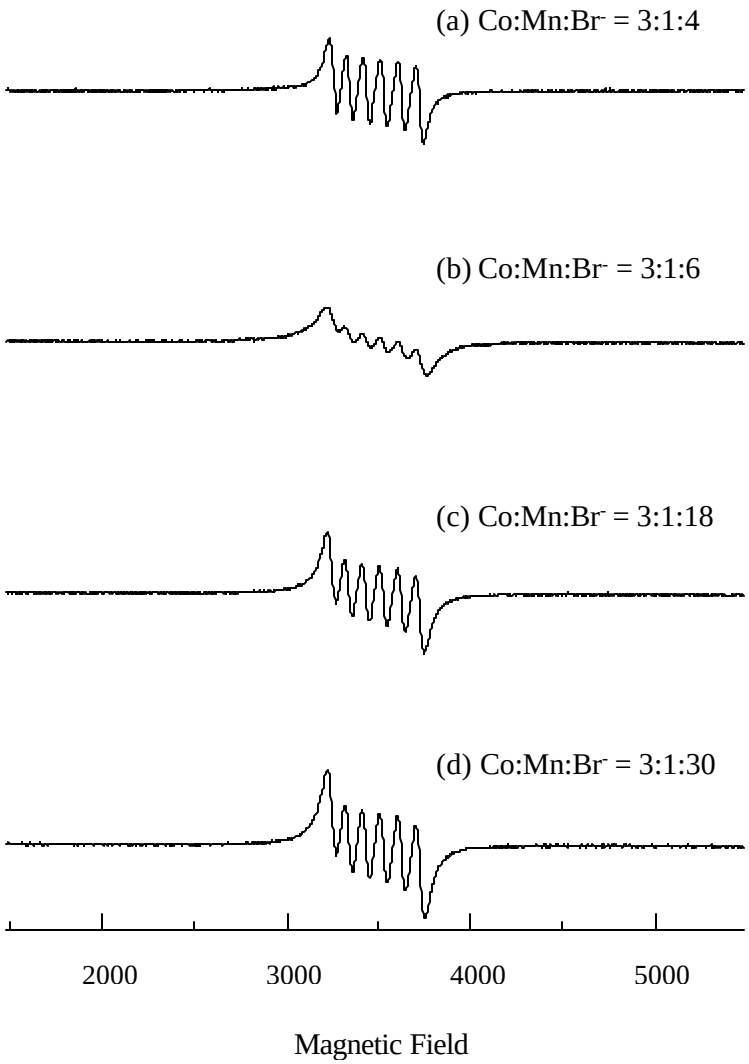

Fig. 4.5 Influence of Br^- on the EPR spectra of $Co(OAc)_2.4H_2O$ (1.03 mmol) / $Mn(OAc)_2.4H_2O$ (0.35 mmol) / NaBr (x mmol) / HOAc (587 mmol) / H_2O (311 mmol) / PX (44.3 mmol) / air; x = 1.35, 2.03, 6.1 and 10.2 for curves (a) – (d), respectively.

EPR studies were also carried out on the following reaction mixtures (containing excess Br^-) to investigate the effect of bromide ion on the speciation.

(vii) $Co(OAc)_2.4H_2O$ (1.03 mmol) / $Mn(OAc)_2.4H_2O$ (0.35 mmol) / NaBr (2.03 mmol) / HOAc (587 mmol) / H_2O (311 mmol) / PX (44.3 mmol) / air; (Co : Mn : Br^- : 3 : 1 : 6 mmol).

(viii) $Co(OAc)_2.4H_2O$ (1.03 mmol) / $Mn(OAc)_2.4H_2O$ (0.35 mmol) / NaBr (6.09 mmol) / HOAc (587 mmol) / H_2O (311 mmol) / PX (44.3 mmol) / air; (Co : Mn : Br^- : 3 : 1 : 18 mmol).

(ix) $Co(OAc)_2.4H_2O$ (1.03 mmol) / $Mn(OAc)_2.4H_2O$ (0.35 mmol) / NaBr (10.2 mmol) / HOAc (587 mmol) / H_2O (311 mmol) / PX (44.3 mmol) / air; (Co : Mn : Br^- : 3 : 1 : 30 mmol).

Fig. 4.5 depicts the EPR spectra at 298 K of the reaction mixtures containing different concentrations of NaBr before reacting with O_2 (air, 0 h). The type of manganese species varies with Br^- concentration. The spin Hamiltonian parameters (Table 4.1), especially g_{iso}, ΔH_{pp} and the spectral width are different. Interestingly, the spectrum for solution (vii) (Co : Mn : Br^- molar ratio = 3 :1 : 6, Fig. 4.5(b)) is similar to the oxygenated solutions (iii) and (iv) with low bromide ion contents (e.g., Co : Mn : Br^- = 3 : 1 : 4 mmol; Fig. 4.3 (b)). The spectra are also similar to that of zirconium containing solution (vi) (Fig. 4.3(f)) and reveal the presence of highly interacting Mn cluster species (g_{iso} = 2.000 and spectral width = 544 G). The spectrum for the solution containing lower amounts of Br^- ions (Fig. 4.5 (a)) corresponds to that of $Mn(OAc)_2.4H_2O$ in HOAc. On the other hand, the spectra for solutions having higher amounts of Br^- ion (Fig. 4.5 (c) and 4.5 (d)) indicate the presence of only weakly interacting Mn(II) ions. Thus, the linear, trimeric structure of $Mn(OAc)_2.4H_2O$ is converted to oligomeric species in the presence of cobalt and Br^- ions. At a Co : Mn : Br^- ratio of 3 : 1 : 6, for example, a majority of the

Co and Mn are present as cluster complexes, $Co_2Mn(O)(OAc)_x$ and $CoMn_2(O)(OAc)_x$. At higher Br^- ion concentrations, a linear acetato bridged chain structure, with weakly interacting Mn ions, is formed.

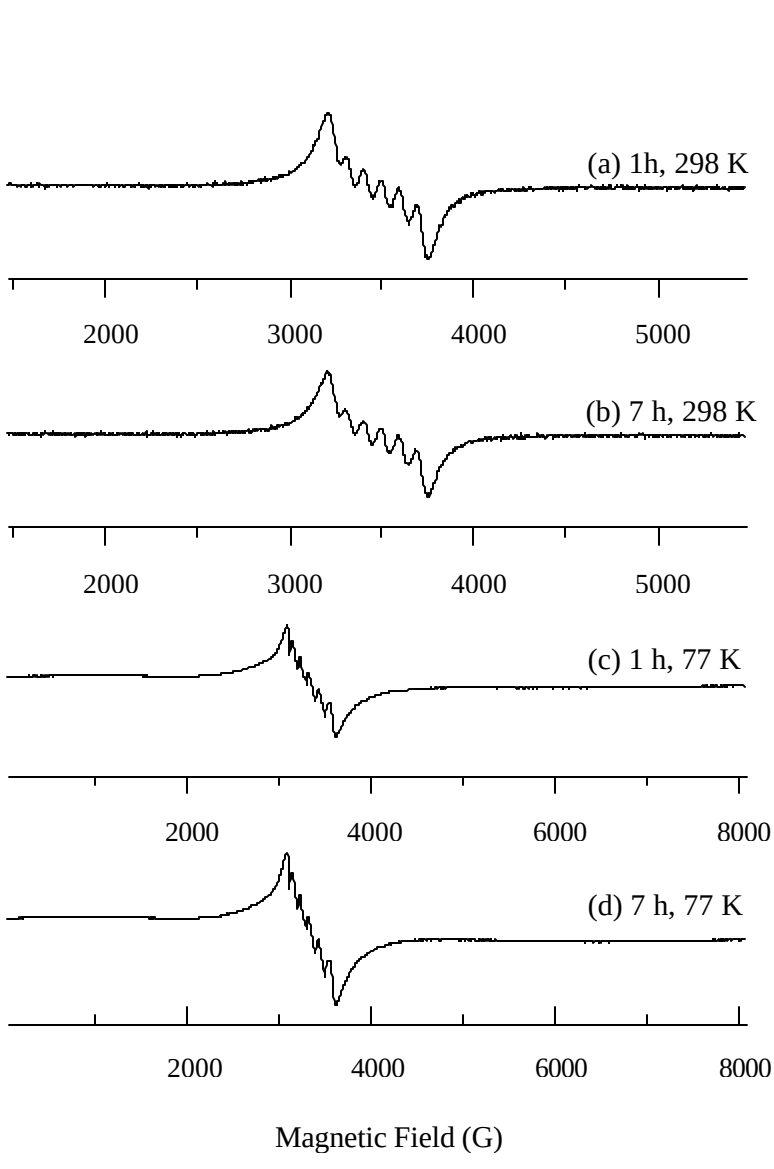

Fig. 4. 6 EPR spectra of $Co(OAc)_2.4H_2O$ (1.03 mmol) / $Mn(OAc)_2.4H_2O$ (0.35 mmol) / NaBr (2.03 mmol) / HOAc (587 mmol) / H_2O (311 mmol) / PX (44.3 mmol) / air: (a) 1 h, 298 K; (b) 7 h, 298 K; (c) 1 h, 77 K; (d) 7 h, 77 K, respectively.

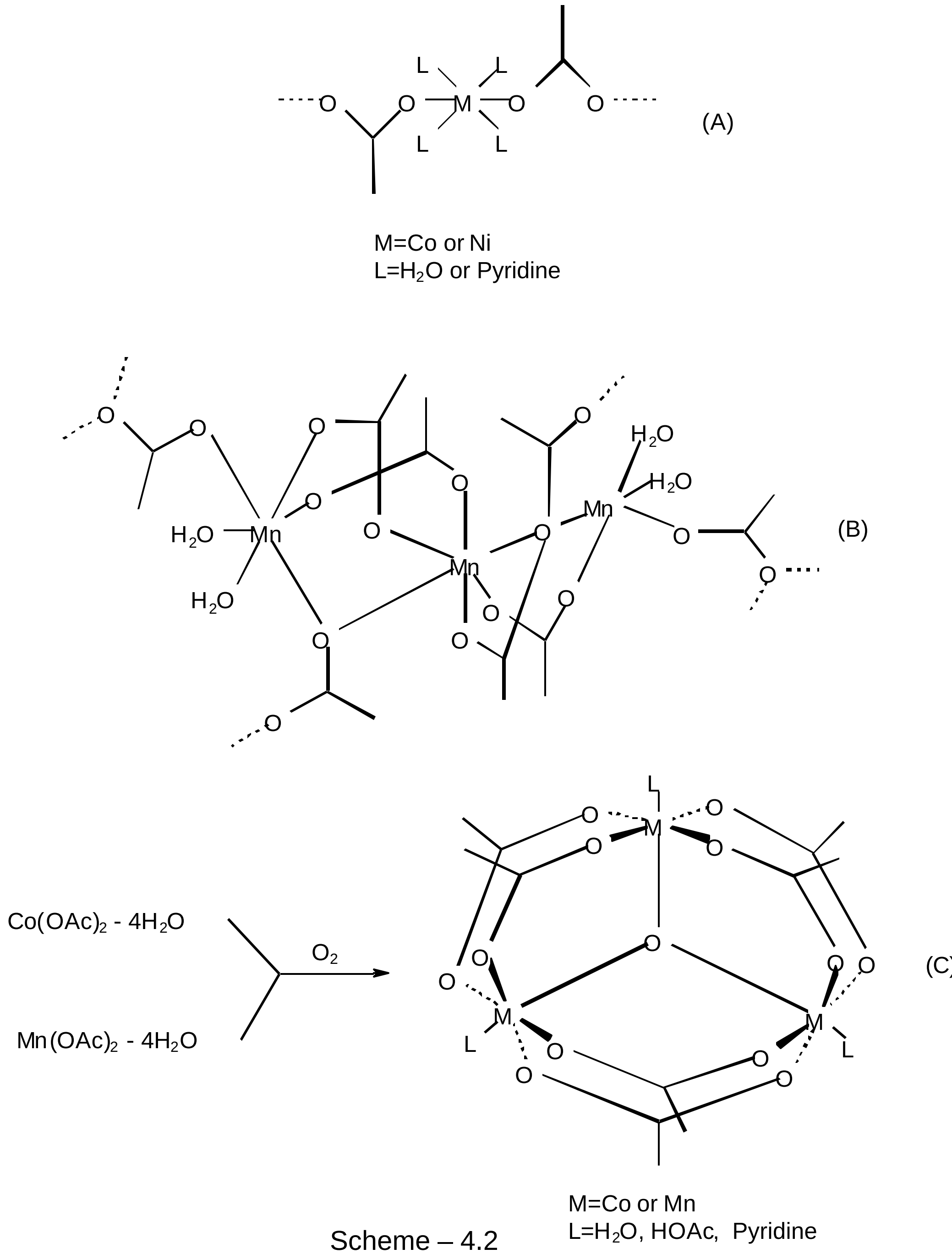

Scheme – 4.2

Typical spectra for solution (vii) are shown in Fig. 4.6. No major changes were noticed in the EPR spectrum during the course of the reaction. The behavior is similar to that of solution (vi) containing zirconium as an additive. In other words, the induction periods to generate the cluster

complexes are reduced considerably by the addition of excess Br^- or zirconium ions. The optimum proportion of the constituents to generate the cluster species was found to be Co : Mn : Br^- = 3 : 1: 6 mmol.

$Co(OAc)_2.4H_2O$ and $Ni(OAc)_2.4H_2O$ have an isomorphous structure in solid state (36) and form one dimensional chains (Scheme 4.2(A)) with acetato ligands bridging adjacent Co or Ni atoms (36). $Mn(OAc)_2.4H_2O$, on the other hand, is trimeric and forms a two dimensional network, with adjacent trimer units interconnected through bridging acetato groups (Scheme 4.2(B)) (37). The symmetry around the metal is octahedral. The cobalt and nickel acetate complexes are present as monomers in HOAc solution while $Mn(OAc)_2.4H_2O$ is present as a trimer (as may be inferred from a comparison of EPR spectra of frozen solutions). Monomeric non-interacting Mn(II) ions in solution show an EPR spectrum at 298 K consisting of six well resolved equally intense hyperfine lines due to the interaction of Mn(II) nuclear spins (S = 5/2, I = 5/2). Frozen solutions of Mn(II), at 77 K, exhibit six major lines due to zero-field transitions of m_S: $|-1/2\rangle \leftrightarrow |+1/2\rangle$, while the other sets of transitions corresponding to m_S: $|\pm 5/2\rangle \leftrightarrow |\pm 3/2\rangle$ and $|\pm 3/2\rangle \leftrightarrow |\pm 1/2\rangle$ are usually not resolved due to the large zero-field anisotropy; they contribute only to the background upon which the six major hyperfine signals are superimposed. Further, two small forbidden transitions due to $\Delta m_I = \pm 1$ appear between the adjacent hyperfine features. In the case of interacting Mn(II) ions, the nature of the spectrum depends upon the magnitude of the exchange interaction (J). If J is small, the linewidths (ΔH_{pp}) will be larger and the hyperfine features are only partially resolved. The intensities of the outmost and the inner hyperfine signals will be different. In frozen solutions, at 77 K, in addition to the

exchange interactions, the dipole-dipole interactions also contribute and as a consequence of this, the sextet hyperfine feature from the zero-field transition, m_S: $|-1/2\rangle \leftrightarrow |+1/2\rangle$ will not be resolved. The EPR spectra of Co / Mn / Br^- (before reacting with oxygen (air)) indeed belong to this category. If J is high, only an exchange-narrowed line is observed in place of the sextet hyperfine pattern. In fact, the cluster complexes formed during the course of the reaction belong to this category. It is pertinent to note that the oxo-bridged $Mn_3(O)((OAc)_6(py)_3$ cluster complex (Scheme 4.2(C)) has an exchange coupling constant of 10.2 cm^{-1} while $Mn(OAc)_2.4H_2O$ has a value of 0.5 cm^{-1}. The difference between the spectral patterns before and after reacting with oxygen, especially for solutions (iii) and (iv) are due to the formation of oxo-bridged Mn cluster complexes. The higher resolution in the hyperfine pattern (Fig. 4.3(d) and 4.3(h)) after interacting with oxygen is an indication of formation of monomeric Mn(II) ions. The structures of the various species are shown in Scheme 4.2.

4.3.2 Aerial Oxidation of *Para*-Xylene

The conversion and product distribution in the oxidation of PX over Co/Mn, Co/Mn/Zr, Co/Mn/Ce and Ni/Mn/Zr catalyst systems are presented in Table 4.2. Under mild conditions (363 K, continuous air-flow (1 atm)), *p*-tolyl alcohol (A), *p*-tolualdehyde (B), *p*-toluic acid (C), 4-carboxybenzaldehyde (D) and terephthalic acid (E) are the main products in the oxidation of PX. Co or Mn acetates alone gave low conversions and *p*-tolualdehyde was the major oxidation product (Runs 1 and 5, Table 4.2). A combination of Co and Mn salts resulted in much higher conversions. The catalyst with Co to Mn mmol ratio of 3:1 showed the highest conversion;

Table 4.2 Catalytic Activity Data for the Oxidation of *Para*-Xylene[a]

Run No.	Catalyst composition[b] (mmol)	Time (h)	Conv. (wt%)	TOF[c]	Product Distribution (wt%)[d]				
					A	B	C	D	E
1	Co(1.03)	8.0	28.2	1.5	2.6	91.5	5.9	-	-
2	Co(1.03)+Mn(0.35)	16.0	98.0	2.0	0.4	18.2	76.4	2.0	3.0
2A	Co(1.03)+Mn(0.35)	8.0	99.7	3.9	5.7	46.6	18.2	13.0	16.5
2B	Co(1.03)+Mn (0.35)	7.0	97.3	4.5	2.4	34.0	38.4	15.2	10.0
2C	Co(1.03)+Mn (0.35)	6.3	99.5	5.1	2.8	36.0	36.6	17.4	7.0
2D	Co(1.03)+Mn(0.35)	4.5	99.2	7.0	3.5	44.5	27.8	17.0	7.2
3	Co(0.7)+Mn (0.7)	16.0	81.0	1.1	5.5	19.4	71.5	3.0	0.3
4	Co(0.35)+Mn (1.03)	16.0	31.6	0.6	1.6	94.6	3.8	-	-
5	Mn (1.03)	8.0	12.0	0.6	1.5	96.4	2.1	-	-
	Effect of Zirconium								
6	Co(1.03)+Mn(0.35)+ Zr (0.1)	7.5	92.0	3.7	1.7	33.3	36.0	21.0	8.0
6A	Co(1.03)+Mn(0.35)+ Zr(0.1)	5.9	96.0	5.8	7.6	60.0	8.5	12.5	11.4
7	Co(1.03)+Mn(0.35)+ Zr(0.1)	6.5	93.4	3.8	3.8	33.7	53.8	7.4	1.3
8	Co(1.03)+Mn(0.35)+ Zr(0.6)	7.5	86.8	3.0	3.4	24.1	64.6	6.0	1.9
9	Co(1.03)+Mn(0.35)+ Zr(0.05)	10.0	81.6	2.5	2.2	33.8	56.3	6.5	1.2
10	Co(0.35)+Mn(1.03)+ Zr(0.1)	6.5	38.0	1.8	6.2	93.6	0.2	-	-
11	Co(0.35)+Mn(1.03)+ Zr(0.1)	10.0	55.0	1.6	8.1	91.0	0.9	-	-
12	Co(0.35)+Mn(1.03)+ Zr(0.1)	16.0	87.8	1.7	2.8	30.2	63.5	1.5	2.0
13	Co(0.35)+Zr(1.03)	5.0	16.0	0.7	6.2	90.3	3.5	-	-

Table 4.2 (contd …) Catalytic Activity Data for the Oxidation of *para*-Xylene [a]

Run No.	Catalyst composition[b] (mmol)	Time (h)	Conv. (wt%)	TOF	Product distribution (wt.%)[d]				
					A	B	C	D	E
	Effect of Cerium								
14	Co(1.03)+Mn(0.35)+ Ce(0.1)	10.5	51.5	1.5	11.6	80.4	8.0	-	-
14A	Co(1.03)+Mn(0.35)+ Ce(0.1)	8.5	98.5	3.5	8.6	51.7	29.7	7.0	3.0
15	Co(0.35)+Mn(1.03)+ Ce(0.1)	10.5	41.0	1.2	10.7	88.6	0.7	-	-
16	Co(0.35)+Ce(1.35)	5.0	15.5	1.5	51.8	42.7	5.5	-	-
	Effect of Nickel								
17	Ni(1.03)+Mn(0.35)	16.0	17.0	0.3	17.3	82.7	-	-	-
18	Ni(0.7)+Mn(0.7)	16.0	24.0	0.3	19.3	66.8	13.9	-	-
19	Ni(0.35)+Mn(1.35)	16.0	13.2	0.3	6.2	90.9	2.9	-	-
20	Ni(0.35)+Mn(1.35)+ Zr(0.1)	16.0	67.1	1.2	15.2	58.4	26.0	0.2	0.2

[a]Reaction Conditions: Medium– *p*-xylene(44.3 mmol)+NaBr(1.35 mmol)+H_2O(311 mmol)+ HOAc(587 mmol); Air-atmospheric pressure; Temperature-363 K.

[b]Sources of Co, Mn, Ni, Zr and Ce are $Co(OAc)_2.4H_2O$, $Mn(OAc)_2.4H_2O$, $Ni(OAc)_2.4H_2O$, $Zr(OH)_4$ and $Ce(NO_3)_3.6H_2O$, respectively. Values in the parentheses refer to the number of mmol of catalysts. In runs 2A, 6A and 14 A, 2.03 mmol of NaBr was used. In runs 2B, 2C and 2D, 3.51, 6.09 and 10.2 mmol of NaBr were used respectively.

[c]Turnover Frequency (TOF) = mole of *p*-xylene converted per mole of metal catalyst per hour.

[d]A = *p*-tolyl alcohol, B = *p*-tolualdehyde, C = *p*-toluic acid, D = 4-carboxybenzaldehyde and E = terephthalic acid.

p-toluic acid was the major oxidation product and 4-CBA and TA were the minor oxidation products. When the catalyst contained more Mn than Co (Run 4), *p*-tolualdehyde was the major product. A novel and interesting finding is the significant enhancement in the catalytic activity and yield of TA formed at

higher Br^- concentrations (compare Run 2 with Runs 2A – 2D). The values of the turnover frequencies for PX conversion (TOF) have increased by three and half times with increasing Br^- concentrations. Similar conversions are attained more quickly.

Addition of Zr enhanced the conversion and the product contained higher amounts of 4-CBA and TA (Runs 6 – 13). PX conversion is, however, suppressed at high Zr concentrations (compare Runs 7 and 8). The promotional effect of Br^- is also observed (compare Runs 6 and 6A).

Conversions with Ce were lower (Runs 14 – 16). Ce-containing catalysts showed higher selectivity for *p*-tolualdehyde. A novel finding is that the Co/Ce catalyst, in the absence of Mn, was the only catalyst among the various catalyst systems to exhibit a high selectivity for *p*-tolyl alcohol (Run 16), a specialty chemical. At similar or even lower conversion levels, other catalyst systems like Co/Zr (Run 13), Ni/Mn (Run 17) and Mn (Run 5) exhibited much lower selectivities for *p*-tolyl alcohol. Again, Br^- enhances significantly both the TOF and yield of TA (compare Runs 14 and 14 A). The activity of Ni/Mn catalysts is illustrated in the Runs 17 – 19. The conversions in the absence of cobalt, even after 16 h of reaction time, are very low. *p*-Tolualdehyde was the major product. Addition of Zr to Ni/Mn catalyst (Run 20) enhances the activity significantly. Although *p*-tolualdehyde was the major product, small quantities of 4-CBA and TA were also formed. The high conversion levels and the presence of 4-CBA and TA even in the absence of cobalt are surprising, novel findings.

Partenheimer reported (12) that the oxidation of acetic acid to CO_2 in the system cobalt-O_2-HOAc was promoted by Co(III). In the investigations

reported here, loss of HOAc was not observed at 363 K with Co/Mn, Ni/Mn or Co/Mn/Ce catalyst systems even at near-complete conversion of PX (Run 2). This may perhaps be due to the fast reduction of Co(III) to Co(II) by Mn(II). Co(III) ions are, hence, not available for the oxidation of HOAc. Loss in HOAc (about 10%) was observed at this temperature only when Zr was used. An interesting observation is that the oxidation of HOAc to CO and CO_2 depends more on the catalyst/promoter system and the temperature of oxidation than on the PX conversion level. Hence, it is possible, at least in principle, to reduce the HOAc loss by choice of a catalyst and solvent system that can oxidize *p*-tolualdehyde, *p*-toluic acid and 4-CBA to TA at lower temperatures.

The EPR spectra of the solutions with different Br^- ion concentrations at 298 K and at reaction time of 3 h were deconvoluted. The ratio of the intensity of cluster complexes ($Co_2Mn(O)(OAc)_x$ and $CoMn_2(O)(OAc)_x$), to $Mn(OAc)_2.4H_2O$ increases with increasing $[Br^-]/([Co] + [Mn])$ ratio, reaching a maximum for Co : Mn : Br^- = 3 : 1 : 6 mmol and then decreases (Fig. 4.7(a)). The catalytic activity (TOF), on the other hand, increases continuously with Br^- concentration (Fig. 4.7(b)). The amounts of 4-CBA and TA formed during the oxidation reaction (Fig. 4.7(c)) follow changes in the ratio of intensity of cluster complexes to $Mn(OAc)_2.4H_2O$. Cluster complexes (like $Co_2Mn(O)(OAc)_x$ and $CoMn_2(O)(OAc)_x$), probably play an important role in the further oxidation of *p*-toluic acid to 4-carboxybenzaldehyde and terphthalic acid.

The catalytic activity studies in the oxidation of PX reveal the following:

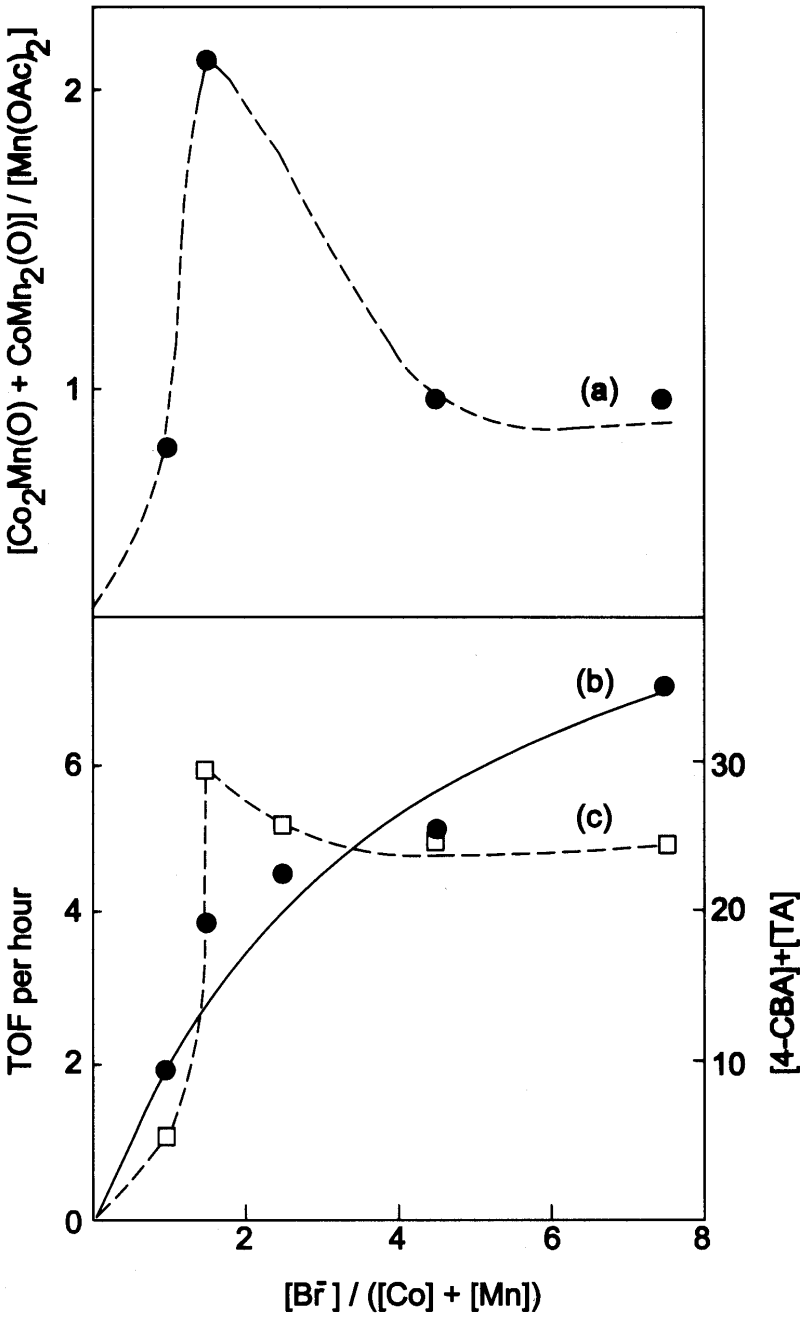

Fig. 4.7 Variation of the intensity ratio of cluster complexes $[Co_2Mn(O) + CoMn_2(O)]$ to $Mn(OAc)_2$ species (curve (a)). TOF per hour (curve (b)) and ([4-CBA] + [TA]) (curve (c)) vs $[Br^-]/([Co]+[Mn])$. The signal intensities of cluster and $Mn(OAc)_2$ complexes were estimated from the EPR spectra (298 K) of the solutions recorded at a reaction time of 3 h.

(1) Catalytic activity is synergistically enhanced when both Co and Mn are present and Co is in excess.

(2) Zr in small quantities enhances the PX conversion and selectivity for 4-carboxybenzaldehyde and terephthalic acid significantly. The combination of Co/Mn/Zr with mmol ratio of 7 : 3 ≤ 0.1 was found to give the highest conversion of PX and yield of TA among the systems studied.

(3) While the Ce-containing catalysts were less active than those containing Zr, their selectivity for *p*-tolyl alcohol was much higher.

(4) While the Ni/Mn catalysts were also much less active than Co/Mn samples, their activity could be enhanced significantly by Zr.

(5) High concentrations of bromide ion enhanced, significantly, both PX conversion and yield of TA, and

(6) There is a correlation between the yield of 4-CBA + TA and the concentration of the Co/Mn cluster complexes.

4.4 Role of Co/Mn Cluster Catalysts in the oxidation of *Para*-Xylene

The aerial oxidation of PX by Co/Mn/Br^- catalyst system follows a free radical chain mechanism (3). Co(III) is the radical initiating species formed from $Co(OAc)_2.4H_2O$ either by reaction with O_2 or with adventitious peroxides present in acetic acid.

$$Co(OAc)_2 + O_2 \rightarrow Co^{III}(O_2^{\bullet})(OAc)_2 \qquad [1]$$

$$Co(OAc)_2 + ROOH\ (trace) + HOAc \rightarrow Co(OAc)_3 + RO^{\bullet} + H_2O \qquad [2]$$

The $Co(OAc)_3$ then reacts rapidly with $Mn(OAc)_2$ generating $Mn(OAc)_3$; $Co(OAc)_3$ is reduced to $Co(OAc)_2$ in the process

$$Co(OAc)_3 + Mn(OAc)_2 \rightarrow Co(OAc)_2 + Mn(OAc)_3 \qquad [3]$$

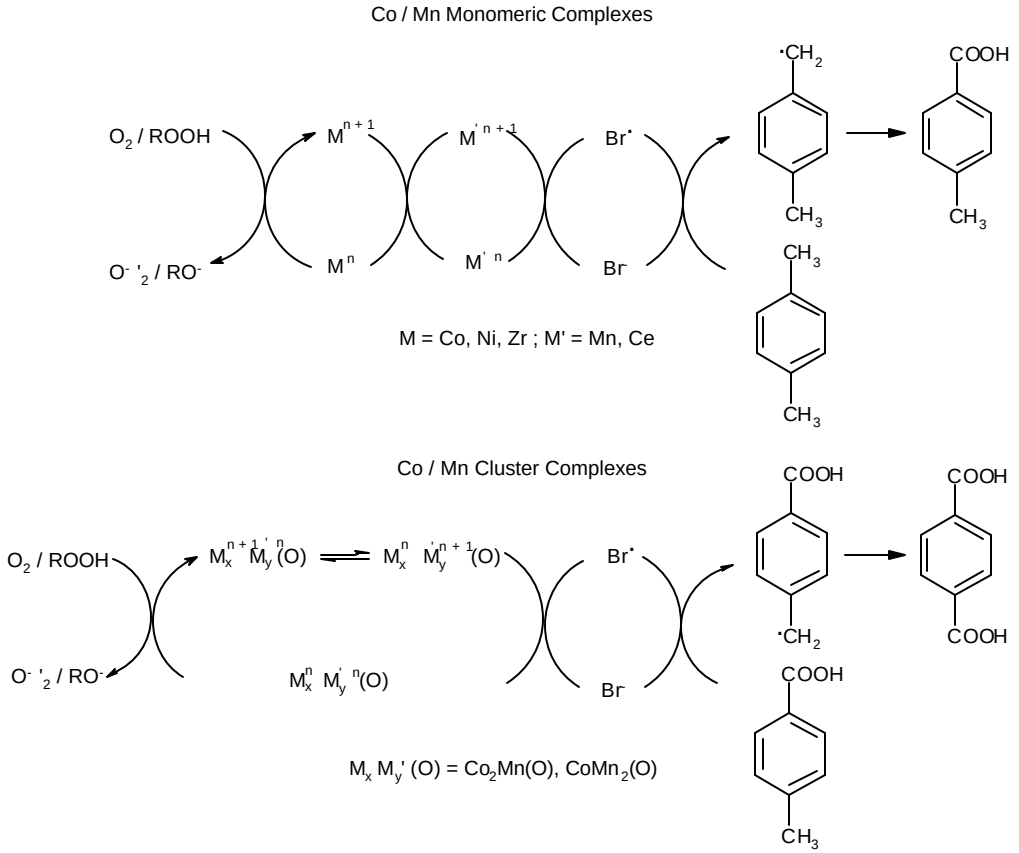

Fig. 4.8 Reaction pathways.

The Mn(III) ion, in turn, abstracts an electron from Br^- generating the bromine radical $Br^\bullet$, a crucial species which abstracts a hydrogen atom from the methyl group of PX and initiates the oxidation of *para*-xylene.

$$Mn(OAc)_3 + Br^- \rightarrow Mn(OAc)_2 + Br^\bullet + OAc^- \quad [4]$$

$$Br^\bullet + H_3CC_6H_5CH_3 \rightarrow HBr + H_3CC_6H_5CH_2^\bullet \quad [5]$$

$$H_3CC_6H_5CH_2^\bullet + ROOH \rightarrow H_3CC_6H_5CH_2OOH + R^\bullet \quad [6]$$

Cerium, probably, functions similar to manganese, while nickel and zirconium can substitute for cobalt. This model is shown schematically in Fig. 4.8 and is an extension of that proposed by Partenheimer (3, 18, 19). The role of dioxygen in generating the Co(III) species from Co(II) is supported by electronic and EPR spectral results (Fig. 4.1(a) and Fig. 4.3).

Electronic spectroscopic results (Fig. 4.1) show that in the system Co/Mn/Br/HOAc/ H_2O/PX/O_2, Mn(III) cluster complexes could be detected in addition to $Co(OAc)_2$. It is also probable that $Co(OAc)_3$ and Co(OAc)Br are also present and are not seen due to their extremely short half-lives arising from their very high redox activities. The band at 630 nm in the electronic spectra (Fig. 4.1(a)) provides evidence for the formation of Co(III) species. The intensity of this band increases continuously during the course of the reaction indicating the enhanced formation of Co(III) species. However, in the presence of PX or Mn(II) salt, this band corresponding to Co(III) is absent (Fig 4.1(b)). It is probably consumed fast in the oxidation of Mn(II) to Mn(III). The spectral bands at 460 and 350 nm (Fig. 4.1(c)) corresponding to the monomeric and Mn(III) cluster complexes present during the reaction indicate that their half life is relatively longer than that of the Co(III) species. The presence of the Mn(III) cluster complexes under reaction conditions is also supported by the

EPR results (Fig. 4.3 – 4.5). More specifically, solutions with an excess of manganese (Co : Mn = 1 : 3 mmol) contain homonuclear $Mn_3(O)(OAc)_x$ type clusters (Scheme 4.2) as the major species with a minor component being $CoMn_2(O)(OAc)_x$ clusters (Fig 4.4, Table 4.1). Solutions with an excess of cobalt (Co : Mn : 3 : 1 mmol) contain heteronuclear clusters of the type $Co_2Mn(O)(OAc)_x$ (Scheme 4.2) as a predominant species and $Co_3(O)(OAc)_x$ and $Mn_2Co(O)(OAc)_x$ (Scheme 4.2) as the minor ones. The cluster complexes showed a broad EPR signal below the free spin value (g = 2.0023) at 298 K. They become EPR silent at 77 K, probably due to the antiferromagnetic interactions among the manganese atoms of the cluster. The presence of Zr(IV) ions enhances the concentration of the Mn(III) cluster complexes (Fig. 4.3) as well as the rate of oxidation of PX (Table 4.2).

A similar enhancement in the cluster complex formation was also observed at high Br^- ion concentrations (Fig. 4.5) The concentrations of the cluster complexes were high in the solutions with Co/Mn/Br^- mmol ratios of 3 : 1 : 6 (Fig. 4.5 (b)). The Mn(III) cluster complexes probably play a significant role in the oxidation of bromide ion to bromide atom. When Co/Br^- or Mn/Br^- alone are used as catalysts, the PX conversions are very low (compared to the systems containing both Co and Mn). More importantly, 4-CBA and TA are not observed among the products. The further oxidation of *p*-toluic acid to 4-CBA and TA is significantly enhanced by (1) the simultaneous presence of Co and Mn, (2) presence of Zr, and (3) optimal amounts of Br^- (Table 4.2). Spectroscopic studies revealed that in the initial stages of the reaction, Co(III) and Mn(III) are present as monomeric species (Figs. 4.3(a) and 4.4(a)). Cluster complexes were observed only after 3 – 5 h. Comparative spectral and

catalytic data (Tables 4.1 and 4.2) suggest, that while monomeric complexes can abstract a hydrogen atom from the methyl group of the PX (to form *p*-methylbenzyl radical which undergoes further oxidation to *p*-toluic acid), the further oxidation of *p*-toluic acid is more difficult. The $p\text{-}s^{+}$ Hammett substituent constant changes from -0.31 (for PX) to +0.42 (for *p*-toluic acid). The reduction in the ring electron density results in the abstraction of hydrogen atom from methyl group in *p*-toluic acid being 4.9 times slower. Monomeric complexes, probably, cannot abstract a hydrogen atom from *p*-toluic acid. Cluster complexes are apparently required. Support for this hypothesis comes also from runs containing small quantities of zirconium as well as high amounts of bromine (Runs 2A – 2D, 6A, 14A). In these cases, the spectroscopic data (Figs. 4.3 and 4.5) indicate that the cluster complexes $Co_2Mn(O)(OAc)_x$ and $CoMn_2(O)(OAc)_x$ are formed even at the start of the reaction leading to higher values of TOF and conversion of *p*-toluic acid to 4-CBA and TA. Although the present study does not evince, unequivocally, the exact compositions of the cluster complexes, it is proposed that bimetallic clusters like $Co_2Mn(O)(OAc)_x$ and $CoMn_2(O)(OAc)_x$ play a vital role in the oxidation of *p*-toluic acid to terephthalic acid.

It is evident from the combined spectroscopic and catalytic studies that the actual catalytically active species in the PX oxidation are multinuclear oxo-bridged Co/Mn cluster systems. High catalytic activity and increase in the yield of terephthalic acid was observed when the heteronuclear cluster complexes like $Co_2Mn(O)(OAc)_x$ and $CoMn_2(O)(OAc)_x$ are present in significant concentrations in the reaction mixture.

4.5 Conclusions

The identities of the complexes of Co and Mn present during the aerobic oxidation of *para*-xylene at 363 K by the Co / Mn / Br^- system in acetic acid solvent are investigated by electronic and EPR spectroscopies. Both the specific catalytic activity (turnover frequency, TOF) for *para*-xylene conversion and the yield of terephthalic acid are enhanced by (1) the presence of both cobalt and manganese in the catalyst system, (2) additives like Zr and Ce, and (3) an optimal concentration of Br^-. The reaction mixtures contain in addition to $Co(OAc)_2$ and $Mn(OAc)_2$, many additional species like Co(OAc)Br, $Co(OAc)_3$, $Co_3(O)(OAc)_x$, $Co_2Mn(O)(OAc)_x$, $CoMn_2(O)(OAc)_x$.

An interesting finding from the combined spectroscopic and catalytic studies is that the system exhibited high catalytic activity and yield of terephthalic acid when heteronuclear cluster complexes like $Co_2Mn(O)(OAc)_x$ and $CoMn_2(O)(OAc)_x$ are present in significant concentrations in the reaction mixture.

4.6 References

1. U. S. Patent No. US 2 833 816 (1958).
2. PCT Int. Appl. WO 9 931 038 A1 (1999).
3. Partenheimer, W., *Catal.Today,* **23,** 69 (1995).
4. *"Dioxygen Activation and Homogenous Catalytic Oxidation"* in: Simandi, L. I., (Ed.), Elsevier, Amsterdam, Vol. **66** (1991).
5. *"The Activation of Dioxygen and Homogenous Catalytic Oxidation"* in Barton, D. H. R., Martell, A. E., and Sawyer, D. T., (Eds.), Plenum Press, New York (1993).
6. Parshall, G. W., and Ittel, S. D., *"Homogenous Catalysis: The Application and Chemistry of Catalysis by Soluble Transition Metal Complexes"*, John Wiley & Sons Inc., New York, (1992).
7. Steinmetz, G. R., and Sumner, C. E., *J. Catal.*, **100,** 549 (1986).

8. Kamiya, Y., *J. Catal.,* **33,** 480 (1974).

9. Hay, A. S., and Blanchard, H. S., *Can. J. Chem.,* **43,** 1306 (1965).

10. Hendriks, C. F., Van Beek, H. C. A., and Heertjes, P. M., *Ind. Eng. Chem. Prod. Res. Dev.,* **18,** 38 (1979).

11. Harustiak, M., Hronec, M., and Ilavsky, J., *J. Mol. Catal.,* **53,** 209 (1989).

12. Partenheimer, W., *J. Mol. Catal.,* **67,** 35 (1991).

13. Zaidi, S. A. H., *Appl. Catal.,* **27,** 99 (1986).

14. Zaidi, S. A. H., *Appl. Catal.,* **42,** 247 (1988).

15. Guochuan, Y., Zuwei, X., Guoying, C., Shuhua, F., and Xiaodan, H., *Appl. Catal. A: General ,* **185,** 277 (1999).

16. U. S. Patent Nos., US 4 786 753 and US 5 453 538.

17. *"Catalytic Oxidations: Principles and Applications,* in Sheldon, R. A., and Van Santen, R. A., (Eds.), World Science, Netherlands Institute for Catalysis Research, Singapore, (1995).

18. Partenheimer, W., and Kaduk, J. A., *Stud. Sur. Sci. Catal.,* **66,** 613 (1991).

19. Gipe, R. K., and Partenheimer, W., *Stud. Sur. Sci. Catal.,* **110,** 1117 (1997).

20. Jones, G. H., *J. Chem. Res. (S),* 207 (1982).

21. Jones, G. H., *J. Chem. Soc., Chem. Comm.,* 536 (1979).

22. Koubek, E., and Edwards, J. O., *J. Inorg. Nucl. Chem.,* **25,** 1401 (1963).

23. Sumner Jr., C. E., *Inorg. Chem.,* **27,** 1320 (1988).

24. Sumner Jr., C. E., and Steinmetz, G. R., *J. Am Chem. Soc.,* **107,** 6124 (1985).

25. Ziolkowski, J. J., Pruchnik, F., and Szymanska-Buzar, T., *Inorg. Chim. Acta,* **7,** 473 (1973).

26. McGarvey, B. R., in *" Transition Metal Chemistry",* Carlin R. L., (Ed.), Marcel Dekker, New York, Vol. **3**, 89 (1968).

27. Lever, A. B. P., *"Inorganic Electronic Spectroscopy",* Elsevier, Amsterdam, (1968).

28. Kuska, H. A., and Rogers, M. T., in *"Coordination Chemistry"*, Martell, A. E., (Ed.), Van Nostrand-Reinhold, New York, Vol **1**, 186 (1971).

29. Deshpande, S., Srinivas, D., and Ratnasamy, P., *J. Catal.*, **188,** 261 (1999).

30. Vincent, J. B., Chang, H. –R., Folting, K., Huffman, J. C., Christou, G., and Hendrickson, D. N., *J. Am. Chem. Soc.*, **109,** 5703 (1987).

31. McCusker, J. K., Jang, G. H., Wang, S., Christou, G., and Hendrickson, D. N., *Inorg. Chem.*, **31,** 1874 (1992).

32. Cannon, R. D., and White, R. P., *Inorg. Chem.*, **36,** 195 (1988).

33. Suresh, E., Bhadbhade, M. M., and Venkatasubramanian, K., *Polyhedron*, **16,** 3941 (1997).

34. Beattie, J. K., Hambley, T. W., Klepetko, J. A., Masters, A. F., and Turner, P., *Polyhedron*, **15,** 2141 (1996).

35. McGarvey, B. R., in " *Transition Metal Chemistry"*, Carlin R. L., (Ed.), Marcel Dekker, New York, Vol. **3**, 89 (1968).

36. Van Niekerk, J. N., and Schoening, F. R. L., *Acta Crystallogr.*, **6,** 227 (1953).

37. Bertaut, E. F., Qui Duc, T., Burlet, P., Burlet, P., Thomas, M., and Moreau, J. M., *Acta Crystallogr .*, **30B**, 2234 (1974).

Chapter-5

Solid, Zeolite-Y-Encapsulated (μ_3-Oxo)(μ-Acetato)-Bridged Co/Mn Cluster Catalysts for Aerial Oxidation of *Para*-Xylene

5.1 Introduction

Commercially, terephthalic acid (TA) is manufactured by the homogenous dioxygen oxidation of *para*-xylene (PX) in acetic acid (HOAc) medium, using a Co/Mn/Br^- catalyst system (1 - 5). However, it is desirable, in the commercial process, to replace the conventional homogeneous catalyst system by a heterogeneous solid catalyst system, and the reduction or elimination of 4-carboxybenzaldehyde (4-CBA) and other impurities from TA (which necessitate elaborate hydrogenation and recrystallization procedures) in the manufacture of purified TA required for the polyester industry. One such method of heterogenization of the homogeneous catalysts is the encapsulation of active metal complexes inside the pores of zeolites or zeolitic materials (6 - 10). Most of the work on PX oxidation in liquid phase has been confined to homogenous catalysts. However, reports on solid catalysts for PX oxidation are scarce. Hashimoto et al reported CeO_2 incorporated mordenite catalysts for the oxidation of PX in the presence of O_2 (11). Centi et al reported studies using Fe-Mo oxide clusters inside zeolites ZSM-5, boralite, silicalite and Fe-silicalite (12). The catalytic activity of Co, Cu, Cr, Ni or Mn species supported on chemically modified silica gel in the aerial oxidation of PX to *p*- toluic acid was investigated by Chisem et al (13). Kishimoto et al observed 90% PX conversion and 62.6% TA selectivity over an alumina-supported $W_{12}Sb_3Fe_2O_x$ catalyst (14). However, none of these solid catalysts can replace the existing commercial catalyst as PX conversions and TA purities are remarkably low. In some cases *p*-toluic acid is the major product.

In situ electronic and EPR spectroscopic studies, presented in Chapter 4, identified the formation of μ_3-oxo-bridged heteronuclear Co/Mn cluster

complexes (Fig. 5.1) in the homogeneous medium, during the course of the PX oxidation reaction. In this chapter, these cluster complexes are synthesised independently and encapsulated in the supercages of zeolite-Y. The various clusters studied are $[Co_3(O)(CH_3COO)_6(pyridine)_3]^+$, $[Mn_3(O)(CH_3COO)_6(pyridine)_3]^+$ and $CoMn_2(O)(CH_3COO)_6(pyridine)_3$, (hereafter referred to as $Co_3(O)$, $Mn_3(O)$ and $CoMn_2(O)$, respectively).

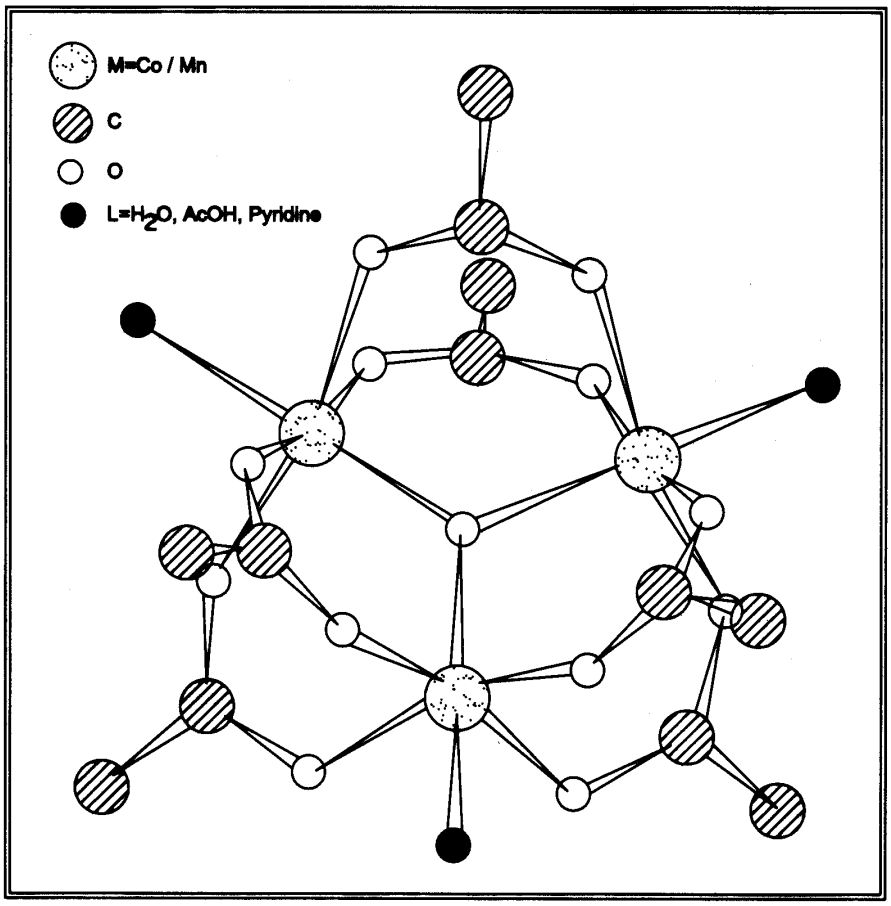

Fig. 5.1 Structure of μ_3-oxo-bridged Co/Mn cluster complex.

The "neat" and solid, encapsulated cluster complexes were characterized by various physicochemical techniques including FT-IR, UV-visible and EPR spectroscopies. The catalytic activities of the cluster

complexes in the aerial oxidation of PX were investigated. The novel, solid catalysts comprising of (μ_3-oxo)(μ-acetato)-bridged Co/Mn cluster complexes oxidize selectively, *para*-xylene to terephthalic acid with dioxygen.

5.2 Experimental

The materials such as $Co(CH_3COO)_2.4H_2O$, $Mn(CH_3COO)_2.4H_2O$, NaBr, glacial acetic acid, pyridine, PX and others were used as received. The procedures for the synthesis of the "neat" and encapsulated (μ_3-oxo)(μ-acetato)-bridged Co/Mn cluster complexes and the procedures for the catalytic activity tests are described in Chapter 2.

5.3 Results and Discussion

5.3.1 Physicochemical Characterization

5.3.1.1 Elemental Analysis

The chemical composition of the "neat" and cluster complexes was estimated by elemental (C, H & N) and ICP-AES analyses (see Chapter 2).

5.3.1.2 X-ray Diffraction Studies

No major changes were observed in the XRD patterns of zeolite-Y on encapsulation of (μ_3-oxo)(μ-acetato)-bridged Co/Mn cluster complexes, indicating that encapsulation did not alter the framework structure of zeolite-Y.

5.3.1.3 Thermogravimetric Analysis

The TGA-DTG profiles of different catalysts are shown in Fig. 5.2. The peak maximum around 480 K in the DTG of $Co_3(O)$ corresponds to loss of coordinated pyridine and that at 549 K is due to the decomposition of acetate ligand. The weight losses in two stages in the range 563 - 663 K correspond to decomposition of counterion ClO_4^-, initially into ClO and then to chlorine. The weight loss in the range 818 - 936 K corresponds to decomposition of

secondary products like $CoCO_3$ (formed from the acetate) into cobalt oxide-type materials.

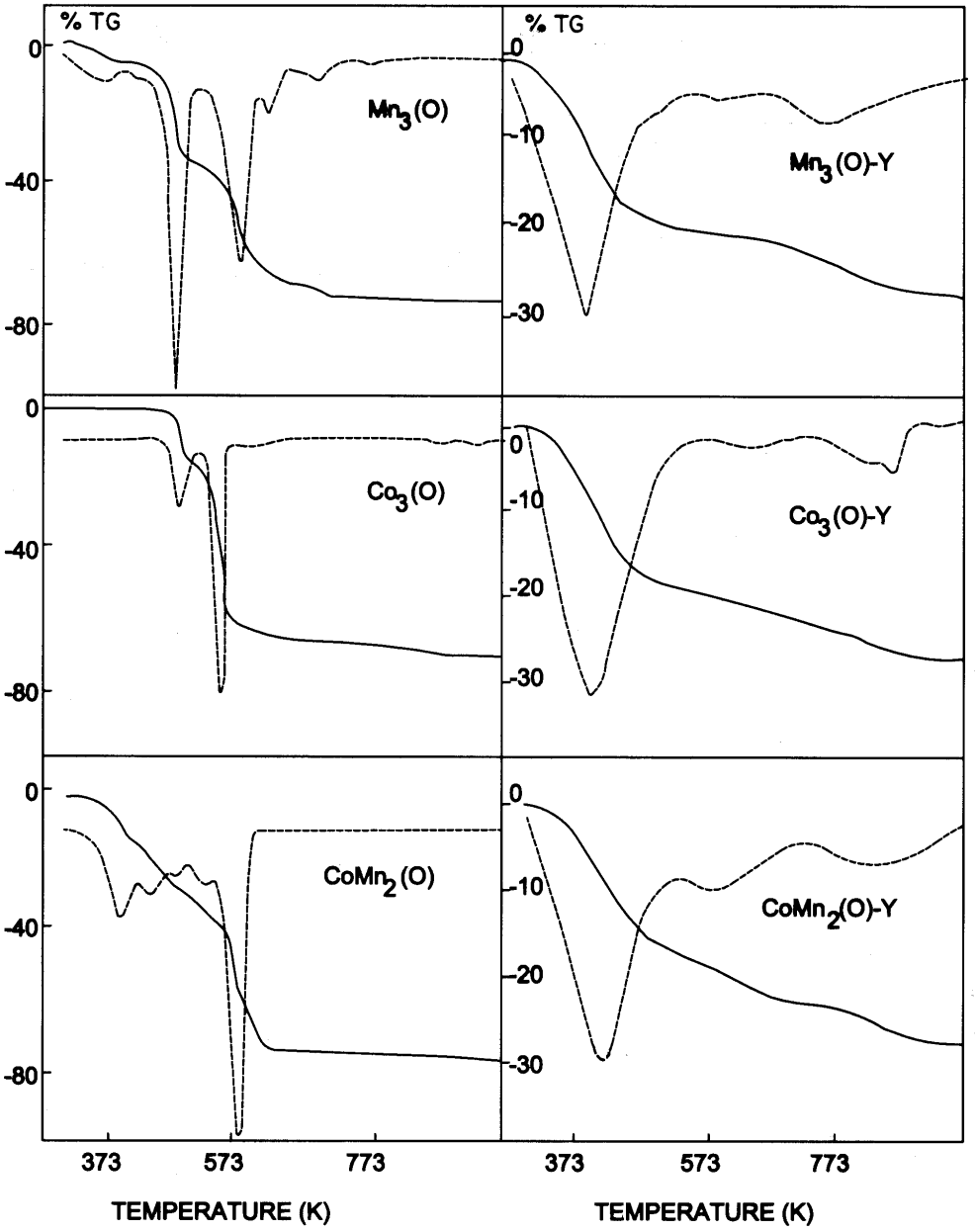

Fig. 5.2 TGA (—) and DTG (---) profiles of "neat" and encapsulated μ_3-oxo-bridged cluster complexes.

In $Mn_3(O)$ cluster, the DTG peak at 388 K is due to the loss of water. Pyridine decomposition is observed at 454 - 495 K (peak maximum - around 484 K). The decomposition of acetate in $Mn_3(O)$ occurs in the range 497 - 603 K, with peak maximum at 577 K. The peaks with maxima at 616 and 700 K are due to decomposition of the ClO_4^- ion.

The weight loss with a peak maximum at around 390 K in "neat" $CoMn_2(O)$ cluster complex is due to water loss. The three DTG peaks, due to loss of pyridine, in the temperature range 423 - 529 K, arise perhaps from differences in bond strengths of pyridine coordinated to Co and Mn ions. The decomposition of acetate occurs at 563 K. In case of the zeolite-Y-encapsulated catalysts, the peaks corresponding to adsorbed/bound water dominate those of acetate and pyridine ligands (Fig. 5.2). The DTG peaks of the latter appear as shoulders in the range 493 - 593 K. The broad multi-step peak in the range 723 - 923 K is due to the decomposition of secondary carbonates (formed from the acetate) during thermal analysis.

5.3.1.4 FT-IR Spectroscopy

The FT-IR bands of the zeolite framework and adsorbed water overlap those of the acetate and pyridine ligands (Fig. 5.3). "Neat" $Mn_3(O)$ and $Co_3(O)$ cluster complexes (Curves a and b, respectively) show additional peaks around 1092, 1072, 1047, 1032 and 762 cm^{-1} due to the ClO_4^-. The μ_3-oxo-bridge in $Mn_3(O)$ shows a characteristic peak at 665 cm^{-1}. The position of this peak is sensitive to the coordinated metal ion and occurs at 692 and 685 cm^{-1} for $Co_3(O)$ and $CoMn_2(O)$, respectively (Curves b and c, respectively). The spectral assignments of different bands for "neat" and encapsulated complexes are presented in Table 5.1. The COO^- vibrational modes of acetato groups shift

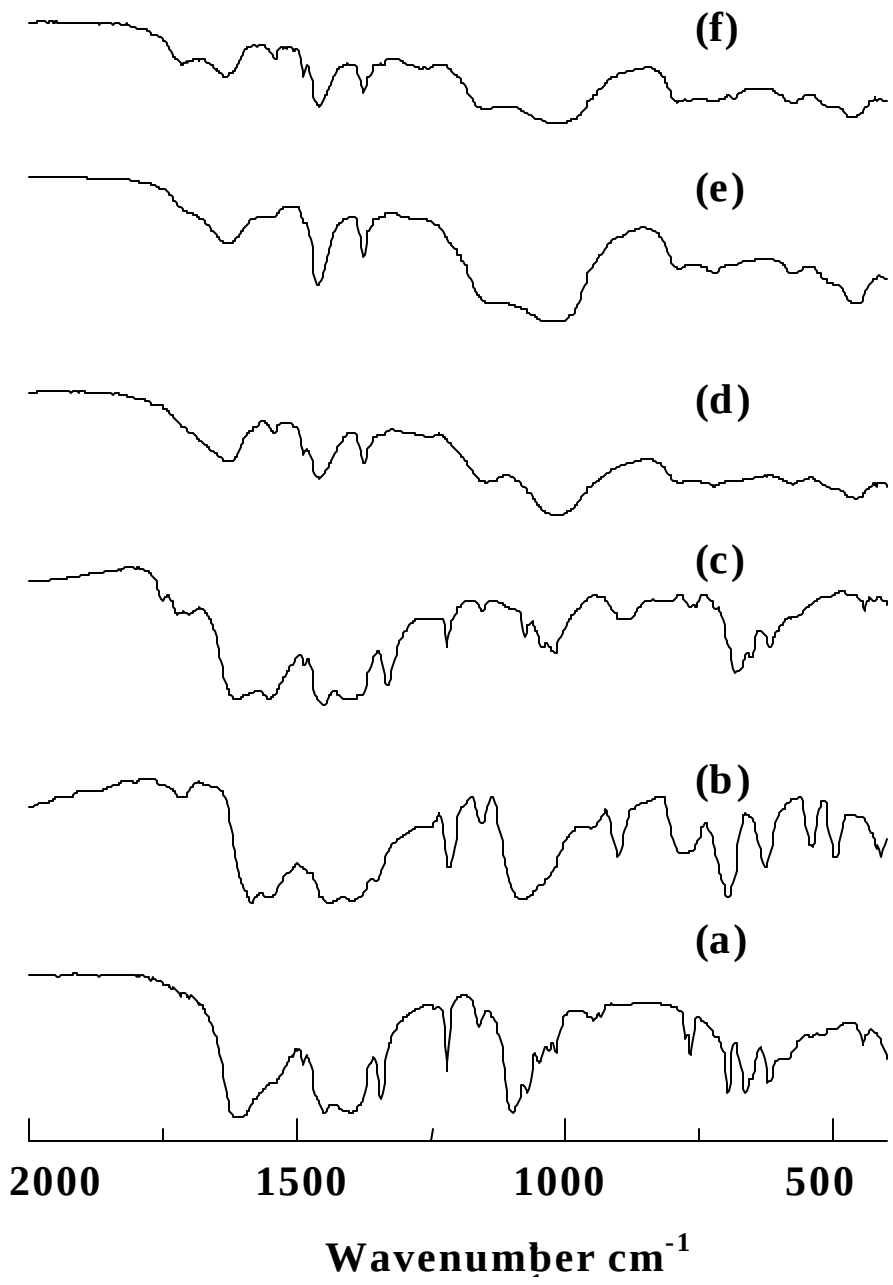

Fig. 5.3 FT-IR spectra (in Nujol mull) of: (a) $Mn_3(O)$, (b) $Co_3(O)$, (c) $CoMn_2(O)$, (d) $Mn_3(O)$-Y, (e) $Co_3(O)$-Y and (f) $CoMn_2(O)$-Y.

Table 5.1: FT-IR Assignments for "Neat" and Encapsulated (μ_3-Oxo)(μ-Acetato)-Bridged Metal Cluster Complexes

	$Mn_3(O)$		$Co_3(O)$		$CoMn_2(O)$	
Assignment	"Neat" (cm^{-1})	Encapsulated (cm^{-1})	"Neat" (cm^{-1})	Encapsulated (cm^{-1})	"Neat" (cm^{-1})	Encapsulated (cm^{-1})
C-H stretch (asym. & sym.)	2924	2924	2924	2924	2924	2924
COO^- asym. stretch	1605	1624	1609	1635	1616	1635
COO^- sym. stretch	1404	1458	1402	1463	1404	1458
CH bending (CH_3)	1456, 1342	1489, 1340	1452, 1352	1463	1448, 1350	1489, 1340
COO^- deform.	617	a	623	a	619	a
C=N stretch (Py)	1558	1545	1558	1550	1553	1545

[a]Masked by zeolite bands.

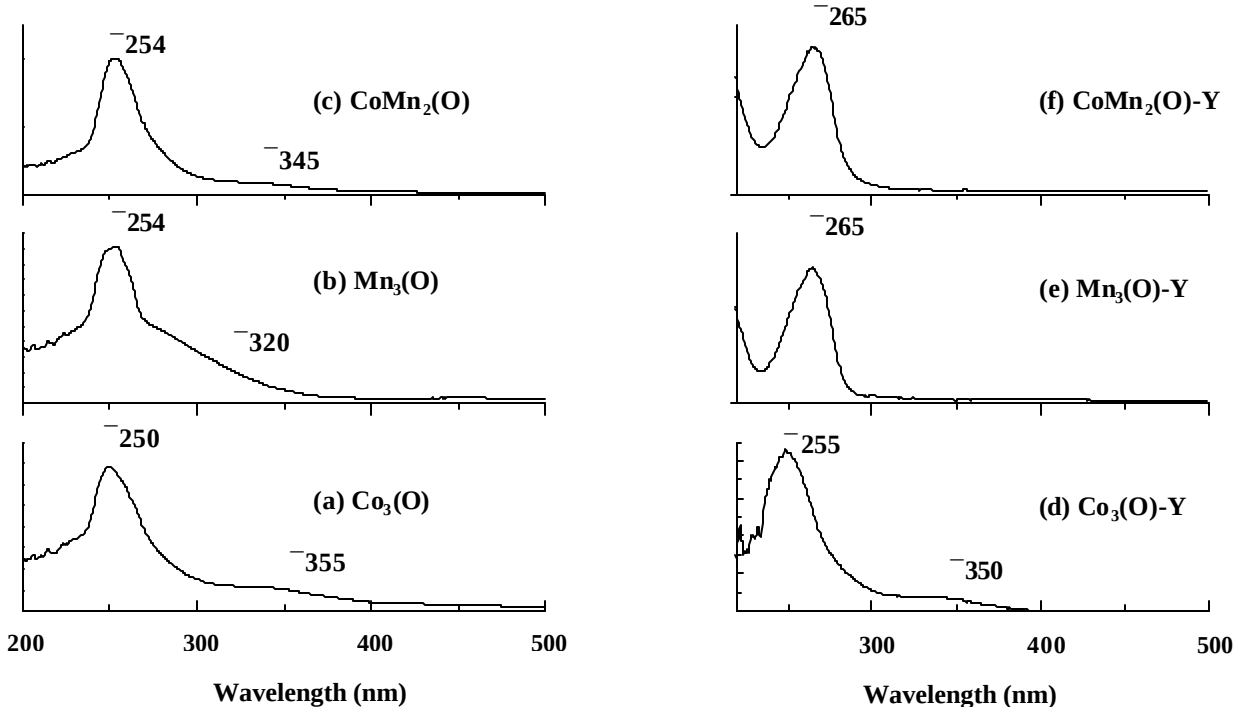

Fig.5.4 UV-visible (for "neat") and diffuse reflectance UV-visible (for encapsulated) spectra of (μ_3-oxo)(μ-acetato)-bridged cluster complexes: (a) $Co_3(O)$, (b) $Mn_3(O)$, (c) $CoMn_2(O)$, (d) $Co_3(O)$-Y, (e) $Mn_3(O)$-Y and (f) $CoMn_2(O)$-Y.

to lower energy (i.e., towards higher wavenumbers) on encapsulation (Fig. 5.3 and Table 5.1). The separation ($\Delta\nu$) between $\nu_{as}(COO^-)$ and $\nu_s(COO^-)$ is in the range 165 - 212 cm^{-1}, indicative of bidentate COO^- coordination in *syn-syn* mode to two metal ions (15).

5.3.1.5 UV-Visible Spectroscopy

Acetic acid solutions of the "neat" cluster complexes show an intense UV band, of ligand origin, around 254 nm and a shoulder at 280 nm (Fig. 5.4; Curves a - c). In addition to these, a weak, partially resolved band, characteristic of a μ_3-oxo-bridge, is also observed at around 320 nm for $Mn_3(O)$ and at 355 and 345 nm for $Co_3(O)$ and $CoMn_2(O)$, respectively. The position of the latter band is sensitive to the coordinated metal ion and is attributed to oxygen $\Rightarrow$ metal charge transfer transitions. This band is seen even in the diffuse reflectance UV-visible spectra of encapsulated cluster complexes (Curves d - f of Fig. 5.4). However, due to the dilution in the zeolite matrix, it could be seen only in $Co_3(O)$-Y (Curve d). The observation of these bands confirms the presence and structural integrity of these cluster complexes in the cavities of zeolite-Y.

5.3.1.6 EPR Spectroscopy

The "neat" $Mn_3(O)$ cluster complex shows a broad, isotropic signal at g = 2.01 with a peak-to-peak linewidth (ΔH_{pp}) of 500 G. The isotropic nature of the EPR signal is due to the small zero-field interaction in the cluster complex. The position and ΔH_{pp} of the signal are invariant to temperature, in the range 77 - 298 K. However, the intensity of the EPR signal, determined by the double integration method, increases with decreasing temperature (Fig. 5.5, Curve a)

indicating that the antiferromagnetic interaction (among Mn(III) ions, resulting in a S = 2 ground

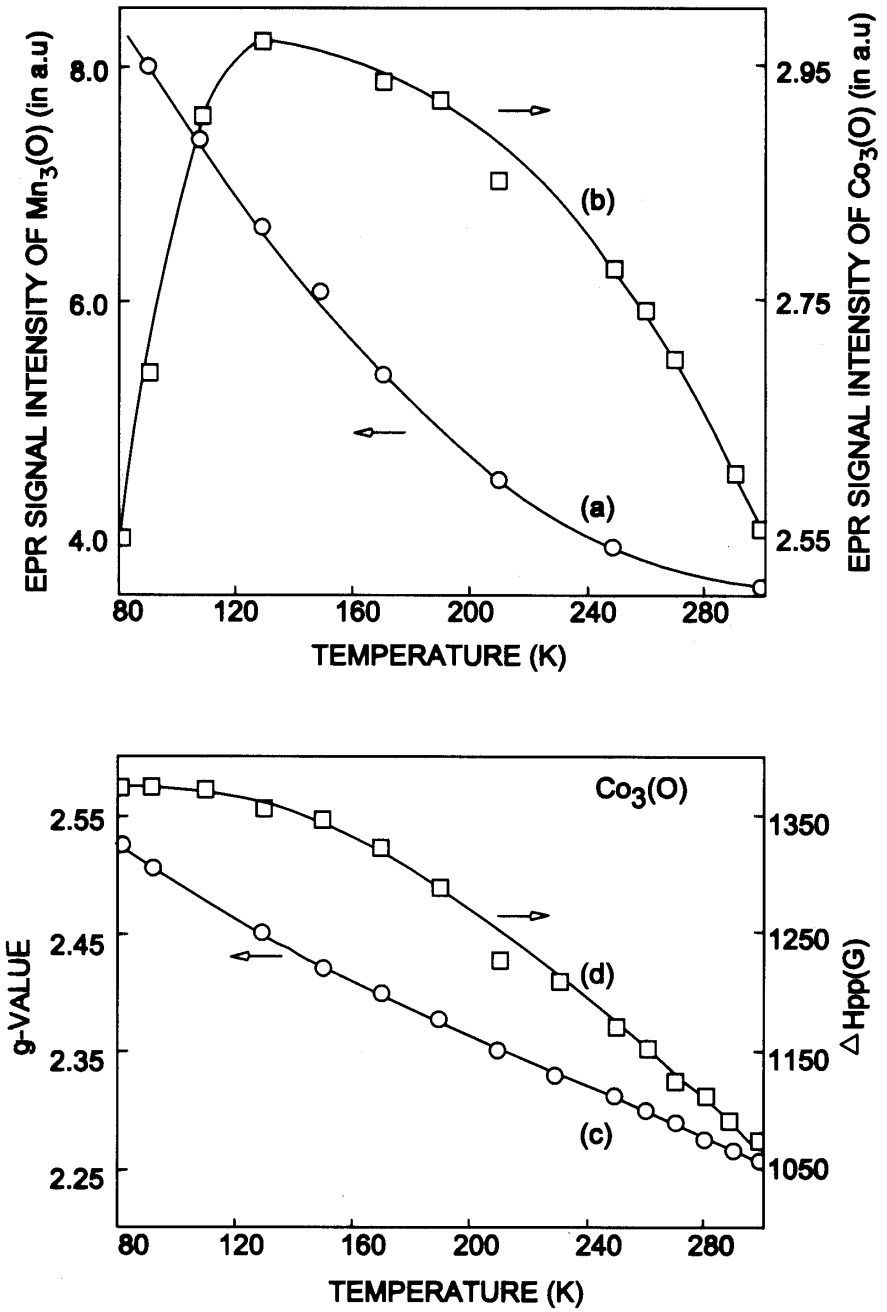

Fig. 5.5 Variation of EPR signal intensity with temperature for (a) "neat" $Mn_3(O)$ and (b) $Co_3(O)$ cluster catalysts. Variation of (c) g-value and (d) linewidth (ΔH_{pp}) with temperature for "neat" $Co_3(O)$ cluster complex.

state) is rather weak in this complex. This is the first report on the EPR characteristics of this cluster complex. Its magnetic behaviour was reported by Vincent et al (16), who found the exchange coupling constant (J) to be -10.2 cm^{-1}. EPR results are in agreement with the small J values reported by them (16). Polycrystals of the "neat" $Co_3(O)$ cluster complex also show isotropic signals at 300 K, but at a higher g value (2.259) and with a larger linewidth (1075 G). Unlike $Mn_3(O)$, the variation with temperature of the signal intensity, g value and linewidth (Fig. 5.5, Curves b – d, respectively) of the "neat" $Co_3(O)$ cluster complex indicate strong antiferromagnetic interaction. The Curie temperature is around 130 K for the $Co_3(O)$ cluster. It is below 77 K for Mn_3O. $CoMn_2(O)$, on the other hand, is EPR-silent throughout the temperature range.

The encapsulated $Mn_3(O)$ cluster complex ($Mn_3(O)$-Y) shows a broad EPR signal at g = 2.012 with barely resolved manganese hyperfine features superimposed on the broad signal (Fig. 5.6, curve a). Encapsulated $Co_3(O)$ complexes ($Co_3(O)$-Y) also exhibit a broad signal at g = 2.210 (Fig. 5.6, curve b), the intensity of which decreases at low temperatures and disappears totally at 77 K. The variation of the signal intensity in the "neat" and encapsulated $Co_3(O)$ complexes is similar and indicates strong intramolecular antiferromagnetic interactions. $Co_3(O)$-Y samples also revealed trace amounts of a Mn(II) ion impurity present in the parent zeolite sample (marked by asterisk "*" in Fig. 5.6). Mixed metal clusters encapsulated in zeolite-Y showed (Fig. 5.6, curve c) Mn–like spectrum at g = 2.026. A shift in g value from 2.012, typical of $Mn_3(O)$-Y cluster, is due to the presence of Co in the trinuclear unit, confirming the structural integrity of the $CoMn_2(O)$ cluster in

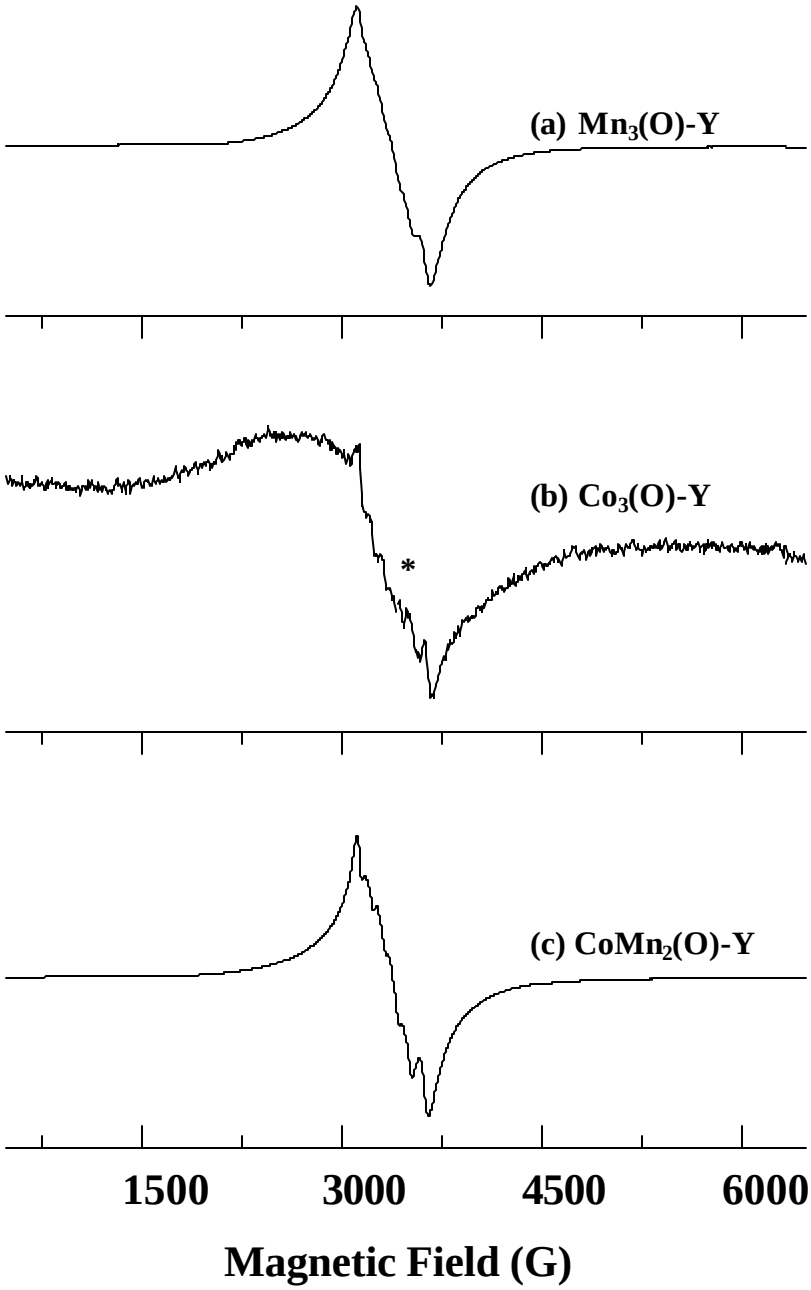

Fig. 5.6 X-band EPR spectra of encapsulated (μ_3-oxo)(μ-acetato)-bridged Co/Mn cluster complexes at 298 K: (a) $Mn_3(O)$-Y, (b) $Co_3(O)$-Y. The broad signal is due to the encapsulated cobalt cluster (the six sharp signals marked by asterisk (*) are due to Mn impurity), (c) $CoMn_2(O)$-Y.

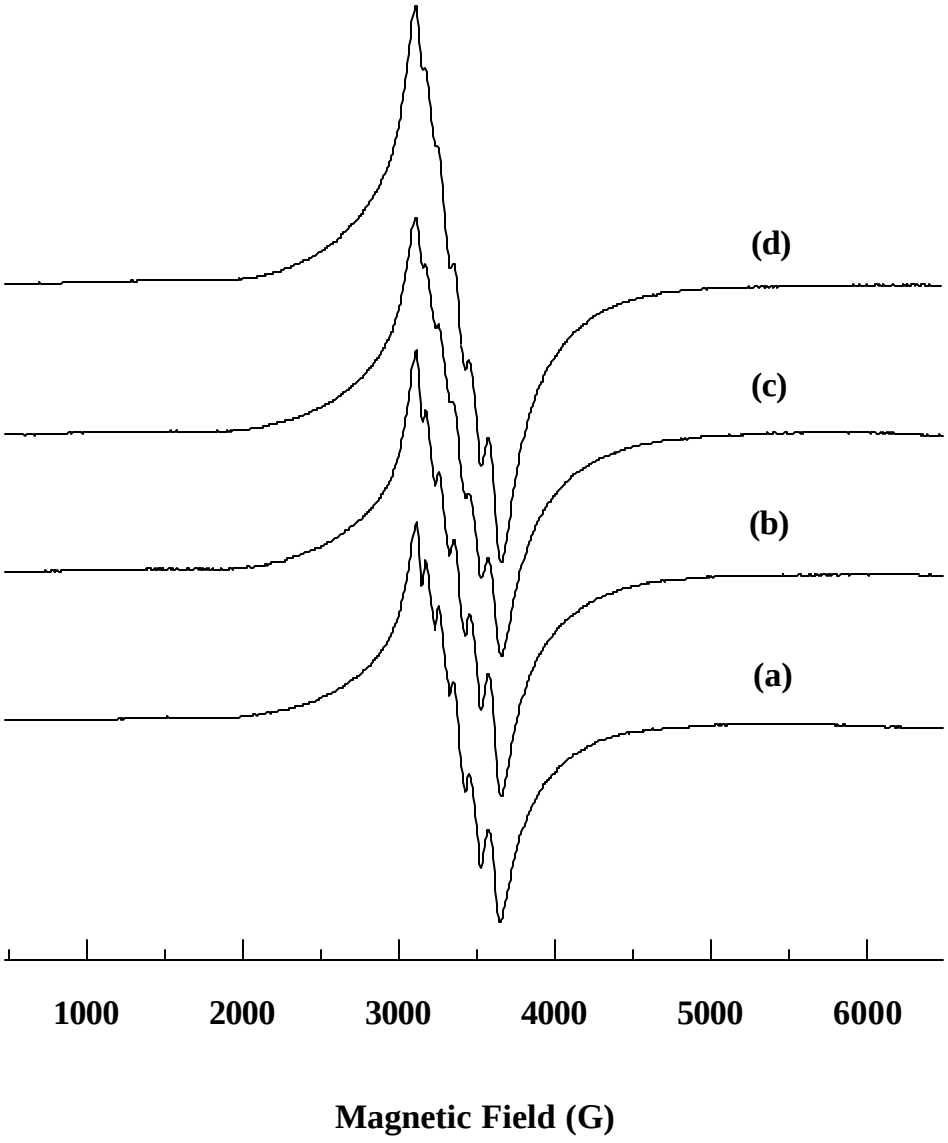

Fig. 5.7 EPR spectra (at 82 K) of $Mn_3(O)$: (a) $Mn_3(O)$ + HOAc + NaBr; (b) $Mn_3(O)$ + HOAc + NaBr after 1 h at 473 K; (c) $Mn_3(O)$ + HOAc + NaBr after 1 h at 473 K and 550 psig air; (d) $Mn(CH_3COO)_2.4H_2O$ + HOAc + NaBr after 1 h at 473 K and 550 psig air.

zeolite-Y, a conclusion also reached from the FT-IR and UV-visible spectral data.

5.3.1.7 Stability of Cluster Complexes under Reaction Conditions

Fig. 5.7 shows the EPR spectra of $Mn_3(O)$ complex and NaBr dissolved in acetic acid and heated in air (550 psig) to 473 K for 1 h (Fig. 5.7, curves a – c). The spectral features reveal the structural stability of these oxo-bridged cluster complexes under typical reaction conditions. Heating a mixture of $Mn(CH_3COO)_2.4H_2O$ solution in acetic acid, NaBr and air (550 psig), in fact, converts the linear manganese acetate into a trimeric $Mn_3(O)$ cluster complex (Fig. 5.7, compare Curves a and d). This observation also confirms that the Mn cluster complexes are formed during the course of the reaction even with the conventional catalyst system ($Co/Mn/Br^-$), as postulated in Chapter 4.

5.3.2 Catalytic Activity Studies

In the commercial process for the selective oxidation of PX to TA, in addition to complete conversion of PX, it is also essential to get as high a selectivity for TA as possible. Particularly, it is desirable to suppress or eliminate the 4-CBA impurity. In current practice, 4-CBA occurs to the extent of 0.1 – 0.5% in the crude product. In the following sections the activities of the "neat" and zeolite-Y-encapsulated cluster catalysts are reported. The catalytic data are presented in Tables 5.2 – 5.5. The reaction did not proceed to any significant extent, in the absence of catalyst.

Table 5.2 Effect of Solvent and Halide Ion on the Oxidation of *para*-Xylene over Co/Mn Catalysts in Homogeneous Medium Reaction Conditions: *Para*-Xylene (2 ml) + NaBr (0.0836 g) + H_2O (5.6 ml) + HOAc (38 ml); Oxidant = Air; Reaction time = 45min; Temperature = 473 K; Pressure = 550 psig.

Run No.	Catalyst (mmol)	Solvent/ Halide ion	Conv. (%wt)	TON[b]	Product Distribution (%Wt.)[c]					
					A	B	C	D	E	F
1	$Co(OAc)_2$(0.43)+$Mn(OAc)_2$(0.14)	1,4-dioxane Br^-	35.1	11	11.2	88.5	0.3			
2	$Co(OAc)_2$(0.43) + $Mn(OAc)_2$(0.14)	AcOH, Cl^-	18.0	6	1.7	74.7	23.6			
3	$Co(OAc)_2$(0.43) + $Mn(OAc)_2$(0.14)	AcOH, Br^-	100	32	0	0	0.9	0.1	97.7	1.3
4	$Co_3(O)$ (0.041)	1,4-dioxane Br^-	17.3	78	23.8	76.2	0			
5	$Mn_3(O)$(0.039)	1,4-dioxane Br^-	46.0	216	14.0	84.6	1.4			
6	$CoMn_2(O)$(0.041)	1,4-dioxane Br^-	23.5	106	24.0	74.8	1.2			
7	$Co(OAc)_2$(0.43)+$Mn(OAc)_2$(0.14)	AcOH[a]	2.3	1	6.8	52.5	40.7			
8	$Co_3(O)$ (0.041)	AcOH[a]	4.3	20	0	63.7	36.3			
9	$Mn_3(O)$(0.039)	AcOH[a]	0.5	2	0	70.9	29.1			
10	$CoMn_2(O)$(0.041)	AcOH[a]	7.5	34	1.6	75.2	23.3			

[a]Reaction without any halide ion.
[b]Turnover number (TON) = moles of *para*-xylene converted per mole of metal catalyst.
Products: A = *p*-Tolyl alcohol, B = *p*-Tolualdehyde, C = *p*-Toluic acid, D = 4-Carboxybenzaldehyde, E = Terephthalic acid and F = Benzoic acid. Liquid products A and B were estimated using GC. Products C to F were estimated using HPLC.

Table 5.3 Oxidation of *para*-Xylene over $Co(CH_3COO)_2.4H_2O$ and $Mn(CH_3COO)_2.4H_2O$ Salts in Homogeneous Medium Reaction Conditions: Reaction Time = 2h; Temperature = 473 K; Other Conditions are the Same as in Table 5.2

Run No.	Catalyst (mmol)[a]	Pressure (psig)	Conv. (%wt)	TON[b]	Product Distribution (%Wt.)[c]					
					A	B	C	D	E	F
1	Co(0.43)	200	84.7	36	1.6	39.4	21.4	8.8	28.4	0.3
2	Co(0.43)+Mn(0.14)	200	83.4	27	0	40.3	23.0	6.4	30.1	0.2
3	Co(0.28)+Mn(0.28)	200	89.1	30	0	44.4	24.6	10.4	20.1	0.6
4	Co(0.14)+Mn(0.44)	200	87.4	28	0	43.6	25.3	13.3	17.3	0.5
5	Mn(0.44)	200	89.1	38	0	44.0	24.7	12.9	17.2	1.2
6	Co(0.43)	350	100	43	0	0	14.1	2.2	83.6	0.1
7	Co(0.43)+Mn(0.14)	350	100	32	0	0	0.8	0.01	98.8	0.4
8	Co(0.28)+Mn(0.28)	350	100	33	0	0	1.6	0.1	98.2	0.1
9	Co(0.14)+Mn(0.44)	350	100	32	0	0	5.0	0.2	92.8	2.0
10	Mn(0.44)	350	100	42	0	0	23.7	5.0	70.9	0.4
11	Co(0.43)+Mn(0.14)	550	100	32	0	0	0.7	1.4	96.9	0.01
12	Co(0.28)+Mn(0.28)	550	100	33	0	0	0.36	0.03	99.6	0.01
13	Co(0.14)+Mn(0.44)	550	100	32	0	0	0.44	0.05	99.5	0.01
14	Mn(0.44)	550	99	42	0	0	7.3	1.0	91.7	0.02

[a]Sources of Co and Mn are $Co(CH_3COO)_2.4H_2O$ and $Mn(CH_3COO)_2.4H_2O$, respectively.
[b]Turnover number (TON) = moles of *para*-xylene converted per mole of metal catalyst.

Table 5.4 Catalytic Activity of "Neat" Co/Mn Cluster Catalysts in the Selective Oxidation of *para*-Xylene in Homogeneous Medium: Effect of Pressure and Reaction Time (Reaction Conditions: Reaction temperature = 473 K; Other Conditions are the Same as in Table 5.2)

Run No.	Catalyst (mmol)	Pressure (psig)	Reaction Time (min)	Conv. (%wt)	TON	Product Distribution (%Wt.)[c]					
						A	B	C	D	E	F
1	$Co_3(O)(0.041)$	550	15	67.7	307	0.5	26.5	20.1	46.7	5.3	0.9
2			30	75.6	343	0.5	33.6	25.3	33.3	6.4	0.9
3			45	86.7	393	0	42.5	26.0	11.7	19.5	0.3
4	$Mn_3(O)(0.039)$	550	15	79.4	373	0	37.6	27.4	22.9	11.2	0.9
5			30	64.5	303	0	22.5	26.1	10.3	40.8	0.3
6			45	100	470	0	0	27.0	8.0	64.9	0.1
7			120	100	470	0	0	1.6	0.1	98.2	0.1
8	$CoMn_2(O)(0.041)$	550	15	100	449	0	0	4.0	0.3	95.7	0
9			30	100	449	0	0	6.1	0.9	93.0	0
10			45	100	449	0	0	4.7	0.7	94.6	0
11			60	100	449	0	0	1.8	0.4	97.8	0
12			120	100	449	0	0	0.8	0.1	99.0	0.1

Turnover number (TON) = moles of *para*-xylene converted per mole of metal catalyst.

Table 5.5 Catalytic Activity of Solid Catalysts: m_3-Oxo-Bridged Co/Mn Clusters Encapsulated in Zeolite -Y

Reaction Conditions: Catalyst = 0.2995 g, Tempe rature = 473 K and Pressure = 550 psig; Other Conditions are the Same as in Table 5.2

Run No.	Catalyst (g.mmol of metal)	Time (min)	Conv. (%wt)	TON	Product Distribution (%Wt.)[c]					
					A	B	C	D	E	F
1	Mn_3(O)-Y (0.075)	60	74.8	183	0	33.1	47.3	8.1	10.4	1.1
2		150	80.4	197	0	37.8	30.8	1.7	29.7	0
3		240	99.9	245	0	0	20.1	0.7	79.2	0
4	Co_3(O)-Y (0.036)	60	65.6	341	13.4	18.4	13.0	37.5	15.2	2.5
5		150	72.0	374	10.5	14.0	10.7	39.8	20.7	4.3
6	$CoMn_2$(O)-Y (0.09)	60	74.4	151	0	0	6.4	0.8	92.8	0.1
7		150	100	203	0	0	1.1	<0.01	98.9	0
8		240	100	203	0	0	0.6	0.01	99.4	0

Turnover number (TON) = mole s of *para*-xylene converted per mole of metal catalyst.

5.3.2.1 Effect of Solvent and Halide Ion

When the reactions were carried out with NaCl in place of NaBr (Table 5.2), the conversions are markedly lower (compare Runs 2 and 3). The conversions are also low in the absence of the halide ion (Runs 7 – 10), or when 1,4-dioxane is used in place of acetic acid (Runs 1 and 4 – 6). Hence, both acetic acid and the bromide ion are essential for high activity and selectivity.

5.3.2.2 *Para*-Xylene Oxidation over Cobalt and Manganese Acetates Salts

When mixtures of the cobalt and manganese acetates are used, the clusters are formed in about 15 min at higher pressures (350 – 550 psig) and temperatures (above 473 K) when compared to about 4 h at atmospheric pressure and 363 K. The combination of cobalt and manganese acetates in mmol ratio of 3 : 1, 1 : 3, and 1 : 1 yield cluster complexes of the type $Co_2Mn(O)$, $CoMn_2(O)$ and a mixture of $Co_2Mn(O)$ and $CoMn_2(O)$, respectively (Chapter 4). Both conversion and selectivity are higher when Co and Mn are present together (Table 5.3). Complete conversion of PX and >95 wt.% selectivity to TA are obtained at 550 psig and 473 K (Table 5.3; Runs 7, 8, 11 – 14).

5.3.2.3 *Para*-Xylene Oxidation over "Neat" Co/Mn Cluster Catalysts

At 473 K and a pressure of 550 psig, 100% PX conversion and >98 wt.% TA selectivity are obtained with the cluster catalysts ($Mn_3(O)$ and $CoMn_2(O)$) (Table 5.4, Runs 7 and 12). Complete conversion of PX is achieved within 15 min with $CoMn_2(O)$ (Run 8). However, TA selectivity improved when reactions are continued for a longer time (Runs 8 – 12). $Co_3(O)$ exhibits low PX conversions and TA selectivity. $Mn_3(O)$, on the other hand, yielded

100% PX conversion and high TA selectivity at longer reaction times (Run 7). It may be noted that the heteronuclear cluster catalyst $CoMn_2(O)$ is more active and yields higher TA selectivity than the homonuclear $Co_3(O)$ and $Mn_3(O)$. The concentration of 4-CBA is also, in general, less with the former.

5.3.2.4 *Para*-Xylene Oxidation over Solid Catalysts

When the complexes are encapsulated in zeolite-Y, complete conversions are achieved only at longer reaction times (Table 5.5), perhaps, due to diffusional limitations in the zeolite. Easy separability and reusability are major advantages of the solid catalysts. Another interesting feature with the encapsulated $CoMn_2(O)$ cluster catalyst (Run 8) is the very low concentration of the 4-carboxybenzaldehyde impurity (around 0.01%). It may be noted that the activity and selectivity of both the "neat" and encapsulated cluster complexes follow the trend $CoMn_2(O) > Mn_3(O) > Co_3(O)$ confirming the superiority of the heteronuclear complexes.

5.3.2.5 Catalyst Leaching Tests

The molecular dimensions of the $M_3(O)$ (M = Co, Mn) cluster is about 10.8 Å. It can be accommodated in the supercages of zeolite-Y (~12 Å). The cluster is, however, larger than the openings of the windows of the zeolite's supercage and after formation it is, hence, locked inside the supercage making its loss during the reaction difficult (Fig. 5.8). AAS and EPR spectroscopic techniques investigated leaching of metal ions from the solid catalyst at the end of the reaction. While AAS did not reveal any leaching of metal ions, EPR estimated that about 0.5% of the encapsulated manganese in the solid catalyst was leached into solution (about 50 ppm of Mn in solution). This amount cannot account for the observed catalytic activity. Catalytic runs with this trace

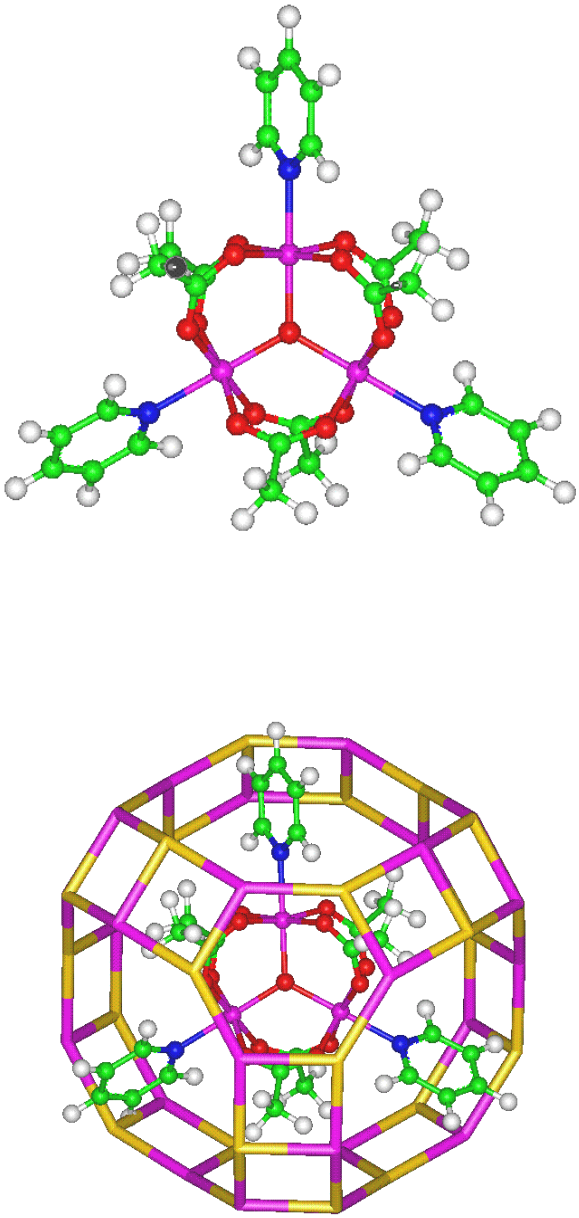

Fig. 5.8 Molecular model of "neat" and zeolite-Y-encapsulated (μ_3-oxo)(μ-acetato)-bridged Co/Mn cluster complexes.

amounts of metal ions in solution exhibited low PX conversions (28 wt.%) with *p*-tolyl alcohol (A) and *p*-tolualdehyde (B) as products; TA was not detected.

5.4 Mechanism of *Para*-Xylene Oxidation

5.4.1 Role of Bromide

During the reaction, Co(III) oxidizes Mn(II) to Mn(III) ions, being itself reduced to Co(II). The Mn(III) ion, in turn, abstracts an electron from the bromide ion to form a bromine atom. The bromine atom subsequently abstracts a H-atom from the $-CH_3$ group (forming HBr) and initiates the oxidation reaction. A similar abstraction of an electron from the chloride ion by Mn(III) ions to form chlorine atom (and Mn(II)) is not favorable because the $E_{1/2}$ of the Mn(III)/Mn(II) couple (1.2 V) is smaller than that of $Cl^{\bullet}/Cl^{-}$ couple (1.36 V). The redox potentials of cobalt, manganese, bromide and chloride ions against NH electrode are given below (17).

$Co(III) + e^{-} \leftrightarrow Co(II)$ ($E_{1/2}$ = 1.92 V)

$Mn(II) \leftrightarrow Mn(III) + e^{-}$ ($E_{1/2}$ = 1.2 V)

$Br^{-} \leftrightarrow Br^{\bullet} + e^{-}$ ($E_{1/2}$ = 1.06 V)

$Cl^{-} \leftrightarrow Cl^{\bullet} + e^{-}$ ($E_{1/2}$ = 1.36 V)

Chlorine atoms ($Cl^{\bullet}$) are also less stable than bromine ($Br^{\bullet}$) and readily form chlorine molecules. The unfavorable redox couple as well as the low concentration of chlorine atoms in solution are responsible for the low PX conversions observed with chloride ions (Table 5.2). Bromide ions are, hence, the promoters of choice.

5.4.2 Role of the Cluster Complexes

The CV data of cobalt and manganese acetates and "neat" $Co_3(O)$ and $CoMn_2(O)$ cluster complexes are presented in Table 5.6. Fig. 5.9 shows the CV

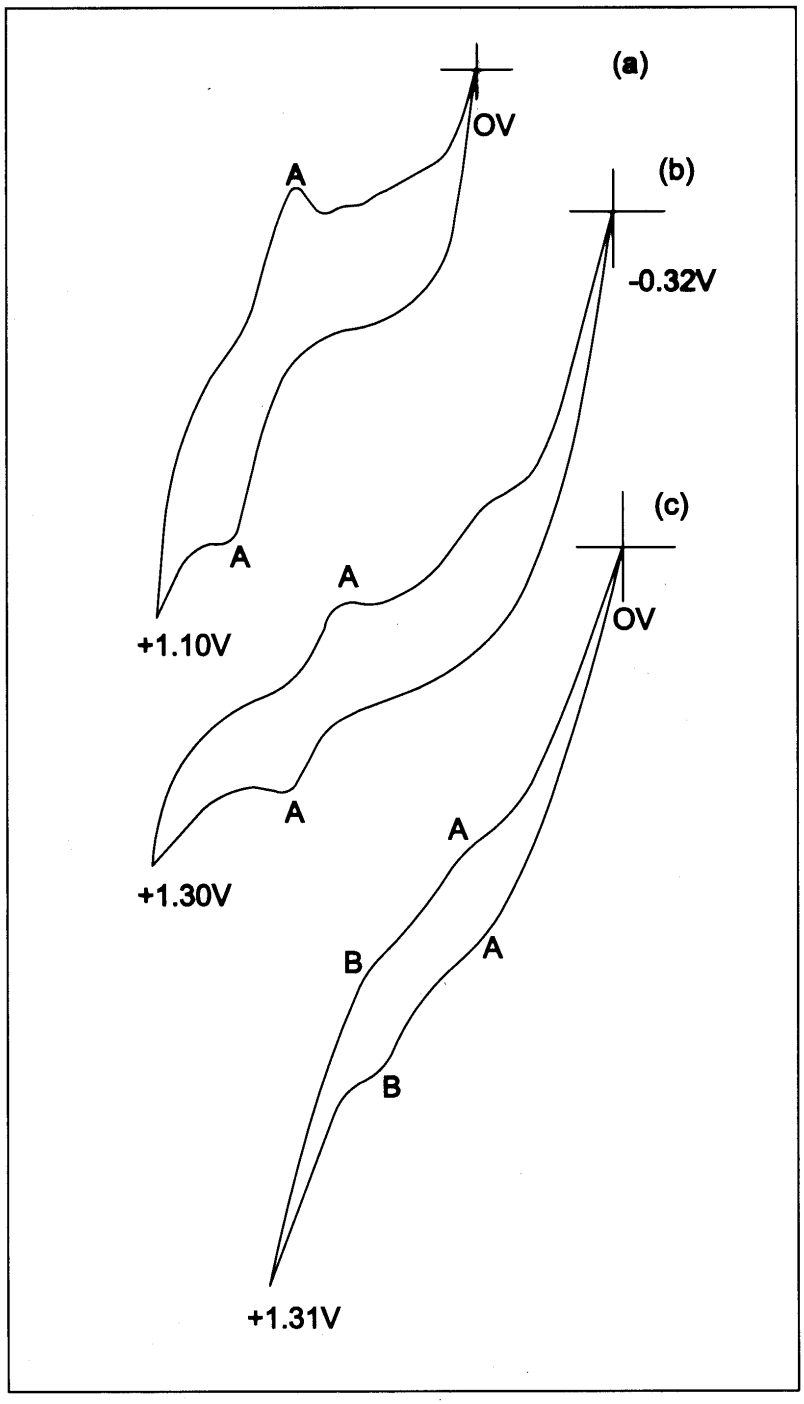

Fig. 5.9 Cyclic voltammograms of (a) $Co(CH_3COO)_2.4H_2O$, (b) $Co_3(O)$, and (c) $CoMn_2(O)$. Redox couples A and B are indicated.

Table 5.6 Cyclic Voltammetric Data of "Neat" (μ_3-Oxo)(μ-Acetato)-Bridged Co/Mn Cluster Complexes

Complex	Redox Couple	$E_{1/2}$ (in V)[a]	ΔE (in V)[b]
$Co(CH_3COO)_2.4H_2O$	A : Co^{III} / Co^{II}	+0.75	0.21
$Mn(CH_3COO)_2.4H_2O$	A : Mn^{III} / Mn^{II}	+0.75	0.30
$Co_3(O)$	A : $Co_3^{III}(O)$ / $Co^{II}Co_2^{III}(O)$	+0.69	0.22
$CoMn_2(O)$	A: $Co^{III}Mn_2^{III}(O)$/$Co^{II}Mn_2^{III}(O)$	+0.56	0.04
	B: $Co^{III}Mn^{IV}Mn^{III}(O)$/$Co^{III}Mn_2^{III}(O)$	+0.93	0.05

[a]$E_{1/2}$ = half -wave potential with reference to saturated calomel electrode.
[b]ΔE = separation between the cathodic and anodic peaks of the redox couple.

of cobalt acetate, $Co_3(O)$ and $CoMn_2(O)$ (Curves a – c, respectively). The redox couple A (Fig. 5.9) is due to changes in the oxidation state of Co (between +2 and +3). $CoMn_2(O)$ (Curve c) shows an additional redox couple (B) due to $Mn^{III} \leftrightarrow Mn^{IV}$ transitions of one of the two Mn ions in $CoMn_2(O)$. The $E_{1/2}$ value for couple A is lower for $CoMn_2(O)$ (+0.56 V) compared to $Co_3(O)$ (+0.69 V) and cobalt and manganese acetates (+0.75 V), respectively (Table 5.6). Lower $E_{1/2}$ values are indicative of greater ease of electron transfer. The redox couples of $CoMn_2(O)$ are reversible while those of the others are quasi-reversible (note the smaller ΔE values for $CoMn_2(O)$ (0.04 V) compared to $Co_3(O)$ (0.22 V), cobalt acetate (0.21 V) and manganese acetate (0.30 V)) (Table 5.6). The low $E_{1/2}$ and ΔE values indicative of more facile $Co^{II} \leftrightarrow Co^{III}$ transitions in $CoMn_2(O)$, are, perhaps, responsible for its higher catalytic activity.

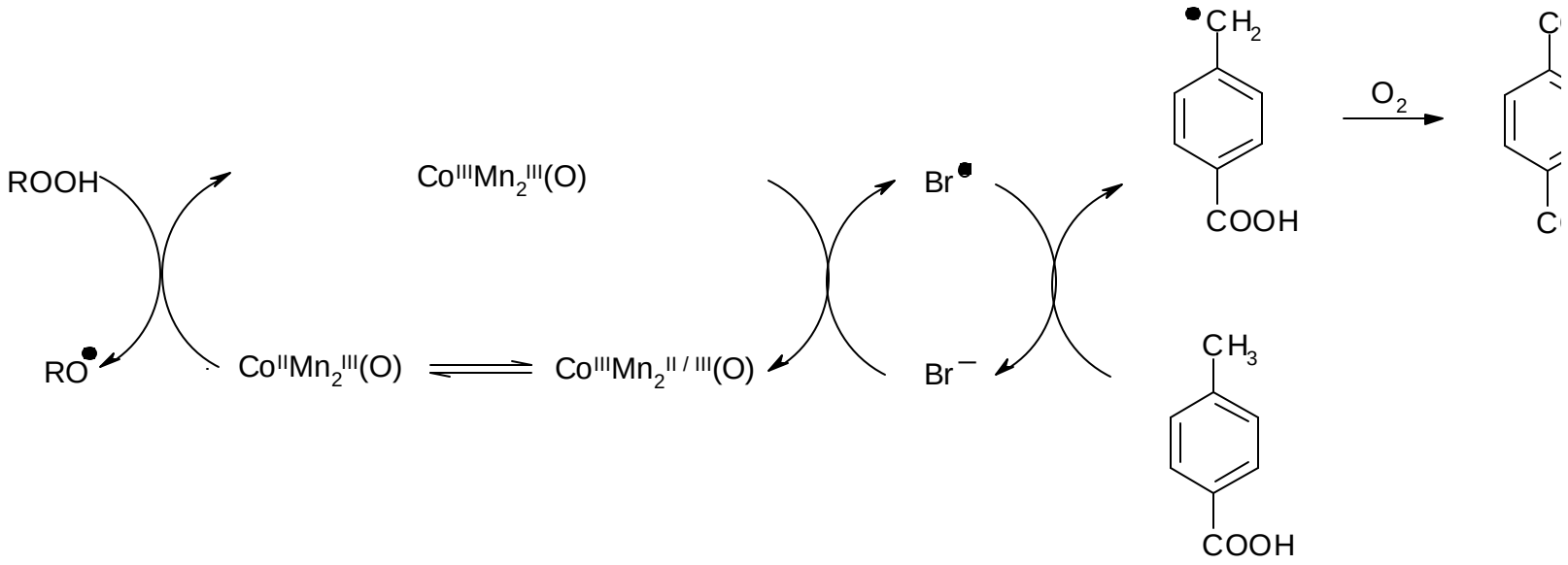

Fig.5.10 Catalytic oxidation of *para*-toluic acid over $CoMn_2(O)$-Y

The aerial oxidation of PX by Co/Mn/Br^- catalyst system follows a free radical chain mechanism (1). The mechanism of the oxidation reaction is believed to begin with H-atom abstraction from the methyl group by bromine atoms (forming HBr) (1). The resultant benzyl radical adds to O_2 and proceeds through the hydroperoxide to *p*-tolyl alcohol (A), *p*-tolualdehyde (B) and *p*-toluic acid (C) (18). H-atom abstraction from the methyl group in *p*-toluic acid (C) generates a secondary benzyl radical, which follows the same pathway to yield eventually, TA (E). The former reaction (oxidation of PX to *p*-toluic acid) is easier and even mononuclear Co or Mn complexes accomplish this significantly (19). Further oxidation of *p*-toluic acid to TA, however, is difficult and only the catalyst system Co/Mn/Br^-, in HOAc, at high pressure and temperature, achieves 100% conversion of PX with >95% selectivity to TA. The reduction in ring electron density (in going from PX to *p*-toluic acid) makes H-abstraction from the methyl group of *p*-toluic acid about 4.9 times more difficult. Monomeric complexes cannot abstract H-atoms from *p*-toluic acid; (μ_3-oxo)(μ-acetato)-bridged heteronuclear Co/Mn clusters ($CoMn_2(O)$) are capable of accelerating the latter reaction step. A plausible reaction mechanism for oxidation by (μ_3-oxo)(μ-acetato)-bridged Co/Mn cluster complexes is shown in Fig. 5.10. It is interesting to note the presence of such oxo- and acetato-bridged Fe, Cu and Mn complexes as active sites in many oxygenase, oxidase and catalase enzymes (20 – 23). Cluster complexes exhibit labile intramolecular electron and spin transfer. This unique property and the basic nature of the μ_3-oxo-bridges account, perhaps, for their superior performance in the selective oxidation of PX.

5.5 Conclusions

(μ_3-Oxo)(μ-acetato)-bridged Co/Mn cluster complexes, both in the "neat" state and when encapsulated in the supercages of zeolite-Y are efficient catalysts for the selective oxidation of PX to TA. The more facile redox behavior of Co between +2 and +3 oxidation states in $CoMn_2(O)$ compared to the homonuclear complexes is responsible for the greater catalytic activity of the former. The zeolite-Y-based heterogeneous catalysts in addition to possessing all the superior activity and selectivity characteristics of the homogeneous catalysts have the advantages of easy separation and reuse. The catalyst is stable at reaction conditions and there is negligible leaching of metal ions into reaction medium. To date, this is the first solid catalyst reported that is both highly active and selective in oxidation of *para*-xylene to terephthalic acid. An interesting advantage with the encapsulated $CoMn_2(O)$ cluster catalyst is a very low concentration of the 4-carboxybenzaldehyde impurity (around 0.01%).

5.6 References

1. Partenheimer, W., *Catal. Today* **23**, 69 (1995).

2. *Catalytic Oxidation: Principles and Applications*, Sheldon, R. A., and Van Santen, R. A. (Eds.), World Scientific, Singapore (1995).

3. Sheldon, R. A. in *The Activation of Dioxygen and Homogeneous Catalytic Oxidation*, Barton, D. H. R., Martell, A. E., and Sawyer, D. T. (Eds.), Plenum Press, New York, 9 (1993).

4. Sheldon, R. A. in *Dioxygen Activation and Homogeneous Catalytic Oxidation*, Simandi, L. I. (Ed.), Elsevier, Amsterdam, Vol. **66**, 573 (1991).

5. Parshall, G. W., and Ittel, S. D., *Homogeneous Catalysis:The Applications and Chemistry of Catalysis by Soluble Transition Metal Complexes*, John Wiley & Sons Inc., New York (1992).

6. Hutchings, G. J., *Chem. Commun.*, 301 (1999).

7. Sabater, M. J., Corma, A., Domenech, A., Fornés, V., and Garcia, H., *Chem. Commun.*, 1285 (1997).

8. Ogunwumi, S. B., and Bein, T., *Chem. Commun.*, 901 (1997).

9. Parton, R. F., Bezoukhanova, C. P., Grobet, J., Grobet, P. J., and Jacobs, P. A., *Stud. Surf. Sci. Catal.* **83**, 371 (1994).

10. Deshpande, S., Srinivas, D., and Ratnasamy, P., *J. Catal.* **188**, 261 (1999).

11. Hashimoto, K., Matzuo, K., Kominami, H., and Kera, Y., *J. Chem. Soc., Faraday Trans.*, **93**, 3729 (1997).

12. Centi, G., Fazzini, F., Fierro, J. L. G., Granados, M. L., Sanz, R., and Serrano, D., *Stud. Surf. Sci. Catal.*, **118**, 577 (1998).

13. Chisem, I. C., Chisem, J., Rafelt, J. S., Macquarrie, D. J., Clark, J. H., and Utting, K. A., *J. Chem. Technol. Biotechnol.*, **74**, 923 (1999).

14. Kishimoto, N., Nakamura, I., and Nagamura, Y., Eur. Pat. Appl. EP 1 099 475, 16 May (2001).

15. Mehrotra, R. C., and Bohra, R., *Metal Carboxylates*, Academic Press, New York (1983).

16. Vincent, J. B., Chang, H.-R., Folting, K., Huffman, J. C., Christou, G., and Hendrickson, D. N., *J. Am. Chem. Soc.*, **109,** 5704 (1987).

17. Douglas, B. E., McDaniel, D. H., and Alexander, J. J., *"Concepts and Models in Inorganic Chemistry*," Wiley, New York, (1994).

18. Metelski, P. D., Adamian, V. A., and Espenson, J. H., *Inorg. Chem.*, **39**, 2434 (2000).

19. Jacob, C. R., Varkey, S. P., and Ratnasamy, P., *Appl. Catal.A*, **182**, 91 (1999).

20. Andersson, K. K., and Gräslund, A., *Adv. Inorg. Chem.* **43**, 359 (1995).

21. *Metal-Oxo and Metal-Peroxo Species in Catalytic Oxidations*, Meunier, B., (Ed.), *Structure and Bonding*, Vol. **97**, pp. 125 - 211 (2000).

22. Beyer, W. F., and Fridovich, I., *Biochemistry* **24**, 6460 (1985).

23. Law, N. A., Caudle, M. T., and Pecoraro, V. L., *Adv. Inorg. Chem.* **46**, 305 (1999).

Chapter-6

Oxidation of Cyclohexanone, Cyclohexanol and Cyclohexane to Adipic Acid over (μ_3-Oxo)(μ-Acetato)-Bridged Co/Mn Cluster Complexes

6.1 Introduction

Adipic acid (AA), a valuable raw material used in the production of Nylon-6,6, fibers, plasticizers and food additives, is manufactured by the oxidation of cyclohexanone, obtained either by hydrogenation of phenol, or more commonly, by the oxidation of cyclohexane (1 - 3). In the first-stage, cyclohexane is oxidized with oxygen (423 – 473 K; 115 – 175 psig), using a soluble cobalt catalyst (usually cobalt naphthenate, cobalt octonate or cobalt acetate) to a mixture of cyclohexanol-cyclohexanone (referred to as KA oil; conversion <10%; selectivity ≈ 70 - 90%). In the second-stage, this mixture is further oxidized, at 343 – 364 K, to AA (yield of AA = 70 - 95%) by 40 – 60% HNO_3 in the presence of copper and vanadium catalysts (2). During the second stage, significant amounts of environmentally harmful NO_x effluents (NO, NO_2 and N_2O) are produced (4, 5). While NO and NO_2 are recycled to the HNO_3 plant, N_2O is usually vented and constitutes a major source of this highly polluting species. Hence, an alternative non-HNO_3 route to AA using cleaner oxidants like O_2 or H_2O_2 is highly desirable.

Although many variations of the initial cyclohexane oxidation (to KA oil) step have been developed, technology for the second stage (conversion of KA oil to AA) is fundamentally the same as that originally developed by Du Pont in the early 1940s (1). A number of alternative processes for producing AA have been investigated but none of them have been commercialized so far (6 – 8). Tanaka (6, 7) has reported a single step, liquid phase, aerial oxidation of cyclohexane to AA (yields of AA = 70 – 75% at cyclohexane conversions of 50 – 75% and 343 – 373 K). BASF has developed a process based on hydrocarboxylation or

carboalkoxylation of butadiene (8). Jacobs and co-workers (9 - 11), Balkus and co-workers (12, 13), Herron et al (14) and Raja and Ratnasamy (15, 16) studied this oxidation with *tert*-butylhydroperoxide or iodosylbenzene (PhIO) over metal phthalocyanine complexes encapsulated in zeolite-Y. Sato *et al.* (17) oxidized cyclohexene with 30% H_2O_2 over $Na_2WO_4.2H_2O$. Recently, Thomas and co-workers (18 - 21) oxidized cyclohexane and n-hexane with air to AA over metal-containing aluminium phosphate molecular sieves. However, none of these studies using solid catalysts have the potential to replace the current commercial process, due to low yields of AA and/or use of expensive oxidants like H_2O_2, *tert*-butylhydroperoxide and PhIO.

In the oxidation of *para*-xylene to terephthalic acid, it was found (Chapters 4 and 5) that (μ_3-oxo)(μ-acetato)-bridged Co/Mn cluster complexes (Fig.6.1) are formed from Co and Mn acetates in acetic acid (HOAc) medium during the oxidation process. These complexes (especially the heteronuclear $CoMn_2(O)$), in both the "neat" state and when encapsulated in zeolite-Y, exhibited higher activity and selectivity in the *para*-xylene oxidation than the individual metal acetates (Chapter 5). The aerial oxidation of cyclohexanone, cyclohexanol and cyclohexane to AA using these (μ_3-oxo)(μ-acetato)-bridged cluster complexes, $CoMn_2(O)(CH_3COO)_6(py)_3$, $[Mn_3(O)(CH_3COO)_6(py)_3]^+$ and $[Co_3(O)(CH_3COO)_6(py)_3]^+$ (hereafter referred to as $CoMn_2(O)$, $Mn_3(O)$ and $Co_3(O)$, respectively; py = pyridine), is reported in this chapter. To date, this is the first non-HNO_3, aerial oxidation route for the preparation of AA from cyclohexanone, wherein the yields of AA are comparable to those obtained in current, commercial practice.

6.2 Experimental

The synthesis and characterization of the "neat" and zeolite-Y-encapsulated (μ_3-oxo)(μ-acetato)-bridged cluster complexes are reported in Chapters 2, 4 and 5. The methodology of the oxidation reactions is presented in Chapter 2.

6.3 Results and Discussion

6.3.1 Oxidation of Cyclohexanone

6.3.1.1 Effect of Cluster Composition and Reaction Temperature

Adipic acid (AA) was the major product, while succinic (SA), glutaric (GA) and valeric acids (VA) were the minor products in the oxidation of cyclohexanone. The composition of the cluster complex has a marked effect on the reactivity (conversion and TOF) and product selectivity. Table 6.1 lists the catalytic activity data of the cluster complexes. Though $Mn_3(O)$ and $CoMn_2(O)$ clusters exhibited similar activity, the yield of AA was more with the former (Table 6.1; Runs 2 and 4). Among the three clusters, $Co_3(O)$ exhibited least activity and AA selectivity (Table 6.1; compare runs 1, 2 and 4). On increasing the temperature from 353 to 423 K, while the conversion and TOF of cyclohexanone increased, the yield of AA passed through a maximum around 373 K (Table 6.1; Runs 3-6).

6.3.1.2 Effect of Pressure and Reaction Time

The conversion of cyclohexanone and AA yield increased with pressure (from 200 to 900 psig) and reaction time (Table 6.2). Under our reaction conditions, complete conversion of cyclohexanone was achieved at 6 h (Table 6.2,

Run No. 12). Product selectivity, however, was less sensitive to changes in pressure and reaction time.

Table 6.1 Selective Oxidation of Cyclohexanone over (μ_3-Oxo)(μ-Acetato) -Bridged Co/Mn Cluster Complexes[a]

Run no.	Catalyst	Temp. (K)	Conv. (wt.%)	TOF	Product distribution (wt.%)			
					SA	GA	VA	AA
1	$Co_3(O)$	363	11.9	136	10.6	15.1	0	74.3
2	$Mn_3(O)$	363	93.7	1104	3.0	13.9	0	83.1
3	$CoMn_2(O)$	353	82.8	941	5.2	18.7	1.1	75.0
4	$CoMn_2(O)$	363	92.2	1048	6.9	14.7	0	78.4
4a	$CoMn_2(O)$	363	90.1	1024	2.3	14.4	3.3	80.0
5	$CoMn_2(O)$	373	97.6	1104	1.9	11.5	0	86.6
6	$CoMn_2(O)$	423	99.9	1130	6.6	21.5	4.7	67.2

[a]Reaction conditions: catalyst weight = 7.5 mg (8.6 – 8.9 μmol); cyclohexanone = 4.21 ml (40.5 mmol); oxidant = air (550 psig when hot); oxidation initiator = MEK (0.114 ml); medium = HOAc (38 ml) + water (1.9 ml); reaction time = 4 h. Run No. 4a was done without MEK.

[b]Turnover frequency (TOF) = number of moles of substrate converted per mole of the catalyst per hour.

Table 6.2 Effects of Pressure and Reaction Time on Product Distribution in the Oxidation of Cyclohexanone over $CoMn_2(O)$ [a]

Run no.	Pressure (psig)	Reaction time (h)	Conv. (wt. %)	TOF[b]	Product distribution (wt.%)			
					SA	GA	VA	AA
1	200	0.75	51.6	3112	0	14.7	5.8	79.5
2	350	0.75	71.0	4282	1.0	13.1	5.7	80.3
3	550	0.75	89.8	5415	2.9	15.7	1.7	79.7
4	700	0.75	94.9	5723	3.2	14.9	3.0	79.0
5	900	0.75	98.2	5922	3.0	13.2	3.8	80.0
6	550	0.25	69.5	12573	3.0	14.9	1.9	80.2
7	550	0.50	84.7	7662	2.7	13.0	2.1	82.1
8	550	1.0	88.0	3980	3.3	15.1	2.1	79.5
9	550	1.5	89.1	2687	2.1	13.4	2.1	82.4
10	550	2	90.6	2049	3.0	15.3	3.3	78.4
11	550	3	90.0	1357	2.3	13.8	2.2	81.7
12	550	6	99.9	755	3.6	17.1	3.0	76.3

[a]Reaction conditions: catalyst weight = 7.5 mg; cyclohexanone = 4.21 ml (40.5 mmol); oxidant = air; oxidation initiator = MEK (0.114 ml); medium = HOAc (38 ml) + water (1.9 ml); temperature = 363 K; [b]Turnover frequency (TOF) = number of moles of substrate converted per mole of the catalyst per hour.

Table 6.3 Selective Oxidation of a Mixture of Cyclohexanol (-ol) and Cyclohexanone (-one) over (μ_3-Oxo)(μ-Acetato)-Bridged Co/Mn Cluster Complexes at 363 K[a]

Run no.	Catalyst	Substrate (-ol : -one)	Overall Conv. (wt.%)	Individual conv. (wt%)		Product distribution (wt.%)			
				-ol	-one	SA	GA	VA	AA
1	$CoMn_2(O)$	0 : 100	92.2	-	92.2	6.9	14.7	0	78.4
2	$CoMn_2(O)$	10 : 90	85.9	100	84.5	3.3	17.5	1.4	77.9
3	$CoMn_2(O)$	20 : 80	84.5	100	80.9	3.4	15.2	1.7	79.7
4	$CoMn_2(O)$	50 : 50	79.1	91.3	65.5	3.3	12.5	1.7	82.5
5	$Mn_3(O)$	0 : 100	93.7	-	93.7	3.0	13.9	0	83.1
6	$Mn_3(O)$	10 : 90	87.1	100	86.1	2.9	16.7	0.8	79.6
7	$Mn_3(O)$	20 : 80	80.5	96.1	75.6	2.2	13.1	0.6	84.1
8	$Mn_3(O)$	50 : 50	84.7	94.7	74.1	2.3	13.3	0.8	83.7

[a]Reaction conditions: catalyst weight = 7.5 mg (8.6 – 8.9 μmol); oxidant = air (550 psig when hot); oxidation initiator = MEK (0.114 ml); medium = HOAc (38 ml) + water (1.9 ml); reaction time = 4 h.

6.3.2 Oxidation of a Mixture of Cyclohexanone and Cyclohexanol

The oxo-bridged clusters are highly efficient in the oxidation of cyclohexanone-cyclohexanol (-one/-ol) mixtures. While the ketone (-one) is oxidized directly to the acid products, the alcohol (-ol) is oxidized initially to -one and then, subsequently to the acid products (1 - 3). The catalytic activity data are presented in Table 6.3. The conversion of –ol increased (from 91 to 100 wt% over $CoMn_2(O)$ and from 94.7 to 100 over $Mn_3(O)$) with increasing concentration of –

one in the reaction mixture (Table 6.3). In the absence of –one the conversion of –ol was very low (45 wt%). In contrast, the individual conversion of –one decreased (from 84.5 to 65.5 wt% over $CoMn_2(O)$ and from 86.1 to 74.1 wt% over $Mn_3(O)$) with increasing concentrations of –ol in the reaction mixture (Table 6.3). In the absence of –ol the conversion of –one was higher (92.2 wt% over $CoMn_2(O)$ and 93.7 wt% over $Mn_3(O)$). The overall conversion of the reaction mixture (-one + -ol) decreased from 92 to 79 wt% over $CoMn_2(O)$ and from 93.7 to 84.8 wt% over $Mn_3(O)$ with increasing –ol concentration. AA selectivities, however, are not significantly changed (80 ± 5%) (Table 6.3).

Table 6.4 Aerial Oxidation of Cyclohexane Over (μ_3-Oxo)(μ-Acetato)-Bridged Co/Mn Cluster Complexes[a]

Run no.	Catalyst	Conv. (wt.%)	TOF[b]	Product distribution (wt.%)					
				-ol	-one	SA	GA	VA	AA
1	$Co_3(O)$	85.6	489	5.0	1.5	16.2	55.0	0.4	22
2	$Mn_3(O)$	41.8	248	-	1.0	59.6	1.1	-	38.3
3	$CoMn_2(O)$	51.6	293	3.7	1.3	31.6	27.2	-	36.2

[a]Reaction conditions: Catalyst weight = 7.5 mg (8.6 – 8.9 μmol); cyclohexane = 4.4 ml (40.7 mmol), oxidant = air (550 psig when hot); oxidation initiator = MEK (0.114 ml); medium = HOAc (38 ml) + water (1.9 ml); reaction time = 8 h. [b]Turnover frequency (TOF) = number of moles of substrate converted per mole of the catalyst per hour.

6.3.3 Oxidation of Cyclohexane

The catalytic activity of the cluster complexes in cyclohexane oxidation decreased in the order: $Co_3(O)$ > $CoMn_2(O)$ > $Mn_3(O)$ (Table 6.4). Succinic and glutaric acids were the major products. It may recalled that adipic acid is the major product in the oxidation of cyclohexanone-cyclohexanol (Tables 6.1 – 6.3).

Table 6.5 Selective Oxidation of Cyclohexanone over (μ_3-Oxo)(μ-Acetato)-bridged Co/Mn Cluster Complexes Encapsulated in Zeolite-Y

Run No.	Catalyst (mg)	Conv. (wt.%)	Product distribution (wt.%)			
			SA	GA	VA	AA
1	$Co_3(O)$-Y (149.8)	3.7	0.6	8.4	0	91.0
2	$Co_3(O)$-Y (299.5)	10.2	0.9	6.6	0	92.5
3	$Co_3(O)$-Y (599.0)	0.6	0.5	8.0	0	91.5
4	$Mn_3(O)$-Y (149.8)	97.1	3.2	14.1	0.2	82.5
5	$Mn_3(O)$-Y (299.5)	96.8	2.8	14.1	1.6	81.5
6	$Mn_3(O)$-Y (599.0)	79.0	4.0	12.5	0.05	83.5
7.	$CoMn_2(O)$-Y (74.9)	98.3	1.8	10.9	0	87.3
8	$CoMn_2(O)$-Y (149.8)	98.4	3.9	15.5	1.3	79.3
9	$CoMn_2(O)$-Y (299.5)	98.4	4.5	16.5	2.0	77.0
10	$CoMn_2(O)$-Y (599.0)	92.7	4.1	16.5	0.1	79.2

[a]Reaction conditions: cyclohexanone = 4.21 ml (40.5 mmol); oxidant = air (700 psig at 298 K); oxidation initiator = MEK (0.114 ml); medium = HOAc (38 ml) + water (1.9 ml); reaction time = 4 h. temperature = 373 K.

6.3.4 Oxidations over $Mn_3(O)$, $Co_3(O)$ and $CoMn_2(O)$ Complexes Encapsulated in Zeolite-Y

The encapsulated complexes exhibited activity similar to the "neat" clusters (compare Tables 6.5 and 6.1). $Mn_3(O)$-Y and $CoMn_2(O)$-Y were more active than $Co_3(O)$-Y. Conversion of cyclohexanone increased with an increase in the amount of the catalyst up to 299 mg and then decreased (Table 6.5). However, significant leaching out of the metal ions during the reaction was observed. This is in contrast to the oxidation of *para*-xylene at 473 K and 550 psig, wherein such leaching was negligible (see Chapter 5).

6.3.5 *In situ* Spectroscopic Studies

In situ electronic and EPR spectroscopies, enabled the identification of the (μ_3-oxo)(μ-acetato)-bridged clusters as the active species in *para*-xylene oxidation (Chapter 4). Similar studies for cyclohexanone oxidation were performed on the following solutions:

1. $Mn(OAc)_2$ in HOAc + pyridine + water (298 K; 363 K for 45 min; 700 psig air, 363 K, 45 min).
2. Solution 1 + MEK (700 psig air, 363 K, 45 min).
3. Solution 2 + cyclohexanone (700 psig air, 363 K, 45 min).
4. A mixture of $Co(OAc)_2$ and $Mn(OAc)_2$ (3:1 mmol ratio) in HOAc + pyridine + water (298 K; 363 K for 45 min; 700 psig air, 363 K, 45 min).
5. Solution 4 + MEK (700 psig, 363 K, 45 min).
6. Solution 5 + cyclohexanone (700 psig, 363 K, 45 min).

6.3.5.1 Electronic Spectroscopy

Solution 1 containing $Mn(OAc)_2$ did not exhibit any absorption in the visible region. However, upon heating at 363 K for 45 min and pressurizing with air (700 psig) a narrow band at 490 nm, a broad band at 445 nm and a shoulder at

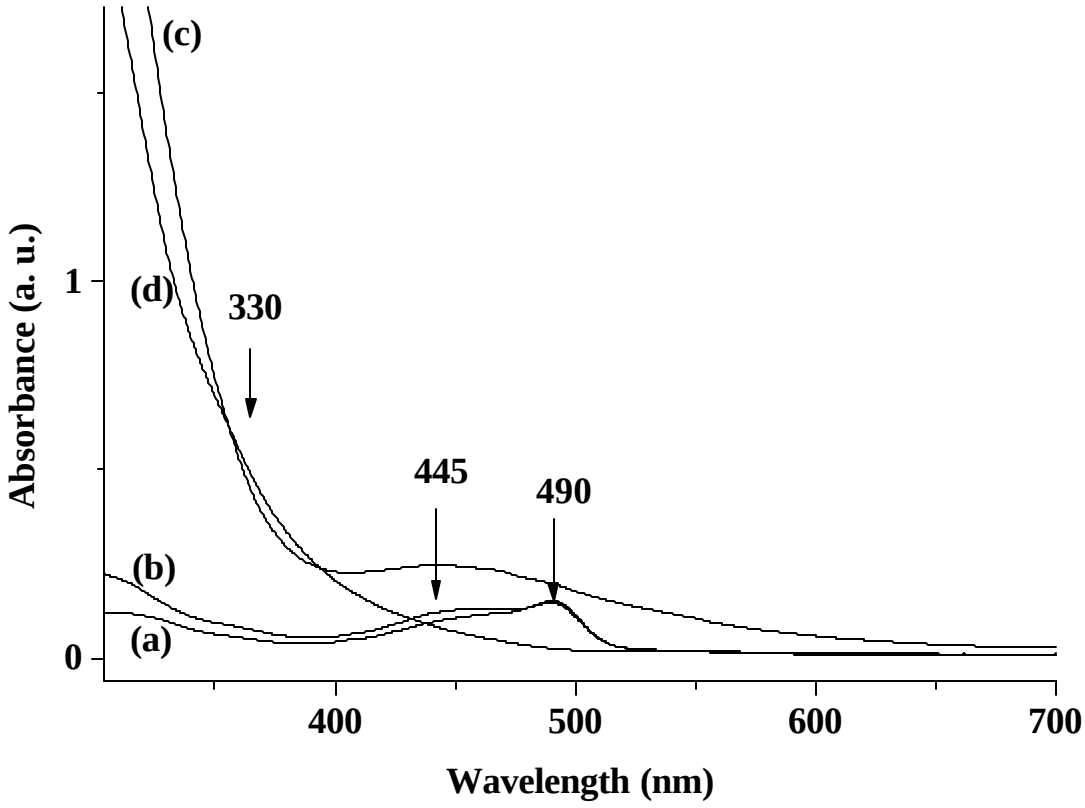

Fig. 6.1 Electronic spectra of manganese complexes: (a) $Mn(OAc)_2$ in HOAc + pyridine + H_2O at 363 K, 45 min; (b) solution in (a) at 700 psig air, 363 K, 45 min; (c) $Mn(OAc)_2$ in HOAc + pyridine + H_2O + MEK at 700 psig air, 363 K, 45 min; (d) $Mn(OAc)_2$ in HOAc + pyridine + H_2O + MEK + cyclohexanone at 700 psig air, 363 K, 45 min.

around 330 nm (Fig. 6.1, curves a and b) were observed. The former (490 nm) corresponds to d-d transition of a monomeric Mn(III) species. The latter two bands are attributed to d-d transition and oxygen $\Rightarrow$ Mn(III) charge transfer transition,

respectively, of (μ_3-oxo)(μ-acetato)-bridged Mn cluster complex ($Mn_3(O)$); the assignment of the 330 nm band was also confirmed from $Mn_3(O)$ cluster complexes prepared independently. As anticipated, the intensities of $Mn_3(O)$ bands increased with the concentration of O_2 (higher pressure of air). When the experiment was conducted with MEK, the color of the solution changed from pale yellow to deep brown. Solution 2 showed intense bands at 445 and 330 nm due to the $Mn_3(O)$ cluster complex (Fig. 6.1, curve c; dilution factor = 20). MEK promoted the oxidation of Mn from +2 to +3 state and formation of the more active $Mn_3(O)$ cluster complex. In the presence of cyclohexanone (solution 3), some reduction in the intensity of $Mn_3(O)$ bands was observed (Fig. 6.1, curve d; dilution factor = 20) suggesting that part of $Mn_3(O)$ is reconverted to Mn(II) species in the presence of cyclohexanone. The $Mn_3(O)$ cluster and Mn(II) species are, perhaps, in a quasi-equilibrium.

Solution 4 containing the mixture of $Co(OAc)_2$ and $Mn(OAc)_2$ (3:1 mmol) exhibited d-d transitions in the visible region, at 524 and 490 nm, corresponding to Co(II) acetate complexes. On heating at 363 K for 45 min and pressurizing with air (700 psig) the intensity of these bands increased (Fig. 6.2, curves a and b). With MEK, solution 5 (700 psig, 363 K, 45 min) showed marked changes in the position and intensity of the UV-visible bands (Fig. 6.2, curve c; dilution = 20). New bands appeared around 570, 455 and 345 nm. The broad band at 570 nm is due to a Co(III) species and those at 455 and 345 nm are characteristic of (μ_3-oxo)(μ-acetato)-bridged Co/Mn cluster complexes ($CoMn_2(O)$) (22). In the presence of cyclohexanone (solution 6), a reduction in the intensity of these bands

(Fig. 6.2, curve d) was observed in addition to the appearance of a weak band at 524 nm corresponding to Co(II) species. The electronic spectroscopic studies of $Mn(OAc)_2$ and a mixture of $Co(OAc)_2$ and $Mn(OAc)_2$ solutions reveal, that during the oxidation reaction a small amount of M(III) ions in the cluster complex are reduced to M(II) species (where M = Co/Mn).

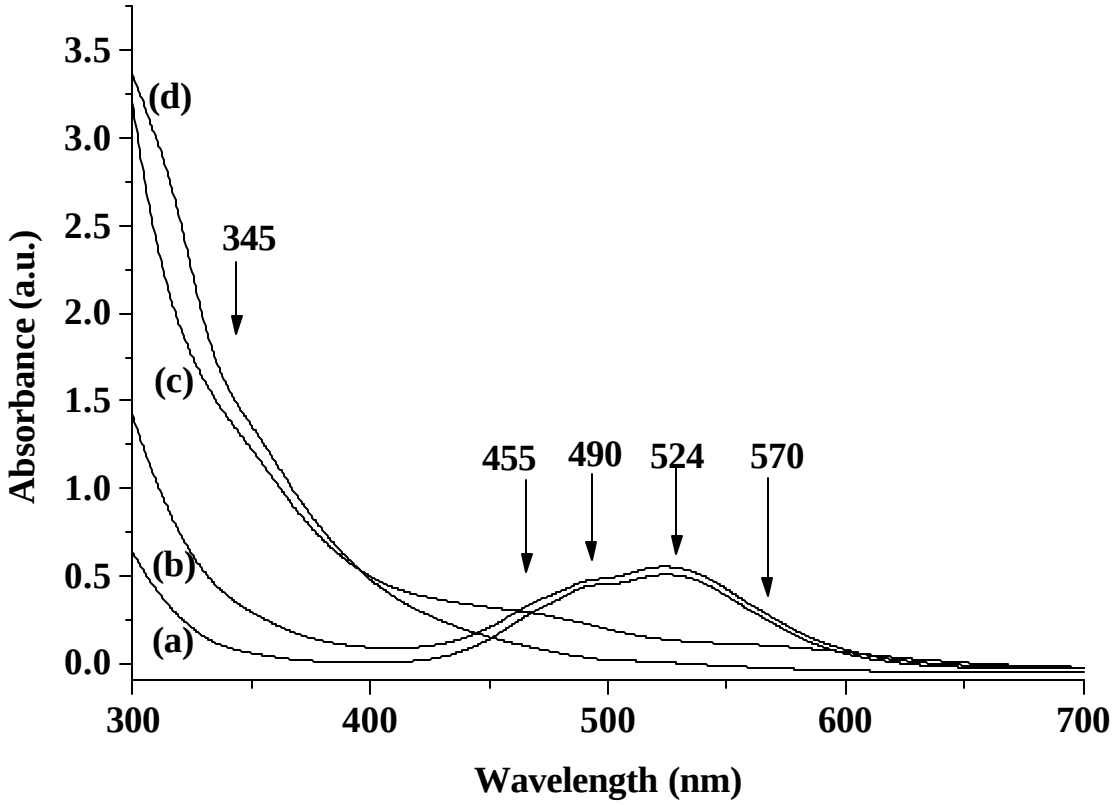

Fig. 6.2 Electronic spectra of cobalt and manganese complexes: (a) $Co(OAc)_2$ + $Mn(OAc)_2$ (3:1 mmol) in HOAc + pyridine + H_2O at 363 K, 45 min; (b) solution in (a) at 700 psig air, 363 K, 45 min; (c) $Co(OAc)_2$ + $Mn(OAc)_2$ in HOAc + pyridine + H_2O + MEK at 700 psig, 363 K, 45 min; (d) $Co(OAc)_2$ + $Mn(OAc)_2$ in HOAc + pyridine + H_2O + MEK + cyclohexanone at 700 psig, 363 K, 45 min.

6.3.5.2 EPR Spectroscopy

Solution 4 containing a mixture of $Co(OAc)_2$ and $Mn(OAc)_2$ showed a resolved sextet line hyperfine pattern (A_{iso} = 94.5 G) centered at g_{iso} = 2.0012 due to the manganese(II) acetate complex (Fig. 6.3, Curve a). Although Co(II) acetate is paramagnetic (S = 3/2), its EPR signals cannot be detected at ambient temperatures due to the short spin lattice relaxation times. When the solution was pressurized with air (700 psig at 363 K for 45 min), the overall spectral intensity decreased (Fig. 6.3, curve b), the signals broadened and the spectral width increased from 524 to 538 G. The center of the hyperfine pattern shifted from g_{iso} = 2.012 to 1.998. These features indicate the formation of magnetically interacting Co/Mn cluster complexes ($CoMn_2(O)$) at high pressure (700 psig) and temperature (363 K) from individual cobalt and manganese acetate salts. This result is in agreement with the electronic spectroscopic studies, wherein these cluster complexes were observed and characterized by bands at 345 and 455 nm (Fig. 6.2). The formal oxidation state of Mn ions changes from +2 to +3 on the formation of the cluster complexes. When MEK was added and the system pressurized with air (700 psig, 365 K, 45 min; solution 5), a significant decrease in EPR signal intensity was observed indicating the formation of more amount of the EPR-silent (μ_3-oxo)(μ-acetato)-bridged Co/Mn clusters (Fig. 6.3, curve c). When cyclohexanone was added (solution 6), the overall intensity increased (solution 6; Fig. 6.3, curve d) due to partial decomposition of the cluster complexes to monomeric Co(II) and Mn(II) species. Similar conclusions were drawn also from the electronic spectroscopic studies (see above).

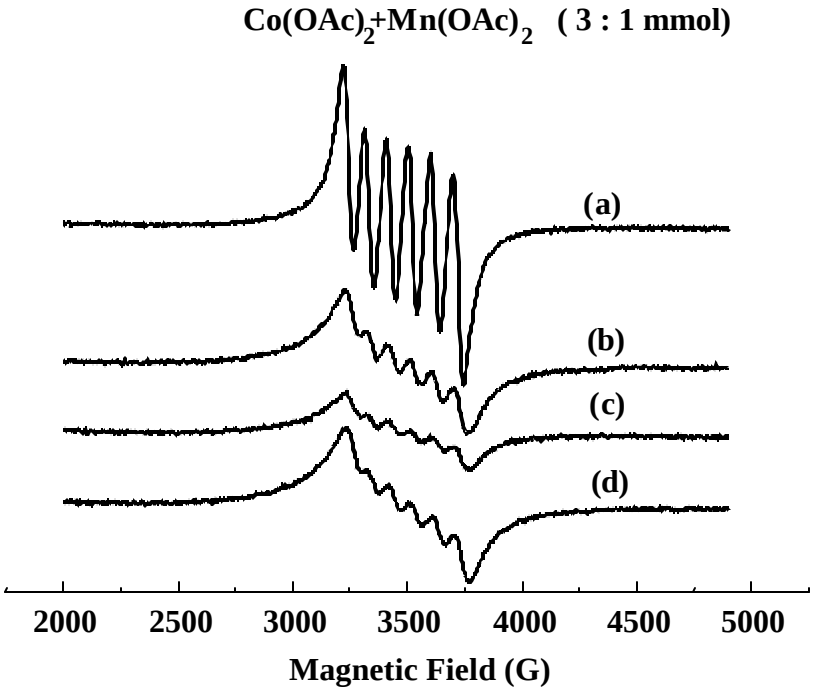

1.

Fig. 6.3 EPR spectra of reaction solutions at 298 K: (a) $Co(OAc)_2$ + $Mn(OAc)_2$ (3:1 mmol) in HOAc + pyridine + H_2O at 363 K, 45 min; (b) solution (a) at 700 psig air, 363 K, 45 min; (c) $Co(OAc)_2$ + $Mn(OAc)_2$ in HOAc + pyridine + H_2O + MEK at 700 psig, 363 K, 45 min; (d) $Co(OAc)_2$ + $Mn(OAc)_2$ (3:1 mmol) in HOAc + pyridine + H_2O + MEK + cyclohexanone at 700 psig, 363 K, 45 min.

6.3.6 Mechanism of Cyclohexanone Oxidation

In the oxidation of cyclohexanone, 1,2-cyclohexanedione is an intermediate (Fig. 6.4) (1). While the keto-form yields the desired product AA, the enol-form leads to other acid impurities (1). The acid impurities (like GA, VA and SA) can form also by oxidative degradation of AA. A plausible mechanism for the degradation of AA is as follows (23):

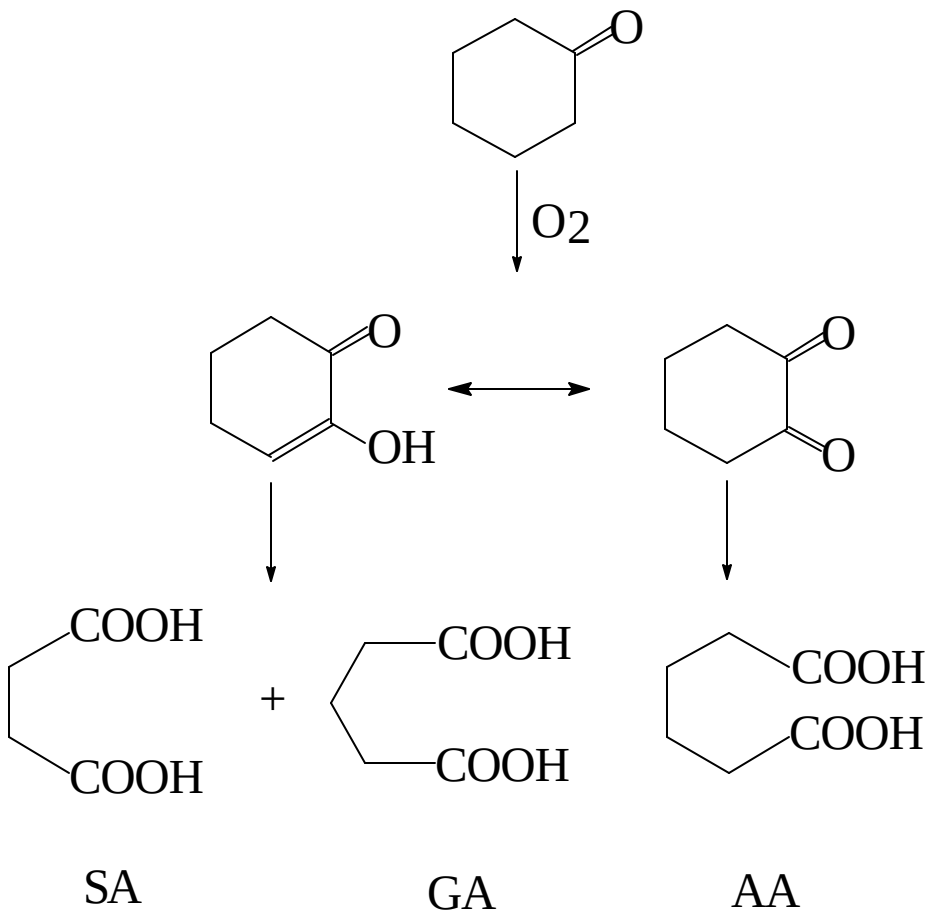

Fig. 6.4 Mechanism of cyclohexanone oxidation.

$$M^{III}(OAc)_3 + HOOC(CH_2)_4COOH \leftrightarrow M^{III}(OAc)_2(OOC(CH_2)_4COOH) + HOAc$$

$$M^{III}(OAc)_2(OOC(CH_2)_4COOH) \rightarrow M^{II}(OAc)_2 + CO_2 + \bullet CH_2(CH_2)_3COOH$$

$$\bullet CH_2(CH_2)_3COOH + O_2 \rightarrow HOOC(CH_2)_3COOH$$

$$M^{III}(OAc)_3 + HOOC(CH_2)_3COOH \leftrightarrow M^{III}(OAc)_2(OOC(CH_2)_3COOH) + HOAc$$

$$M^{III}(OAc)_2(OOC(CH_2)_3COOH) \rightarrow M^{II}(OAc)_2 + CO_2 + \bullet CH_2(CH_2)_2COOH$$

$$\bullet CH_2(CH_2)_2COOH + O_2 \rightarrow HOOC(CH_2)_2COOH$$

Two features may be noted: (1) The decomposition of adipic to glutaric and succinic acids, and (2) the partial reduction of the metal ions (from the tri- to the divalent state). Such a change in the oxidation state of metal ions in cyclohexanone oxidation was indeed observed by *in situ* electronic and EPR spectroscopic studies (*vide supra*). During the oxidation reaction, the metal ions are reoxidized by O_2.

6.4 Conclusions

A novel, non-HNO_3 route for the preparation of adipic acid by aerial oxidation of cyclohexanone or a mixture of cyclohexanone and cyclohexanol or cyclohexane using (μ_3-oxo)(μ-acetato)-bridged Co/Mn cluster complexes is reported. The yields of adipic acid are comparable to those in current processes.

6.5 References

1. Davis, D. D., and Kemp, D. R., in "Kirk-Othmer Encyclopedia of Chemical Technology," Kroschwitz, J. I., and Howe-Grant, M., (Eds.), Wiley, New York, Vol. **1**, 466, 1991.

2. Castellan, A., Bart, J. C. J., and Cavallaro, S., *Catal. Today*, **9**, 237 (1991).

3. Dumas, T., and Bulani, W., in "*Oxidation of Petrochemicals: Chemistry and Technology*," Applied Science Publishers Ltd., London (1974).

4. Thiemens, M. H., and Trogler, W. C., *Science*, **251**, 932 (1991).

5. Schuchardt, U., Cardoso, D., Sercheli, R., Pereira, R., da Cruz, R. S., Guerreiro, M. C., Mandelli, D., Spinacé, E. V., and Pires, E. L., *Appl. Catal. A: General*, **211**, 1 (2001).

6. Tanaka, K., *CHEMTECH*, 555 (1974).

7. Tanaka, K., *Hydrocarbon Processing*, 114 (1974).

8. Chauvel, A., Delmon, B., and Holderich, W. F., *Appl. Catal. A*, **115**, 173 (1994).

9. Parton, R. F., Vankelecom, I. F. J., Casselman, M. J. A., Bezoukhanova, C. P., Uytterhoeven, J. B., and Jacobs, P. A., *Nature*, **370**, 541 (1994).

10. Thisbault-Starzyk, F., Parton, R. F., and Jacobs, P. A., *Stud. Surf. Sci. Catal.*, **84**,

1419 (1994).

11. Parton, R. F., Peere, G. J., Neys, P. E., Jacobs, P. A., Claessens, R., and Baron, G. V., *J. Mol. Catal. A: Chemical*, **113**, 445 (1996).

12. Balkus Jr., K. J., Eissa, M., and Levado, R., *J. Am. Chem. Soc.*, **117**, 10753 (1995).

13. Balkus Jr., K. J., Eissa, M., and Levado, R., *J. Am. Chem. Soc.*, **117**, 10753 (1995).

14. Herron, N., Stucky, G. D., and Tolman, C. A., *J. Chem. Soc. Chem. Commun*., 1521 (1986).

15. Raja, R., and Ratnasamy, P., *Catal.*, Lett., **48**, 1 (1997).

16. Raja, R., and Ratnasamy, P., *US Pat. No. 5,767,320* (1998).

17. Sato, K., Aoki, M., and Noyori, R., *Science*, **281**, 1646 (1998).

18. Dugal, M., Sankar, G., Raja, R., and Thomas, J. M., *Angew. Chem. Int. Ed*., **39**, 2310 (2000).

19. Raja, R., Sankar, G., and Thomas, J. M., *Angew. Chem. Int. Ed*., **39**, 2313 (2000).

20. Thomas, J. M., Raja, R., Sankar, G., and Bell, R. G., *Nature*, **398**, 227 (1999).

21. Luna, F. J., Ukawa, S. E., Wallau, M., and Schuchardt, U., *J. Mol. Catal. A: Chemical*, **117**, 405 (1997).

22. Vincent, J. B., Chang, H.-R., Folting, K., Huffman, J. C., Christou, G., and Hendrickson, D. N., *J. Am. Chem. Soc.*, **109**, 5703 (1987).

23. Schulz, J. G. D., and Onopchenko, A., *J. Org. Chem.*, **45**, 3716 (1980).

Chapter-7

Overall Conclusions

7.1 Summary and Conclusions

Multinuclearity is a common phenomenon in metalloenzymes and proteins, involved in multi-electron redox transformations. It is therefore, aimed to heterogenize multinuclear metal complexes, by encapsulating them inside the supercages of zeolite-Y, as model systems. It is further aimed to investigate the consequences of encapsulation on the structure and catalytic properties of these multinuclear metal complexes.

The metal complexes studied in this work are: (1) dinuclear Cu-acetato and Cu-chloroacetato complexes (Chapter 3), and (2) trinuclear (μ_3-oxo)(μ-acetato)-bridged Co/Mn complexes (Chapters 4 – 6). These complexes have been encapsulated in supercages of zeolite-Y by the "flexible ligand synthesis" method. While a majority of studies reported so far are on mononuclear metal complexes, the present work is unique, in that, it is the first detailed report on encapsulated metal cluster complexes of this type. It may be noted at this juncture, that such oxo- and acetato-bridges are a common occurrence in the active sites of metalloenzymes. Interestingly, Co/Mn cluster complexes are the active species (as revealed by *in situ* spectroscopic studies, Chapters 4 and 6) in the selective hydrocarbon oxidations involving cobalt and manganese acetate salts and molecular oxygen.

The formation and structural integrity of these multinuclear metal complexes have been investigated by a variety of physicochemical techniques viz., chemical and thermal analyses, XRD, FT-IR, UV-visible, EPR and CV. Molecular modeling studies have provided supportive evidence for the location of the cluster

complexes inside the supercages of zeolite-Y. The molecular dimensions of these clusters are larger than the pore opening of the zeolitic supercages. Hence, once formed within the supercages, the complexes cannot exit, unless they decompose or the zeolite structure collapses. Catalytic activities of the "neat" and encapsulated complexes have been investigated in three commercially important selective oxidation reactions viz., (a) regio-selective hydroxylation/oxidation of phenol to *ortho*-benzoquinone (by dimeric acetato-bridged Cu complexes, Chapter 3) and (b) oxidation of *para*-xylene (PX) to terephthalic acid (TA), (Chapters 4 and 5) and (c) oxidation of cyclohexane, cyclohexanol and cyclohexanone to adipic acid (AA) (by trimeric (μ_3-oxo)(μ-acetato)-bridged Co/Mn cluster complexes, Chapter 6). The oxidations have been performed using an environmental-friendly, cheap and clean oxidant, molecular oxygen. The encapsulated clusters have exhibited enhanced catalytic activities and in some cases, improved selectivities compared to the "neat" complexes. Notably, the solid, zeolite-Y-encapsulated cluster catalysts can be easily separated from the reaction mixture and hence, processes involving them will be cleaner, more eco-friendly and economical. The various conclusions drawn from different chapters are briefly outlined below.

The zeolite-Y-encapsulated dinuclear Cu-acetato (CuAc) and Cu-chloroacetato (CuClAc) complexes have mimicked functionally the enzymatic activity of monooxygenase enzyme "tyrosinase". Upon encapsulation inside the supercages of zeolite-Y, the catalytic activity (TOF) of CuAc has enhanced by about 17 times while that of CuClAc by about 250 times. The cause for the

enhanced activity of these dimers upon encapsulation has been investigated by detailed variable temperature EPR spectroscopy (Chapter 3). The EPR studies have provided unequivocal evidence for the formation and integrity of CuAc and CuClAc complexes. Further, EPR spectroscopy has revealed a decrease in Cu-Cu separation of the dimer complexes by ~ 0.2 Å, upon encapsulation. The shortening of the Cu-Cu bond induces a relatively greater overlap of metal orbitals of the dimer copper atoms inside the restricted confines of the zeolite supercages. The consequent enhanced *trans*-axial lability of the phenolate and O_2 ligands enhances the catalytic oxygenase activity of CuAc and CuClAc dimers on encapsulation in zeolite-Y. Thus, the structural basis for the enhanced catalytic activity observed in case of the zeolite-Y-encapsulated CuAc and CuClAc complexes (tyrosinase mimicking "zeozymes"), has been established. It is interesting to note that while most of the known catalyst systems yield hydroquinone and catechol as products of phenol hydroxylation, CuAc, on the contrary, selectively hydroxylates phenol to catechols (monophenolase activity) and further oxidizes the catechol to *ortho*-benzoquinone (diphenolase activity).

Terephthalic acid (TA), an important raw material in polyester industry, is commercially manufactured by the aerial oxidation of *para*-xylene (PX), using the $Co/Mn/Br^-$ catalyst system, in homogenous acetic acid medium. Although the process has been optimized to yield purities of TA in the range 96 - 99%, the actual catalyst formed during the reaction and responsible for the aerial oxidation of PX has not been identified. The structure of the active species in PX oxidation is now established through detailed *in situ* electronic and EPR spectroscopic

investigations (Chapter 4). The optimum zirconium and Br^- ion concentrations enhance the formation of the catalytically active species, trimeric (μ_3-oxo)(μ-acetato)-bridged Co/Mn complexes, in the reaction mixture containing Co(II) and Mn(II) acetates (3:1 mmol) (Chapter 4).

To substantiate the inferences in Chapter 4, the (μ_3-oxo)(μ-acetato)-bridged Co/Mn cluster complexes have been synthesized independently. These cluster complexes have indeed shown comparable PX oxidation activities to the conventional Co/Mn acetate catalysts (Chapter 5). The cluster complexes have been heterogenized, by encapsulating inside the supercages of zeolite-Y. The heteronuclear cluster, $CoMn_2(O)$ has exhibited superior activity compared to the "neat" homonuclear Co and Mn cluster complexes, $Co_3(O)$ and $Mn_3(O)$, respectively. The solid catalysts have exhibited comparable activity to that of the "neat" cluster complexes and the commercial Co/Mn-acetate catalyst (Chapter 5). More interestingly, the formation of 4-carboxybenzaldehyde (4-CBA), a worrisome impurity in the commercial process has been suppressed significantly using the solid, $CoMn_2(O)$-Y catalyst. Spectroscopic studies have revealed that the catalysts are stable at reaction conditions and leaching of metal ions into the reaction mixture (containing PX), is minimal. It may be noted that this is the first report on an efficient solid catalyst for the manufacture of TA.

The Co/Mn cluster complexes have also exhibited efficient activity in the oxidation of cyclohexanone to adipic acid (Chapter 6). Commercially, adipic acid is prepared by oxidizing cyclohexanone with HNO_3. This process produces significant amounts of environmentally harmful NO_x effluents. Aerial oxidation

with the (μ_3-oxo)(μ-acetato)-bridged Co/Mn cluster catalysts, is an alternative non-HNO_3 route. Interestingly, the cluster complexes yield adipic acid comparable to that obtained in the current commercial practice. To date, it is the first non-HNO_3 oxidation route for the preparation of adipic acid from cyclohexanone. The cluster complexes are also active in the oxidation of cyclohexanol and cyclohexane.

The work, detailed in the thesis, provides a deeper insight into the structure and catalytic activity of multinuclear metal cluster complexes encapsulated in large pore zeolite-Y. These encapsulated materials ("zeozymes") are true "ship-in-a-bottle complexes" and have been found to efficiently activate dioxygen in some commercially important catalytic reactions. In dimeric Cu-acetato complexes, the metal ion is directly involved in the activation of dioxygen. On the contrary, in (μ_3-oxo)(μ-acetato)-bridged Co/Mn cluster complexes, the metal and bromide ion combination initially abstracts a proton from the substrate *para*-xylene or cyclohexanone, which in turn adds to dioxygen forming hydroperoxide, that initiates and propagates the autoxidation reaction. The results presented in this thesis contribute to the areas of Green Chemistry and Technology.

List of Research Publications

1. The structural basis for the enhanced oxygenase activity of copper acetate dimers encapsulated in zeolites
   Suhas Chavan, D. Srinivas and Paul Ratnasamy
   Topics Catal., 11/12, 359 - 367 (2000).

2. Structure and catalytic properties of dimeric copper(II) acetato complexes encapsulated in zeolite-Y
   S. Chavan, D. Srinivas and P. Ratnasamy
   J. Catal., 192, 286 – 295 (2000).

3. Formation and role of cobalt and manganese cluster complexes in the oxidation of *p*-xylene
   S. A. Chavan, S. B. Halligudi, D. Srinivas and P. Ratnasamy
   J. Mol. Catal. A: Chemical, 161, 49 – 64 (2000).

4. A novel, zeolite-encapsulated μ_3-oxo Co/Mn cluster catalyst for the oxidation of *para*-xylene to terephthalic acid
   Suhas A. Chavan, D. Srinivas and Paul Ratnasamy
   Chem. Commun., 1124 – 1124 (2001).

5. Selective oxidation of *para*-xylene to terephthalic acid by μ_3-oxo bridged Co/Mn cluster complexes encapsulated in zeolite-Y
   S. A. Chavan, D. Srinivas and P. Ratnasamy
   J. Catal., 204, 409 – 419, (2001).

6. Aerial oxidation of cyclohexane, cyclohexanone and cyclohexanol to adipic acid, by a non-HNO_3 route, over μ_3-oxo-bridged Co/Mn cluster complexes
   S. A. Chavan, D. Srinivas and P. Ratnasamy
   J. Catal., (communicated).

List of Patents

1. Process for the production of aromatic carboxylic acids (Ref No. NF267/2001)
   Applied for Indian, European and US patents.

2. A process for the preparation of encapsulated oxo-bridged organometallic cluster catalysts (Ref No. NF270/2001)
   Applied for Indian, European and US patents.

3. An improved process for the preparation of adipic acid
   Applied for Indian, European and US patents.

4. A process for the preparation of *meta*-phenoxybenzaldehyde
   Applied for Indian, European and US patents.

List of Papers Presented on Conferences/Symposia

1. An insight into the molecular structure and magnetic behavior of dimeric copper acetate encapsulated in zeolite-Y: Variable temperature EPR investigations
   Suhas Chavan, P. M. Suryavanshi, D. Srinivas and Paul Ratnasamy
   5th Symposium of National Magnetic Resonance Spectroscopists held at Indian Institute of Petroleum, Dehradun during February 24 - 26, 1999.

2. Studies on transition metal cluster complexes in selective oxidation of *para*-xylene using molecular oxygen
   S. A. Chavan, S. B. Halligudi, D. Srinivas and P. Ratnasamy
   Fifteenth Indian National Symposium on Catalysis and Second Conference of the Indo-Pacific Catalysis Association (CATSYMP-15 & IPCAT-2) held at National Chemical Laboratory, Pune, India during January 23 - 25, 2001.

3. Selective oxidation of *para*-xylene to terephthalic acid by novel, zeolite-encapsulated metal cluster complexes
   Suhas A. Chavan, D. Srinivas and P. Ratnasamy
   Singapore International Coference (SICC-2) on "Frontiers in Chemical Design and Synthesis" held at National University of Singapore, Singapore during December 18 – 20, 2001.